INFORMATION TO USERS

This material was produced from a microfilm copy of the original document. While the most advanced technological means to photograph and reproduce this document have been used, the quality is heavily dependent upon the quality of the original submitted.

The following explanation of techniques is provided to help you understand markings or patterns which may appear on this reproduction.

1. The sign or "target" for pages apparently lacking from the document photographed is "Missing Page(s)". If it was possible to obtain the missing page(s) or section, they are spliced into the film along with adjacent pages. This may have necessitated cutting thru an image and duplicating adjacent pages to insure you complete continuity.

2. When an image on the film is obliterated with a large round black mark, it is an indication that the photographer suspected that the copy may have moved during exposure and thus cause a blurred image. You will find a good image of the page in the adjacent frame.

3. When a map, drawing or chart, etc., was part of the material being photographed the photographer followed a definite method in "sectioning" the material. It is customary to begin photoing at the upper left hand corner of a large sheet and to continue photoing from left to right in equal sections with a small overlap. If necessary, sectioning is continued again — beginning below the first row and continuing on until complete.

4. The majority of users indicate that the textual content is of greatest value, however, a somewhat higher quality reproduction could be made from "photographs" if essential to the understanding of the dissertation. Silver prints of "photographs" may be ordered at additional charge by writing the Order Department, giving the catalog number, title, author and specific pages you wish reproduced.

5. PLEASE NOTE: Some pages may have indistinct print. Filmed as received.

Xerox University Microfilms
300 North Zeeb Road
Ann Arbor, Michigan 48106

Downloaded from SHAREOK. Persistent Handle URL: https://hdl.handle.net/11244/3535

73-23,958

PASCOE, Ralph Field, 1939-
INDUCTION OF LOCALIZED CORROSION ON A NICKEL ALLOY.

The University of Oklahoma, Ph.D., 1973
Materials Science

University Microfilms, A XEROX Company, Ann Arbor, Michigan

THIS DISSERTATION HAS BEEN MICROFILMED EXACTLY AS RECEIVED.

THE UNIVERSITY OF OKLAHOMA

GRADUATE COLLEGE

INDUCTION OF LOCALIZED CORROSION ON A NICKEL ALLOY

A DISSERTATION

SUBMITTED TO THE GRADUATE FACULTY

in partial fulfillment of the requirements for the

degree of

DOCTOR OF PHILOSOPHY

by

RALPH FIELD PASCOE

Norman, Oklahoma

1973

INDUCTION OF LOCALIZED CORROSION

ON A NICKEL ALLOY

APPROVED BY

DISSERTATION COMMITTEE

INDUCTION OF LOCALIZED CORROSION

ON A NICKEL ALLOY

ABSTRACT

Anodic polarization characteristics of Inconel X-750 are examined as a function of ionic strength, I, and molar anion ratio, r, for the $Cl^-/SO_4^=$ binary anion electrolyte at 30°C. Anodic polarization curves are examined to establish experimental bounds for the investigation of an induction time, τ, for the initiation of localized corrosion.

Current-time fluctuations at constant potential are observed which cannot be explained by the superposition of anodic and cathodic processes on a common surface.

Active site reaction-product-structures are postulated to govern the fluctuations. Evidences of active site surface structures are derived from variations of anion participation in localized corrosion processes and from polarization and induction time phenomena.

ACKNOWLEDGEMENT

The author is pleased to express sincere appreciation to the members of the dissertation committee for their individual and collective contributions toward the completion of this dissertation:

Dr. Raymond D. Daniels, Professor of Metallurgical Engineering and Executive Director of the University of Oklahoma Research Institute, for continued guidance throughout the Ph. D. program. Recent criticism from the industrial community directed toward the "typically narrow" doctoral research program has served to underscore the unusual breadth, flexibility and freedom the author has enjoyed in the selection and execution of the research. Administration and advisement are sure to assume difficult proportions when such wide latitude is given; therefore, this special note of appreciation is given.

Dr. C. M. Sliepcevich, George Lynn Cross Research Professor of Engineering and Dr. Arthur W. Aldag, Jr., Assistant Professor of Chemical Engineering, for making their laboratory equipment available.

Dr. Robert J. Block, Professor of Metallurgical Engineering, for personal instruction in the development of desirable laboratory arts and for making laboratory equipment and supplies available.

Dr. Charles C. Patton, Associate Professor of Petroleum Engineering and Director of the School of Petroleum and Geological Engineering, for discussion which served to focus the authors attention on the practical aspects of corrosion research and for procuring specimen materials.

Dr. Carl E. Locke, Assistant Professor of Chemical Engineering, for participating as a member of the examination committee.

Financial assistance from the School of Chemical Engineering and Materials Science, Dr. C. P. Colver, Director, and the Phillips Petroleum Company Fellowship Program, is appreciated.

Shawn, Russell, Jennifer, Karen and Jonathan Pascoe have contributed significantly to the satisfaction of completing this dissertation.

TABLE OF CONTENTS

	Page
LIST OF TABLES	vi
LIST OF ILLUSTRATIONS	vii
Chapter	
I. INTRODUCTION	1
II. INTERPHASE PROCESSES	4
Orientation in the Total Cell	
Charge-Transfer Reaction	
Passivity and Film Theory	
Critical Pitting Potentials	
III. PITTING THEORIES	19
Mechanical Breakdown Theory	
Deformation Theory	
Displacement Theory	
Catalytic Theory	
IV. EXPERIMENTAL DESIGN	26
Experimental Procedures	
Control Mechanics	
Active Site Potentials	
Induction Time	
V. EXPERIMENTAL RESULTS AND ANALYSIS	46
Polarization Curves	
Potentiostatic-Response Curves	
Attack Mode Photographs	
Induction Time Curves	
VI. DISCUSSION	91
Catalytic and Displacement Theories	
VII. CONCLUSIONS AND RECOMMENDATIONS	96
REFERENCES	99
APPENDICES	106
A. Supplemental Induction Time Curves	
B. Significance of the Transfer Coefficient	

LIST OF TABLES

Table		Page
4.1.	Chemical Composition of Inconel X-750 as Weight Percent .	28
4.2.	Calculated Specific Conductances of HCl/H_2SO_4 Electrolytes at 30°C as a Function of Ionic Strength, I, and Chloride/Sulfate Molar Ratio, r	28
5.1A.	Index of Combinations of I and r for which Anodic Polarization Data are Available	47
5.2A.	Corrosion Potentials of Inconel X-750 at 30°C for Various I and r	53
5.3A.	I-r Equivalents in Ionic Molar Concentrations	54
5.1D.	Index of E, I and r at which Induction Times were Measured	80
5.2D.	Statistical Summary of Correlation Parameters for the Model $\ln t = b_o + b_1 \ln r$	80
5.3D.	Pit Diameters for Various Active Site Current Densities when the Total Current Equals 10 Microamps	86
5.4D.	Induction Times and Active Site Current Densities for Experimental Curves with Propagation Effects Removed . .	88
5.5D.	Statistical Summary of Correlation Parameters for the Model $\log \tau = b_o + b_1 i_a$	88

LIST OF ILLUSTRATIONS

Figure		Page
1.1.	Concepts Applied to the Discussion of Localized Corrosion and where they are Introduced	2
2.1.	Schematic Electrochemical Cell with Separate Anode and Cathode with an Ideal Potential Measuring Device	5
2.2.	Schematic Potential-Distance Curves for Two Different Currents	5
2.3.	Representative E-i Characteristics of the Anodic Interphase	5
2.4.	Metal/Ion Reaction Dynamics	8
2.5.	Redox Reaction Dynamics	8
2.6.	Superposition of Rate Processes to Illustrate One Possible Origin of the Anodic Polarization Curve for a Passivable Metal	11
2.7.	Anodic Polarization Curves Illustrating the Critical Pitting Potential, E_c, and the Protection Potential, E_{pr}	15
3.1.	Experimental Current-Time Curve Illustrating Induction Time Phenomena for 18-8 Austenitic Stainless Steel	25
4.1.	Anodic Polarization Circuit	31
4.2.	Flow Cell Design	31
4.3.	E-i Characteristics Showing: (a) Passivity, (b) Cumulative Processes Associated with Pitting and (c) Schematic Representation of a Completely Active Surface.	33
4.4.	Schematic Potential-Distance Curves for (A) Passive Surface and (B) Active Surface -- Each Potentiostatically Controlled	34
4.5.	Schematic Equipotential Loci under Passive, Active and Pitting Modes with Potentiostatic Control	36
4.6.	Superposition of Anodic and Cathodic Processes on a Common Surface. Active, Unstable and Stable Interaction are Shown	40

Figure		Page
4.7.	I-t Response Characteristics to Selected Disturbances of a Potentiostatically Controlled Anode at I = 0.1	
	a. Equilibrium Current at r = 0, E = +0.7 V	44
	b. On Response After Off Only at r = 0, E = +0.7 V . . .	44
	c. On Response After Off, Rinse, Re-insertion to r = 0 solution at E = +0.7 V	44
	d. On Response After Off, Removal from r = 0 Solution, Rinse, Insertion to r = 1 at E = +0.7 V	44
	e. On Response After Off Only at r = 0, E = +0.4 V . . .	45
	f. On Response After Off Only at r = 0, E = +0.25 V (repeated once)	45
5.1A.	Inconel X-750 Anodic Polarization Curves at 30°C, H_2 Atmosphere, HCl/H_2SO_4, I = 0.1	48
5.2A.	Inconel X-750 Anodic Polarization Curves at 30°C, H_2 Atmosphere, Constant $[H^+]$, I = 2	49
5.3A.	Inconel X-750 Anodic Polarization Curves at 30°C, H_2 Atmosphere, Constant $[H^+]$, I = 5	50
5.4A.	Inconel X-750 Anodic Polarization Curves at 30°C, H_2 Atmosphere, r = 1	51
5.1B.	Potentiostatic-Response Curves for I = 0.1, r = 0 . . .	58
5.2B.	Potentiostatic-Response Curves for I = 0.1, r = 1 . . .	62
5.3B.	Potentiostatic-Response Curves for I = 2, r = 1	68
5.4B.	Potentiostatic-Response Curves for I = 3.2, r = 1 . . .	70
5.1C.	Attack Mode at I = 2, r = 1, E = +1.1 V and at I = 2, r = 0, E = +1.1 V	76
5.2C.	Attack Mode at I = 2, r = 1, E = +0.7 V	77
5.3C.	Attack Mode at I = 2, r = 2, E = +0.7 V and at I = 2, r = 2, E = +0.3 V	77
5.4C.	Cumulative Attack over the Complete Anodic Polarization Curve in N HF	78
5.5C.	Cumulative Attack over the Complete Anodic Polarization Curve in H H_3PO_4	78
5.1D.	Induction Time Curve at I = 0.1, r = 3, E = +0.7 V . .	81
5.2D.	Induction Time Curve at I = 0.1, r = 7, E = +0.4 V . .	81
5.3D.	Calculated i-t Curves for Various Active Site Current Densities	84
5.4D.	Induction Time Curve at I = 0.32, r = 1.5, E = +0.7 V	87
5.5D.	Induction Time Curve for a Flow Cell at I = 0.32, r = 2, E = +0.7 V	89

Figure		Page
5.6D.	Induction Time Curve at I = 0.32, r = 2, E = +0.7 V	90
6.1.	Current-Time Curves for I = 0.1, r = 7 and Various Potentials to Illustrate an Apparent Discontinuity in the Induction Time-Potential Relationship	92
A.1.	Induction Time Curve at I = 0.1, r = 3, E = +0.5 V	107
A.2.	Induction Time Curve at I = 0.1, r = 3, E = +0.6 V	108
A.3.	Induction Time Curve at I = 0.1, r = 7, E = +0.45 V	108
A.4.	Induction Time Curve at I = 0.1, r = 7, E = +0.5 V	109
A.5.	Induction Time Curve at I = 0.1, r = 7, E = +0.6 V	109
A.6.	Induction Time Curve at I = 0.1, r = 7, E = +0.7 V	109
A.7.	Induction Time Curve at I = 0.1, r = ∞, E = +0.2 V	110
A.8.	Induction Time Curve at I = 0.1, r = ∞, E = +0.25 V	111
A.9.	Induction Time Curve at I = 0.1, r = ∞, E = +0.35 V	111
A.10.	Induction Time Curve at I = 0.1, r = ∞, E = +0.4 V	111
A.11.	Induction Time Curve at I = 0.1, r = ∞, E = +0.25 V	112
A.12.	Induction Time Curve at I = 0.32, r = 2, E = +0.5 V	113
A.13.	Induction Time Curve at I = 0.32, r = 2, E = +0.6 V (micropolished)	113
A.14.	Induction Time Curve at I = 0.32, r = 2, E = +0.6 V	114
A.15.	Induction Time Curve at I = 0.32, r = 3, E = +0.4 V	114
A.16.	Induction Time Curve at I = 0.32, r = 3, E = +0.5 V	115
A.17.	Induction Time Curve at I = 0.32, r = 3, E = +0.6 V	115
A.18.	Induction Time Curve at I = 0.32, r = 3, E = +0.7 V	115
A.19.	Induction Time Curve at I = 0.32, r = 7, E = +0.6 V	115
B.1.	Potential Energy-Distance Curves for the Dissolution of a Metal Atom	117
B.2.	Linearized Potential Energy-Distance Curves	117

INDUCTION OF LOCALIZED CORROSION ON A NICKEL ALLOY

CHAPTER I

INTRODUCTION

The study of localized corrosion requires an interdisciplinary approach which includes electrochemical, kinetic, chemical and metallurgical aspects. In actual practice the discipline boundaries fuse together and become all but indistinguishable. Such a frame of reference is quite fluid and, indeed, hardly a frame at all; rather, it is a contextual reference and this is the orientation which the author hopes will be applied by the reader.

For pitting, a particular form of localized corrosion, the context is rather complex as implied in Figure 1.1. If the long-term objective is set as the discovery of the pit initiation mechanism(s), a number of factors appear from the literature and from experimental data which it is hoped will harmonize to increase our understanding of the mechanism or at least point out the next step toward the desired goal.

A definition is in order for the concept of interphase as opposed to interface [3], electric double layer [13, 14] or passive film [29]. Various areas of investigation have introduced the above terms to appropriately describe certain aspects of that region where the metal and electrolyte phases meet. However, it is not strictly correct to think of a passive film without also including an associated film-solution electric double layer [79]. Likewise, the term interface implies a two-dimensional configuration, but the accumulation of mass, e.g., the development of multiple interfaces as in the case of a metal-oxide-solution system, results in a three-dimensional

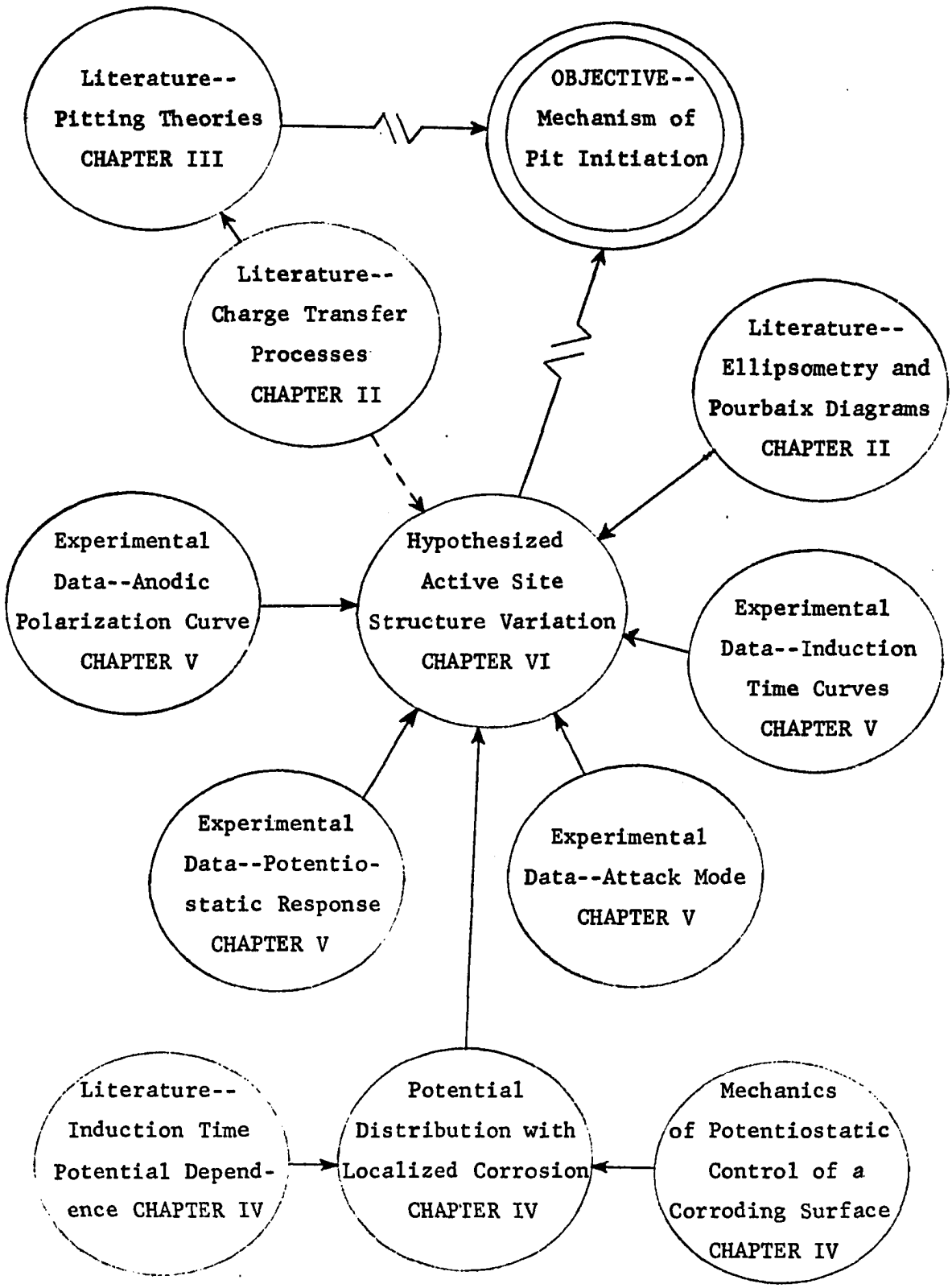

Fig. 1.1.--Concepts Applied to the Discussion of Localized Corrosion and where they are Introduced.

configuration. Much has been said about the semantics, but that argument is left to others. Therefore, the concept of "interphase" is applied to represent the three-dimensional region which cannot be described by the bulk properties of either the metal or solution phases. When describing corrosion processes, such a generalization appears to better convey the state involved since a simple interface model or simple electric double layer model usually cannot be correctly applied. An additional desirable benefit of this approach will be to emphasize the structural aspect of the boundary region and hopefully keep in constant focus the need for spatial orientation. However, caution must be exercised to retain the understanding associated with the more specific concepts.

A factor which greatly influenced the direction this work has taken is the need to obtain kinetic information for the initiation processes associated with localized corrosion, as this should be the shortest route to the mechanism. The "catalytic" theory [30] posed a possible doorway to that kinetic data, and, thus, careful attention to that concept is encouraged.

Great emphasis is directed toward electrolytic contributions to the interphase because a key issue involves the existence and location of potential gradients associated with localized corrosion. This emphasis is, in the authors opinion, a necessary precursor to extended investigation of the effects of metal composition [5, 31, 73], grain structure [34, 80] or surface inclusions [84]. This opinion is based on gradient magnitudes between adjacent anodic and cathodic sites as typically invoked to explain observed localized effects.

The processes which are known to occur in metal-electrolyte interphases are introduced first. Pitting theories are outlined. The physical and philosophical nature of the proposed experimental approach is discussed, and the data are presented. The central issue discussed is a current-time fluctuation in the absence of a large potential fluctuation. An active site reaction-product-structure is postulated to explain the fluctuations and evidences are presented to support the concept.

CHAPTER II

INTERPHASE PROCESSES

Orientation in the Total Cell

A metal immersed in an electrolyte constitutes a heterogeneous electrochemical system. The feature of interest which characterizes the system as electrochemical is charge-transport between phases. There is always an equivalence of electronation and de-electronation processes in a closed system. Both directions of the charge-transfer process occur at an interface, but the planar distribution of transfer sites ranges conceptually from infintesimal to finite discrete sites intermingled on a common surface to pure separated surfaces.

For convenience of discussion consider separated electronation sites or cathodes and de-electronation sites or anodes in an electrolyte as shown in Figure 2.1. If it were possible to measure the potential at all points between a and b for several different current levels, curves of the form schematically illustrated in Figure 2.2 would be obtained, if the interphase processes were all at steady state. If precautions were taken to maintain constant temperature and electrolyte homogeneity, adherence to Ohm's law would be observed for both electronic conduction in the metal electrode bulk, a-a' and b-b', and for ionic conduction in the electrolyte, a"-b" [36]. However, in the interphases, a'-a" and b"-b', the potential versus current (E-i) characteristics may take a variety of commonly recognized forms, some of which are shown in Figure 2.3. Clearly, these cannot be represented by a single, simple equation such as Ohm's law. The reason for diversity of E-i characteristics in the interphase is the variety in kinds and combinations of processes which can occur and, also, because of extreme potential gradients encountered (10^5 - 10^7 V/cm). Some of the possible processes will be briefly discussed in this chapter.

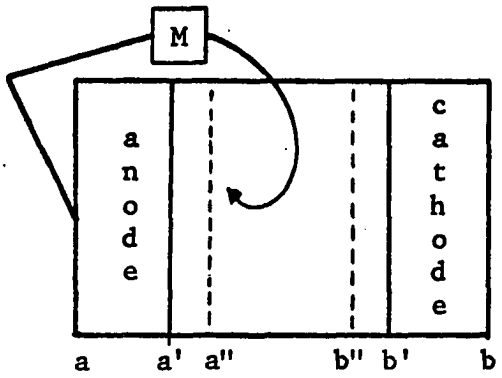

Fig. 2.1.--Schematic Electrochemical Cell with Separate Anode and Cathode with an Ideal Potential Measuring Device.

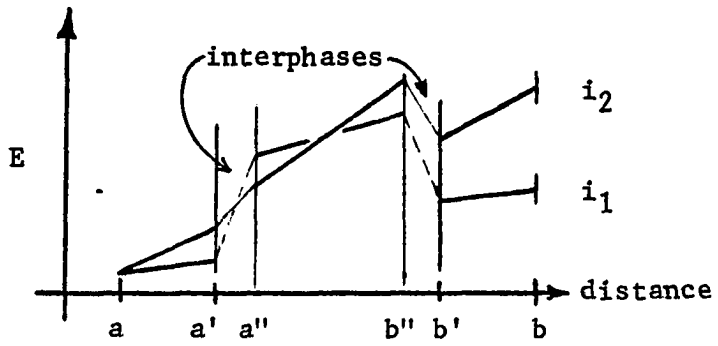

Fig. 2.2.--Schematic Potential-Distance Curves for Two Different Currents.

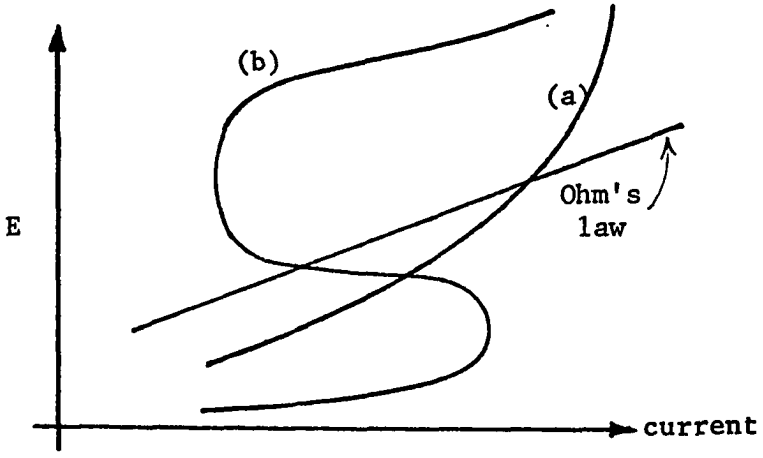

Fig. 2.3.--Representative E-i Characteristics of the Anodic Interphase (Potentiostatic Control Implied).

Charge-Transfer Reaction

Since electronic and electrolytic conduction are sustained by different mechanisms, the interphase must necessarily be the site at which charge carrying chemical species are generated or consumed according to whether the site is an anode or cathode, respectively. The electrochemical equivalents originate in either of two ways [78]:

1) Electron transfer in the interphase occurs when an electron crosses the interface to be accepted or donated by a solution-side species. This is commonly designated as a "redox" reaction.
2) Electrons do not actually cross the interface but remain as an electron residue as cations are ejected (or pulled) from the metal surface during dissolution (or the reverse during deposition). This process is designated the "metal/ion" reaction.

In corrosion studies the metal/ion reaction will always be of concern and it may or may not be associated with parallel or opposing redox reactions. The term "charge-transfer reaction" will be applied to describe both the redox and metal/ion reactions. An examination of the driving force for charge-transfer from an experimental viewpoint suggests three options: (1) an external electron pump which increases the potential difference to accelerate both the anodic and cathodic reactions and (2) an internal electron pump wherein the chemical potential of either the cathodic or anodic reaction increases to accelerate the other. On the basis of work reported elsewhere [18, 72, 83], it is asserted that options 1 and 2 are likely to be equivalent as long as the driving reaction of the internal pump is faster than the reaction being observed, and, second, that the additional species associated with the driving reaction do not influence the observed reaction. The second requirement is a catchall and is difficult to evaluate because of subtleties associated with adsorption, film formation, spatial distribution of anodic and cathodic sites and charge separation at the interphase. (3) The possibility exists, though application has not yet been reported, of superimposing the internal and external electron pumps. Driving one pump

against the other appears to hold promise as a means to experimentally evaluate the equivalence of the options.

Reaction Dynamics. Metal/ion and redox reactions can be viewed as dynamic systems as illustrated in Figures 2.4 and 2.5, respectively. The net reaction rate is the superposition of forward and reverse reaction rates, and the equilibrium state is characterized by forward and reverse reactions of equal rates and opposite direction. The rate magnitude at equilibrium is called the exchange current density, i_o. The potential at equilibrium, E_o, is used as a reference and departures from the equilibrium potential are usually designated as overvoltage, η, for an individual process or polarization for mixed processes, $\eta = E - E_o$.

The arrows in the figures represent direction and magnitude of charge-transport partial processes. The zero external current associated with i_o is accompanied by zero departure from E_o across the interphase. Net positive currents are associated with positive potential departures and negative currents with negative departures.

The special case, where the bulk solution contains none of the electrode metal as ions, renders the concepts of exchange current density and equilibrium potential meaningless; however, this condition is of short duration in the interphase.

Charge-transfer is well characterized [3, 46, 78] for the metal/ion reaction and has been shown to be the sum of the forward and reverse components. When charge-transfer reactions are the slow or rate controlling processes the rate is expressed by the equation:

$$i = i_o\{\exp(-\alpha nf\eta) - \exp[(1-\alpha)nf\eta]\} \qquad \text{Eq. 2.1}$$

where η is the overvoltage, n is the ion charge, $f = F/RT$, F is the Faraday, R is the gas constant and T is the temperature. The significance of the transfer coefficient, α, is shown in Appendix B for the readers convenience. The derivation of Equation 2.1 and the companion Tafel equation is well known [1, 13, 46]. The same equation applies for the redox reaction in which case the charged species is the electron and $n = 1$.

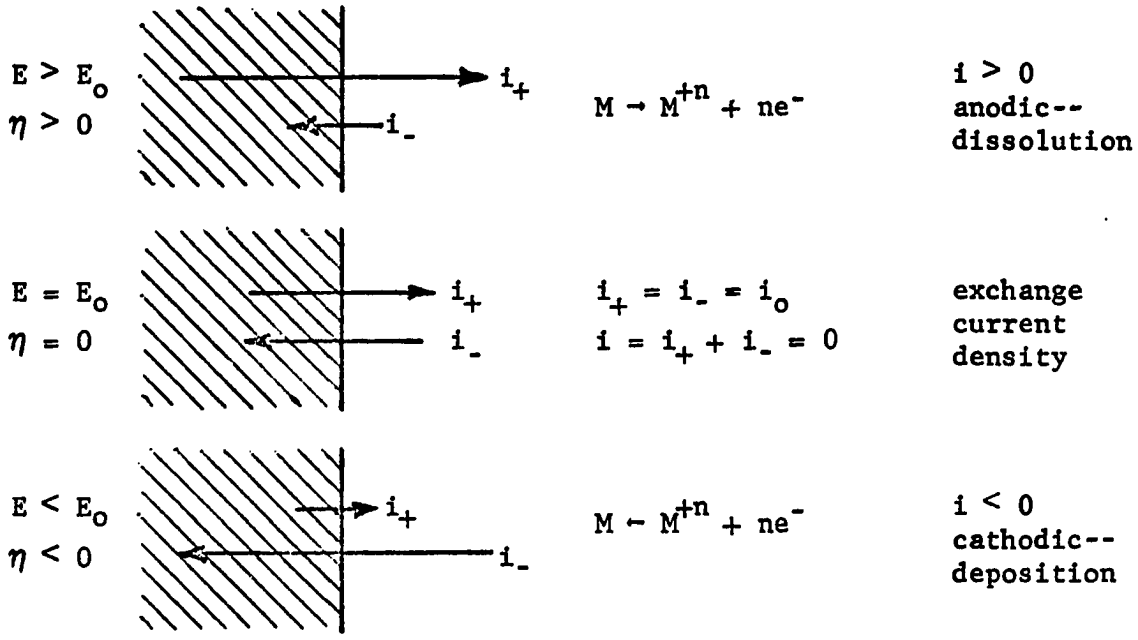

Fig. 2.4.--Metal/Ion Reaction Dynamics [78].

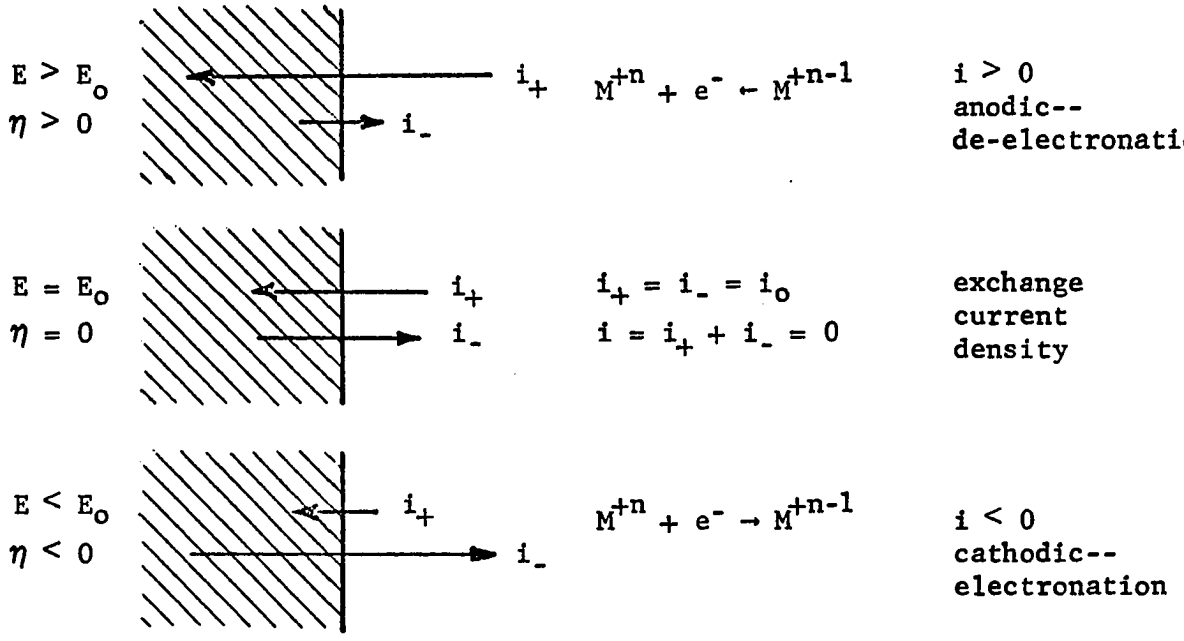

Fig. 2.5.--Redox Reaction Dynamics [78].

The special case of separated anode and cathode is, in terms of reaction dynamics, an approximation where, for example, at the anode the dissolution rate is much, much larger than the deposition rate.

Rate determining steps. The charge-transfer reaction always occurs, but the rate expressed by Equation 2.1 may be masked because of interference from some other process. Three additional types of controlling reaction have been recognized [78].

1) Diffusion Control: Reactant transport to the reaction site may be slower than charge-transfer, resulting in diffusion control and a potential-current relationship based either on Fick's law for laminar or non-flow or on empirical turbulent flow equations.
2) Reaction Control: If a reactant is produced by a chemical reaction which precedes the charge-transfer reaction and if the rate of production of this reactant is slower than it would be consumed under charge-transfer control, then the E-i relationship is dependent on the chemical reaction rate even though the latter is independent of the potential. From equation 2.1, charge-transfer will only be undisturbed if $i \ll i_o$; therefore, at the appreciable current densities associated with localized corrosion, pure reaction control at the active site is quite unlikely.
3) Crystallization Control: The metal/ion reaction involves the dissolution/deposition step which introduces the possibility of a slow orientation of newly formed "ad-atoms" into or out of the crystal structure. In this case the E-i relationship will follow the ad-atom orientation process rather than charge-transfer.

An extended compilation of various modifications and combinations of these four rate controlling steps has been prepared by Vetter [78]. Although the discussion of rate control processes presented here is grossly oversimplified, it serves to orient the reader and implies the care which must be exercised in defining the experimental system and interpreting the resulting data. Indeed, it is well recognized that

interpretive capability appreciably lags experimental capability [1, 3, 86]. The successful analysis of interphase processes which lead to localized corrosion will utilize these fundamental rate concepts to identify the mechanisms, and it will explicate the means by which processes stably coexist on a common surface.

Passivity and Film Theory

Origin of the anodic polarization curve. Hoar [29] described the primary act of passivation as the formation of a tightly held monolayer containing oxide or hydroxide anions and metal cations to form a compact barrier between the metal and the solution. As the potential becomes more noble, the current increases along ACB in Figure 2.6 according to some particular rate process as suggested above. At point C the formation of metal oxide begins to compete for rate control as thermodynamic and kinetic factors become favorable. At potential E_d the dissolution of metal

$$M \rightarrow M^{+2}_{aq} + 2e^- \qquad \text{Reaction 2.1}$$

begins to increase in rate until E_p is reached where oxides begin to form directly as a competing reaction

$$M + H_2O \longrightarrow MO_{solid} + 2H^+ + 2e^-. \qquad \text{Reaction 2.2}$$

To account for the competitiveness of Reaction 2.1 with Reaction 2.2, it was suggested that, as the potential becomes more noble than the potential of zero charge, the water dipoles become increasingly oriented with the oxygen or negative dipole adjacent to the metal. The dissociation of protons from oriented water molecules then provides a kinetically favorable source of adsorbed $O^=$ or OH^-, and the newly formed lattice cations move into position between these anions to maintain electrostatic stability.

As the potential proceeds from E_p to E_f, Reaction 2.2 takes over the rate control to produce the tight monolayer. With this barrier formed, the current density between points D and E in Figure 2.6 must be limited by one or more of the three consecutive steps involved

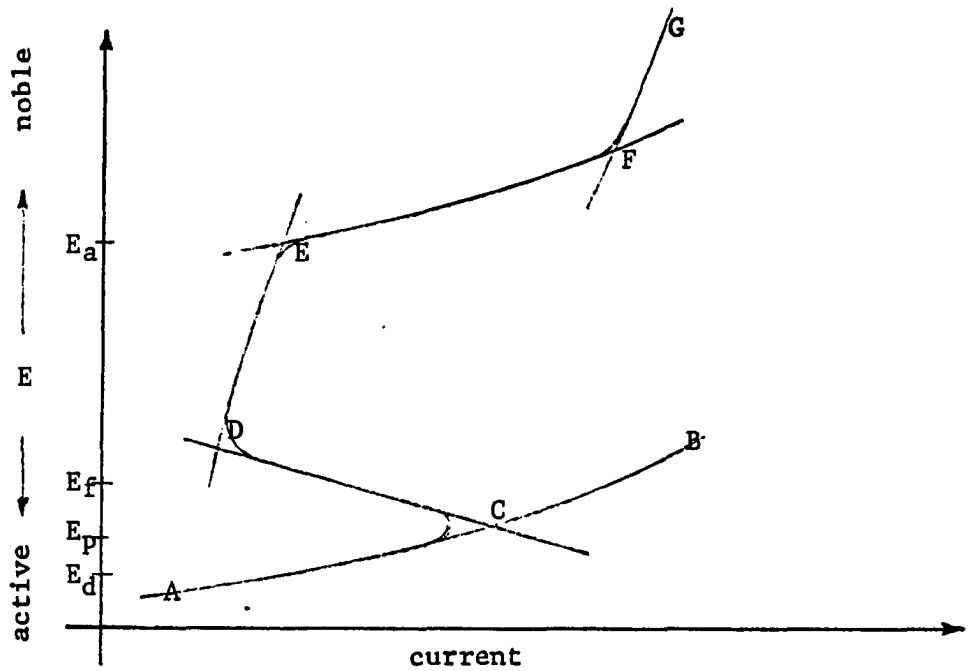

Fig. 2.6.--Superposition of Rate Processes to Illustrate One Possible Origin of the Anodic Polarization Curve for a Passivable Metal (Potentiostatic Control Implied).

A-B: active dissolution via a potential dependent rate determining step.

C-D: dipole reorientation to form the "oxide film".

D-E: passive surface via film protection--a potential independent process.

E-F: film breakdown at E_a to resume active, potential dependent dissolution or oxygen evolution.

F-G: diffusion limited rate determining step.

in getting a newly formed lattice cation into the film, through the film or from the film into solution.

The current increase along EF can be associated with a number of possible reactions:

1) If the film is conductive, a redox reaction such as oxygen evolution may commence at the film-solution portion of the interphase at suitable potentials.
2) If the film is conductive or non-conductive, the increased potential may cause the film to "break apart" to permit the metal/ion reaction to occur with various modes of rate control.
3) As will be discussed further in Chapter III, localized corrosion may occur with pitting, crevice corrosion, grain etching and/or intergranular attack.

Passive film structures. Changes in potential lead to oxide film structure changes with corresponding changes in solubility and conductivity. For example, Frankenthal [19] noted evidence that the film assumed two distinct stages which he designated the primary passivation film and the secondary film. The former is characterized by the absence of hysteresis in the E-i relationship. In this scheme the potential at which the transpassive region commences corresponds to the primary activation potential. In the presence of the secondary film, the activation potential shifts to give an apparent or experimental value.

Vetter [76] discussed film thickening kinetics beyond the initial monolayer and concluded that, in the absence of aggressive anions, the local composition of the oxide depends entirely on the local electric potential and is independent of all other parameters. Conversely, a change in the potential distribution of the oxide film is only possible if the stoichiometry parameter, n, for the oxide MeO_n, also changes throughout the layer. Essential conditions are the constancy of electrochemical potential of the electrons throughout the oxide layer and semiconductor properties of the film. Bianchi, et al., [2] have also emphasized the importance of semiconductive properties of the oxide film.

Bockris, Reddy and Rao [4, 54, 55] used simultaneous galvanostatic polarization and recording ellipsometric techniques to demonstrate at least three different structures in the films formed during the passivation of nickel. A constant current was applied commencing at time, t_o, and the potential and film thickness were monitored with respect to time.

1) $t_o < t < t_1$. The surface remained film free and the potential jumped quickly from -0.39 to +0.01 V SCE. The implication is the formation of a soluble product since no solid accumulation is observed.
2) $t_1 < t < t_2$. The film grew at a linear rate and the potential shifted slightly from +0.01 to +0.06 V SCE. Constancy of potential under galvanostatic conditions indicates a non-passivating film. It was suggested that the soluble products from the preceeding period established the concentrations or surface activity necessary for film formation.
3) $t_2 < t < t_3$. The film thickness remained constant and the potential shift was approximately linear from +0.06 to +1.56 V SCE. The pre-passive film stopped growing and, via some structural transformation, became passive as evidenced by the large noble potential shift.

The refractive index of the film was also monitored and was observed to be continually changing from $t_1 < t < t_3$ which suggests a continuous structure transformation as a function of potential, at least under galvanostatic conditions.

Siejka and Cherki [62] used nuclear microanalysis and an electrolyte prepared from O^{18} enriched water to monitor the role of oxygen fixation in the passive film on nickel. They observed two distinct kinetic regions which they characterized in terms of film thickness. The initial layer was mainly responsible for passivity while film thickening was possibly a manifestation of dynamic equilibrium between the rates of formation and dissolution.

Ebersbach, et al., [15] used potentiostatic control on rotating nickel electrodes to demonstrate that passivation current is independent of angular velocity, i.e., it is not diffusion controlled. Furthermore,

with E held constant, the current decreased exponentially with time in the passive region and the slope of log i/t increased exponentially with potential. These data, along with solubilities of the nickel salts, were used to hypothesize simultaneous active dissolution and passivation processes.

The basis for Pourbaix's work [53] on thermodynamic stability is the recognition that at various potentials certain species are more likely to occur. Although that work has not yet been generally extended to include multicomponent systems, i.e., alloys or multi-anion electrolytes, it appears appropriate to anticipate specific potential regions for which particular reaction products and product structures will predominate.

Critical Pitting Potentials

The reactions associated with the current increase of the transpassive region, AB, as shown in Figure 2.7, may sustain non-localized dissolution. However, the addition of certain specifically active anions, e.g., Cl^-, Br^-, and I^-, has been shown under certain conditions [6, 40, 41, 48, 52, 57, 64, 70] to reduce the potential at which the passive-transpassive shift occurs to some critical potential, E_c, so that the curve follows along CD. In the latter case, corrosion will be highly localized resulting in the formation of pits. Reversal of the potential scan direction at D produces hysteresis effects as shown by DE and passivity is regained at the protection potential E_{pr} [52, 73]. In summary, pitting does not start until $E \geq E_c$ and pits formed do not cease corroding until $E \leq E_{pr}$. In the range $E_{pr} \leq E \leq E_c$, it has been demonstrated that old pits can continue to corrode but no new pits can initiate.

It is desirable to understand the physical meaning of E_c and E_{pr} in terms of interphase processes. Since this has not yet been accomplished in detail, some suggestions from the literature may be useful.

Regarding the protection potential, E_{pr}, Pourbaix [52] recommended this parameter to quantify resistance to pitting corrosion, since

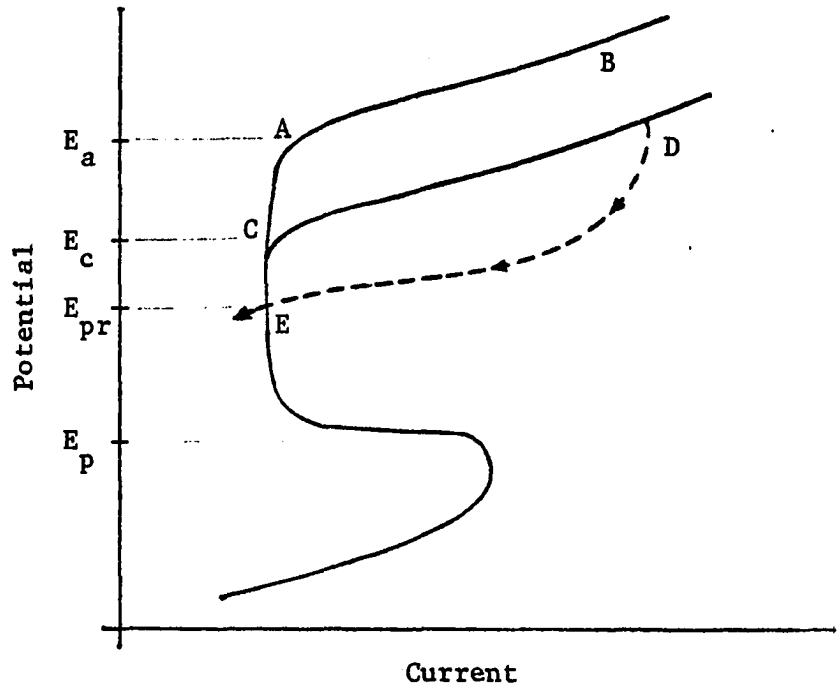

Fig. 2.7.--Anodic Polarization Curve Illustrating the Critical Pitting Potential, E_c, and the Protection Potential, E_{pr}.

it is the potential below which no pitting can occur. The difficulty is that E_{pr} is elusive, apparently because of dependence on experimental technique, surface conditions and specimen history. Wilde and Williams [81, 82] supposed that, after E exceeds E_c and pits initiate, they propagate either as a result of an increase in H^+ activity from hydrolysis of corrosion products or of an increase in Cl^- activity via migration or both of these. When the potential sweep is reversed the propagation process, being potential dependent, decreases in rate until it reaches zero at E_{pr}. If this mechanism is correct, E_{pr} would not be a unique quantity for a given system but should vary as the amount of propagation that has occurred, i.e., a function of increases in H^+ and Cl^- activities in the pit. The value of E_{pr} was observed to be linearly related to the number of coulombs passed in going around the hysteresis loop CDE from E_c to E_{pr}. By conjecture, as H^+ and Cl^- activities are made very large in the bulk solution, E_{pr} should approach E_c because the differences between the in-pit and in-bulk condition approach zero. Also, one might presume that a pit washed with the bulk solution would repassivate when $E_{pr} \leq E \leq E_c$. Both of these situations are reported in the literature [57] and lend support to the non-fundamental nature of E_{pr}, notwithstanding possible usefulness as an evaluation parameter.

The situation regarding the critical pitting potential, E_c, is in slightly better status in that Vermilyea [75] has achieved limited success in rough estimates of E_c from thermodynamic parameters for pure metals and simple electrolytes. For example, consider the reaction

$$M + (n/2)\ H_2O \rightarrow MO_{(n/2)} + n\ H^+ + n\ e^- \qquad \text{Reaction 2.3}$$

which produces an oxide to account for film formation, and

$$M + n\ X^- \rightarrow MX + n\ e^- \qquad \text{Reaction 2.4}$$

which is a dissolution reaction where the product is a salt. Both reactions are potential dependent. The origin of E_c is explained in terms of these reactions by supposing that, if Reaction 2.4 were at equilibrium and were the only reaction occurring, then the potential across the interface is the metal/ion equilibrium potential, E_{eq}.

E_{eq} is calculated from the Nernst equation, using the concentration of the metal ion at the surface rather than bulk properties. If it is then supposed that the reaction is going to the right at some potential, E_r, i.e., at a displacement from equilibrium, then a finite overvoltage, η, is required. Now, if the potential difference from the outer Helmholtz plane to the solution bulk is δE, then

$$E_r - E_{eq} = \eta + \delta E.$$

An anion concentration gradient is established which corresponds to δE at zero flux, or, expressed alternatively, the state is finally reached where the electrochemical potential inside the pit equals the electrochemical potential outside the pit,

$$\mu_p + nFE_p = \mu_b + nFE_b$$

$$\mu_p = \mu_b + nF\,\delta E$$

where the subscripts p and b represent in-pit and bulk characteristics, respectively. Therefore, the chemical potentials of anions are not identical inside and outside the pit. An increasing anion chemical potential inside the pit favors salt formation, while oxide formation is impeded because of the decreased chemical potential of the water. The potential at which the anion chemical potential is sufficiently great to give Reaction 2.4 precedence over Reaction 2.3 is the critical potential above which film ruptures are thermodynamically unable to repassivate. This theory is inadequate for present purposes principally because it does not account for the selectivity of anions, i.e., why some are aggressive and others are not. It does, however, reflect an analytical estimation of the parameter and, therefore, represents a significant step.

Kolotyrkin [38, 39] suggested that the equilibrium

$$MO\begin{matrix}\nearrow H^+ \\ \searrow H^+\end{matrix} + x\ Cl^- \rightleftharpoons M(Cl_x)^{-x} + m\ H_2O \qquad \text{Reaction 2.5}$$

is dependent on Cl^- activity and metal potential. If the Cl^- activity is fixed and the potential dependence is observed, then (1) at $E > E_c$ the reaction shifts right, i.e., the metal dissolves, (2) at E_c the

reaction is at equilibrium and (3) at $E < E_c$ the reaction shifts left and the metal passivates. This concept accounts for the anion selectivity on the basis of ability to form the complex intermediate.

E_c manifests some interesting metal phase dependencies which have been reported in the literature for specific materials. Leckie and Uhlig [41] used 18-8 stainless steel to demonstrate that

1) E_c decreased with increased Cl^- activity,
2) the inclusion of ClO^-, $SO_4^=$, NO_3^- and OH^- caused E_c to increase,
3) E_c was approximately constant from pH 0 to 8, and
4) a temperature decrease caused E_c to increase.

Smialowska and Czachor [66] observed that for a 16 percent Cr, Fe alloy, a sulfate-chloride activity ratio greater than 3.5 prevented stabilization of the anode potential under potentiostatic control, and that E_c for single crystals of 16 Cr/Fe is more positive than for the polycrystalline form.

Although no particular effort is made here to correlate metal compositions with pitting characteristics, one can get a feel for the nature of E_c and the significance of metal composition by noting:

1) Horvath and Uhlig [31] observed the addition of Mo to 15% Cr, 13% Ni stainless steel caused E_c to increase between 25°C and 40°C and decrease at 0°C. The reverse was true for 18-8 stainless steel, where E_c decreased at 25°C and increased at 0°C as the concentration of Mo increased.
2) Bohni and Uhlig [5] demonstrated that for 18% Cr, 10% Ni stainless steel, Re caused E_c to decrease at 0°C and increase at 25°C for both 0.1N NaCl and 0.1N NaBr, but for NaCl, $E_{c,0^oC} > E_{c,25^oC}$ and for NaBr, $E_{c,0^oC} < E_{c,25^oC}$.

It is important to recognize that the distinctive characteristics of E_c and E_{pr} have only recently begun to emerge with clarity. In the older literature it is very difficult to distinguish which concept is being reported; therefore, questions do exist as to the significance of some previous work.

CHAPTER III

PITTING THEORIES

Pitting theories must answer two basic questions: (1) how does the pit start and (2) how does the active site coexist with the passive surface. The initiation mechanism(s) is very likely different from the propagation mechanism(s) since the production of metal ions materially modifies the composition at the reaction site [7, 57]. However, a workable, harmonious transition from initiation to propagation must also be a component to the complete localized corrosion theory.

The second question raises the issue of stability and will be discussed in Chapter IV. Regarding the question of how a pit starts, numerous suggestions have been offered which can be roughly categorized according to whether or not they require pre-existent mechanical irregularities in the passive film. The interpretation of strictly mechanical factors suffers from an inability to explain anion selectivity since ion size or ion mobility do not correlate directly [65]. Therefore, it appears prudent to pursue a non-mechanical route based on electrochemical and chemical parameters and then append possible mechanical debilitation of the film as required.

"Mechanical breakdown," "deformation," "displacement," and "catalytic" theories have been postulated to answer basic questions about pitting propagation and initiation. They constitute a conceptual, rather than comprehensive, cross-section of presently regarded pitting theories which will be summarized in this chapter.

Experimental observations itemized by Kolotyrkin [38] are first noted here for orientation and review of those factors which must fit consistently into the pitting theory.

1) An essential condition is the presence of specifically acting anions.

2) Aggressive anion activity is dependent on the existence of some critical concentration.
3) Two critical potentials exist, i.e., critical pitting potential, E_c, and protection potential, E_{pr} (see Chapter II).
4) Active anions have little effect on the dissolution rate of actively corroding surfaces at $E > E_c$.
5) Active anions have little effect on anodic processes at $E_f < E < E_c$.
6) An essential condition is the higher affinity of the metal for oxygen than the corresponding active anion.
7) The anodic current density is approximately 10^5 times the cathodic current density.
8) An increasing dissolution rate is associated with an increasing number of pits (i.e., area increases) rather than a rate increase in existing pits.
9) For sufficiently large cathodes, an increase in the dissolution rate changes the anode potential, but the cathode potential is unchanged (applicable only for the case of chemically induced pitting).

Mechanical Breakdown Theory [29]

The underlying concept of this theory involves, first, anion adsorption on and water displacement from the metal-oxide surface. This materially reduces the interfacial tension until "peptization" by interfacial charge occurs. The adsorbed anions repel one another, and the oxide film to which the anions are strongly attached is stressed until it breaks apart. Specific details of this theory are itemized along with the observation that the qualitative conditions which lead to pitting are those that also lead to increased anion adsorption.

1) Anions are adsorbed at the film/solution interface according to the following rules: (a) Anions replace adsorbed water molecules, (b) anion adsorption increases as anion concentration increases and as the potential becomes more positive (noble) and (c) anion adsorption increases according to

specific adsorbability properties of the anion.

2) Interfacial tension or interfacial free energy decreases at the oxide/solution interface via the accumulation of mutually repulsive forces between the anions.
3) At some point the interfacial tension is lowered so far, i.e., the accumulation of mutually repulsive charges is so large, that they are pushed apart along with the oxide to which they are attached.
4) Anions move into the crack in the film and force penetration to the metal/oxide interface.
5) Rates are controlled by the factors controlling anion adsorption.

Deformation Theory [58]

As one reviews all of the possible sources of film stress which could conceivably contribute to film rupture, five have been recognized.

1) Interfacial tension of the film (basis of the mechanical breakdown theory).
2) Electrostiction pressure via high electric fields in the film (10^6 - 10^7 V/cm).
3) Internal stress from differences in mobilities of anions and cations in the film with greater anion mobility generating compressive stresses.
4) Internal stresses from partial hydration of the film.
5) Local stresses from impurities and metal surface characteristics.

Deformation theory is an extension of the mechanical breakdown theory made by the inclusion of the electrostriction pressure as a source of stress. The assumption is that these two sources of film stress are the major contributors.

Thermodynamic relationships were derived to show that, at constant film thickness, the film pressure approaches the critical film stress as the electric field strength increases and as the interfacial tension decreases. The critical pitting potential is then interpreted

as the potential above which film pressure exceeds the critical compressive stress of film breakdown. The value of the critical pitting potential is, therefore, dependent on the physical properties of the system, insofar as they dictate the allowable stresses. If the anodic film is rigid anhydrous oxide, brittle cracking occurs and pitting corrosion is promoted. Plastic deformation or flow results from a visco-plastic hydrous oxide film and promotes the generalized corrosion characteristics of the transpassive region.

Displacement Theory [38, 39]

The basis for this theory is the reversible displacement of the passivating oxygen from the metal surface by the aggressive anion as expressed in Reaction 2.5. Specific points to be considered are:

1) Oxygen is bonded to the metal to form the passive layer.
2) Aggressive anions compete reversibly with the oxygen for a place at the metal surface.
3) At the critical pitting potential, E_c, the anions become competitive, rate wise, with oxygen and are capable of displacing oxygen via the formation of metal-anion compounds.
4) A potential increase shifts the overall rate in favor of oxygen displacement by the aggressive anion.
5) A critical concentration, C_c, of aggressive anion is established in the interphase such that $C_c \gg C_b$, where C_b is the bulk concentration.
6) Corrosion localization presumably occurs by the formation of a non-uniformly conducting oxide film which produces concentration pockets at the surface via anion migration. As evidence offered to support this hypothesis, observe that: (a) attempts to purposely corrode a surface uniformly have always produced irregularities, (b) increasing sulfate concentration reduces pit corrosion which implies a migration effect, (c) chloride effects are observed only after an induction time, τ. Induction time is operationally defined as the time between the imposition of a particular set of

aggressive conditions and the commencement of associated aggressive action as measured by an external current increase. The magnitude of τ decreases as chloride concentration increases, which suggests an accumulation period is required to establish a critical concentration and (d) under galvanostatic control, τ increases as current decreases which emphasizes the migration concept.

7) Localized currents rapidly increase by autopropagation in that higher point concentrations induce greater point currents with more rapid migration and, hence, higher point concentrations.
8) Localization is enhanced by the same kinds of macro-nonuniformity that contribute to local cell action. Uneven aeration and temperature fields are contributing factors in the localization.
9) Aggressive anions participate in the localization process by facilitating the elementary act of metal atom ionization. Plausible steps are: (a) chemisorption of the aggressive anion, (b) formation of a surface complex and (c) solvation at some certain potential which must also manifest a concentration dependency. Potential dependence arises from the "polarizability" of anions. Each anion manifests a different polarizability and, therefore, has a different potential dependence.
10) Dissolution processes are inhibited by solution components which exhibit a greater affinity for the metal and forms more stable complexes than the aggressive metal-anion complex by reducing the rate of the solvation step.

Catalytic Theory [30]

The catalytic theory represents a direct experimental method to obtain kinetic information on the collective film breakdown processes. Consider an experimentally established steady-state passive film in the absence of an aggressive anion at a potential, E, such that, if

the aggressive anion were present, pitting would occur, i.e., the potential is more noble than the critical pitting potential. Then, at time zero, introduce the aggressive anion and monitor the time required for pitting to initiate as measured by increased current density.

The results of the experiment suggested above for 18-8 austenitic stainless steel were:

1) the appearance of an induction time of from a few seconds to several hours during which the current remained constant (the induction time was a function of temperature, the noble potential departure from the critical pitting potential, and the chloride concentration),
2) a rapidly increasing current density at the end of the induction time as shown in Figure 3.1, with the onset of visable pitting,
3) an apparent energy of activation of 60 kcal/mole, reflecting the existence of a high energy transition state, involving 2.5 to 4.5 chloride ions. The number of chloride ions participating in the aggressive event is interpreted as the reaction order and was estimated by representing the rate of the breakdown process by $1/\tau$ and calculating the slope of the $\log \tau / \log [Cl^-]$ plot.

The offered explanation for these observations constitutes the catalytic theory of pitting and involves the following steps:

1) Three to four chloride ions adsorb on the oxide film surface around a lattice cation, with preference for a cation adjacent to an anion vacancy. This generates the transition state complex.
2) The metal-chloride complex ejects rapidly and solvates.
3) Ejection "thins" the film which causes the electric field at the site to increase.
4) The intensified electric field, at constant average potential, acts to quickly bring up a new cation.
5) The up-coming cation finds 3 to 4 chloride ions waiting rather than the stable oxide as during the initial event, thus, subsequent events do not require oxide displacement.

6) The cumulative repetition of the above steps at the initial site, along with the activation of adjacent sites, intensifies the electrostatic field and the reaction is accelerated explosively.

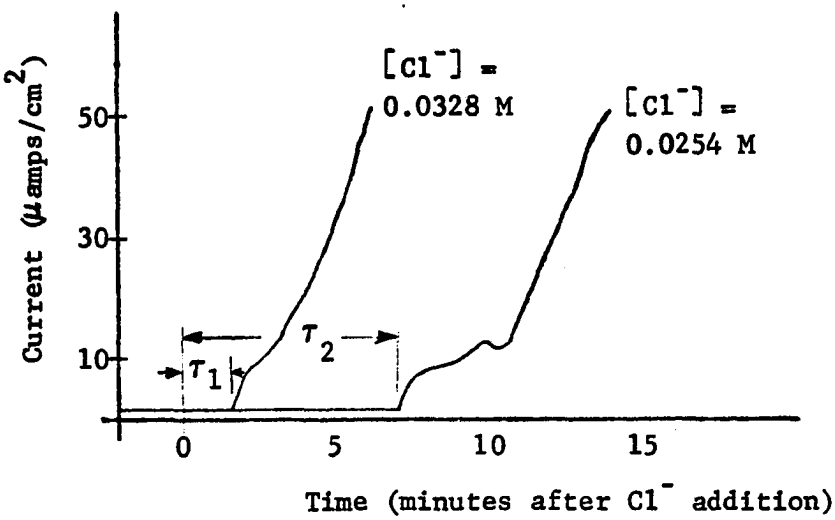

Fig. 3.1.--Experimental Current-Time Curve Illustrating Induction Time Phenomena for 18-8 Austenitic Stainless Steel [30].

CHAPTER IV

EXPERIMENTAL DESIGN

One purpose of the present study is to clarify the experimental significance of induction times and extend the application of the induction time concept to an alloy which will broaden the base for generalizing and testing pitting theories. In terms of the latter point, the particular system of Inconel X-750 in acidic sulfate and chloride solutions at ambient temperatures is examined. This particular selection is advantageous because sulfate and chloride are very broadly encountered in practice. Also, Inconel X-750 is obtainable as a single phase alloy and has moderate resistance to pitting corrosion. Some work has been reported for nickel alloys [31, 50, 63, 74, 85] which serves as a convenient reference for the starting point of this work.

The basic tool used is the potentiostat, and application is directed primarily toward the analysis of transient behavior. Potentiostatic current measurements are straight forward, but they represent the composite of several processes occurring in the interphase as evidenced by non-uniformity of attack, both spatially and time-wise. and by the E-i characteristics as shown in Figure 2.6. The basis by which it is proposed to separate the localized corrosion process rates from the composite is to bundle together those processes which produce pitting and examine them collectively by removing the effects of those processes which occur in the absence of pitting. The operational starting point is the assumption that induction times, which measure the response to an aggressive component, will contain only the information pertaining to the bundled pitting processes.

In this chapter details of the experimental procedures used are outlined, and the mechanics of potentiostatic measurements on locally

corroding surfaces are discussed. Finally, experimental aspects of measuring induction times are presented.

Experimental Procedures

Specimen preparation. Specimens were prepared by heating a one-half inch diameter rod of Inconel X-750 at 2200°F for one hour in an air furnace, followed by water quenching as described by the manufacturer [32]. The rod was then machined to 1.13 centimeters in diameter and cut to 1.4 centimeter lengths. The machined surface was wet-ground with 600 grit silicon-carbide paper to remove the slight ridges left by the machining operation. One side was drilled near the end and a brass pin was pressed into the hole to provide eventual electrical contact. The specimen was washed in boiling benzene and mounted in bakelite to expose only the flat, circular end of the cylinder. The brass pin was drilled and tapped for accomodation on a Stern-Makrides type holder. The exposed electrode surface area for all specimens was 1.00 ± 0.01 square centimeters.

This particular mounting technique avoided gaseous bubble collection and associated crevice corrosion [47] encountered with teflon compression gasket techniques [16]. No evidence of preferential corrosion at the specimen-bakelite juncture was observed at any time. The use of bakelite mounting has been comparatively evaluated [22] and for present objectives the advantages merited its use since it also allowed simplified surface refinishing for repeated use. In this manner variations associated with inherent differences expected among numerous specimens was minimized.

The heat treatment used (solution treated) produces a specimen which is nearly free of precipitates in the grain boundaries [32, 74] and, therefore, is essentially a single phase alloy. The chemical composition of Inconel X-750 is given in Table 4.1.

Solution preparation. Electrolytic solutions were prepared from distilled water and reagent grade chemicals. Stock solutions were prepared at an ionic strength of ten for various molar chloride/sulfate ratios. Dilutions were made to the desired ionic strengths for specific

Table 4.1.--Chemical Composition of Inconel X-750 as Weight Percent (c).

Nickel (a)	74.02
Chromium	14.82
Iron	6.33
Titanium	2.60
Aluminum	0.88
Columbium (b)	0.87
Silicon	0.27
Manganese	0.12
Copper	0.03
Carbon	0.03
Sulfur	0.007

(a) includes a small amount of Cobalt

(b) includes tantalum

(c) International Nickel Company, Huntington Alloy Products Division, Heat No. HT0056X.

Table 4.2.--Calculated Specific Conductances of HCl/H_2SO_4 Electrolytes at 30°C as a Function of Ionic Strength, I, and Chloride/Sulfate Molar Ratio, r.

I	Specific Conductance (mhos/cm)			
	r = 0	r = 1	r = 7	r = ∞
0.1	0.00978	0.0169	0.0308	0.0407
0.32	0.0276	0.0499	0.0956	0.1280
1.0	0.0756	0.1450	0.2900	0.3950
2.0	0.1400	0.2760	0.5680	0.7830

determinations. This method ensured the reproducibility of anion ratios and facilitated reagent preparations. An exception was required for the preparation of electrolytes at constant hydrogen ion concentration, consequently, those solutions were individually prepared.

The specific conductance, k, of solutions used is estimable from data in standard reference handbooks [26, 27]. Table 4.2 lists calculated specific conductances for various ionic strengths, I, and molar chloride/sulfate ratios, r.

It is clear that the bulk concentrations are not those which will be encountered in the interphase [7, 21]. However, it is anticipated that there will exist some functional relationship between the bulk concentrations and interphase concentrations as evidenced by current-concentration dependencies for certain segments of the anodic polarization curves to be introduced in Chapter V.

Ionic strength [8, 27, 37] and anion ratios are used for parametric representation in the present work in order to minimize compositional effects of the electrolyte. For example, as the metal dissolves and the newly formed ions interact with bulk solutions of fixed ionic strength, they will have identical activity coefficients at all values of r. This device improves the likelihood that only specie-specific interactions will be observed as the method of differences is applied at each particular ionic strength. Note that the use of I and r includes all of the information associated with direct use of anion concentrations.

Instrumentation. The cell configuration and instrumentation for anodic polarization follows recommendations by Greene [23, 25] and ASTM [12, 17]. The instrumentation consisted of a Magna Model 4700M research potentiostat, Keithley Model 602 electrometer, Leeds and Northrup Model 8687 potentiometer, Leeds and Northrup Model 4776 and Model 8070-B precision resistors, Hewlett-Packard Model 8875A differential amplifier, Sargent Model SR recorder and a Blue M thermo-regulated immersion heater for the constant temperature bath. The potential step rate was 50 mv each 5.0 minutes with current recorded continuously. A saturated calomel electrode served as the reference and a smooth

platinum electrode was used as the auxiliary. The circuit is shown in Figure 4.1. The test solutions were continuously purged with hydrogen gas for the duration of the test commencing 30 minutes before specimen immersion. The corrosion potential was monitored for one hour prior to polarization. Specimens were wet-ground with 600 silicon-carbide paper and degreased 15 minutes prior to immersion.

The continuous recording arrangement permitted standard potentiostatic data to be obtained, but it also monitored the nature of the response to each potential step and, thus, includes more information than the usual potentiostatic or potentiodynamic curves. These response characteristics are useful to judge stepwise nearness to steady-state conditions and to qualitatively indicate structure changes in the interphase. For purposes of data identification and to facilitate discussion, these i-t traces are designated "potentiostatic-response" curves.

Corroded specimens were immediately removed from the cell, rinsed with distilled water and anhydrous methanol and examined using a Bausch & Lomb Model BVB-73 stereomicroscope. Further examination and photographic work was performed on a Reichert Model Me F universal camera microscope.

A flow cell was constructed for methodology comparisons as shown in Figure 4.2. Identical specimens were mounted as discussed above except electrical contact is from the back side and grooves were machined in the bakelite to seat neoprene"O" rings. Flow characteristics were visually examined by injecting dye at the base of the cell during flow. For the rates used, flow across the faces of the specimens appeared uniform and unobstructed. Much more elaborate flow cell configurations have been proposed [44] and the application of such arrangements may eventually prove desirable. For present purposes the desirable feature is the simplicity of specimen surface preparation and examination.

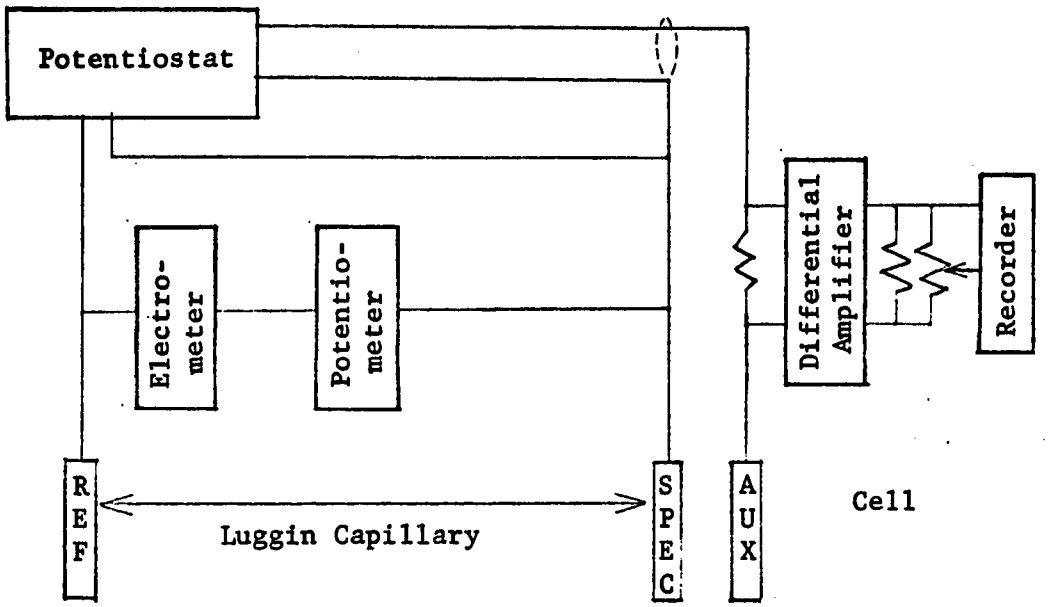

Fig. 4.1.--Anodic Polarization Circuit.

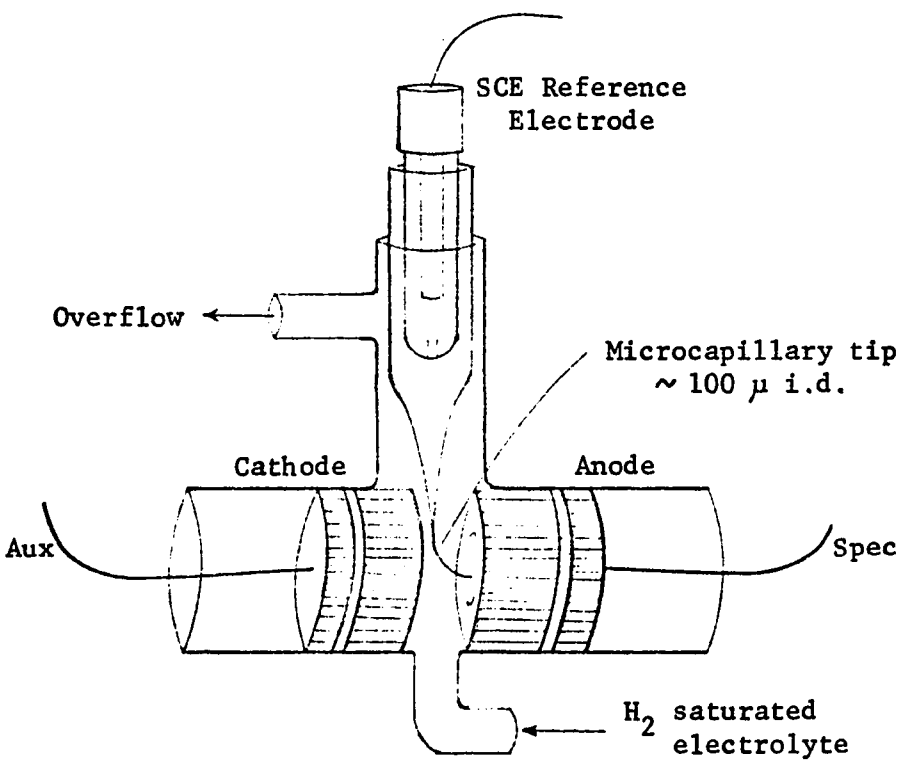

Fig. 4.2.--Flow Cell Design.

Control Mechanics

An important factor in experimental design is the effect of the instrumentation on the tests which are performed and how the instrumentation responds to changes at the electrode surface. This is particularly important in the case of localized corrosion where widely divergent properties are manifest on a common surface. The object of the discussion will be the limitations or restrictions which accompany the application of the potentiostatic technique to localized corrosion. First, a macroscopic picture of what occurs on a passive and on an active surface will be formulated, and then implications of potentiostatic control of a locally corroding surface will be synthesized by merging the passive and active limiting cases. Reference to Figure 4.3 will be helpful where experimental polarization data are given for Inconel X-750. Curve (a) shows the passivation processes, curve (b) represents the cumulative processes associated with pitting and curve (c) shows hypothetical superposition of charge-transfer, diffusion and crystallization control in the absence of passivation.

Passive surfaces. Examination of curve (a) in Figure 4.3 reveals that the current is essentially independent of potential between +0.4 and +1.1 volts. The implication is that charge transport is regulated by chemical factors, semi-conductive properties of the film or edge effects associated with mounting, but, in any case, the current magnitude across the metal surface is very small; therefore, diffusive and convective mass transfer components tend to produce a homogeneous electrolyte outside of the oxide film and the attached electric double layer; hence, specific conductance is independent of position for most of the 2 mm between the capillary probe and the metal surface. The potential-distance curve which accompanies the previous conclusions and observations will be of the form shown in Figure 4.4(A), and the observed potential difference between the probe and the metal surface will be very close to the same value at all points on the surface.

Active surfaces. An experimental E-i curve cannot be obtained for a completely active surface on Inconel X-750 at the potentials for which passivity is also manifested. A hypothesis of what might happen

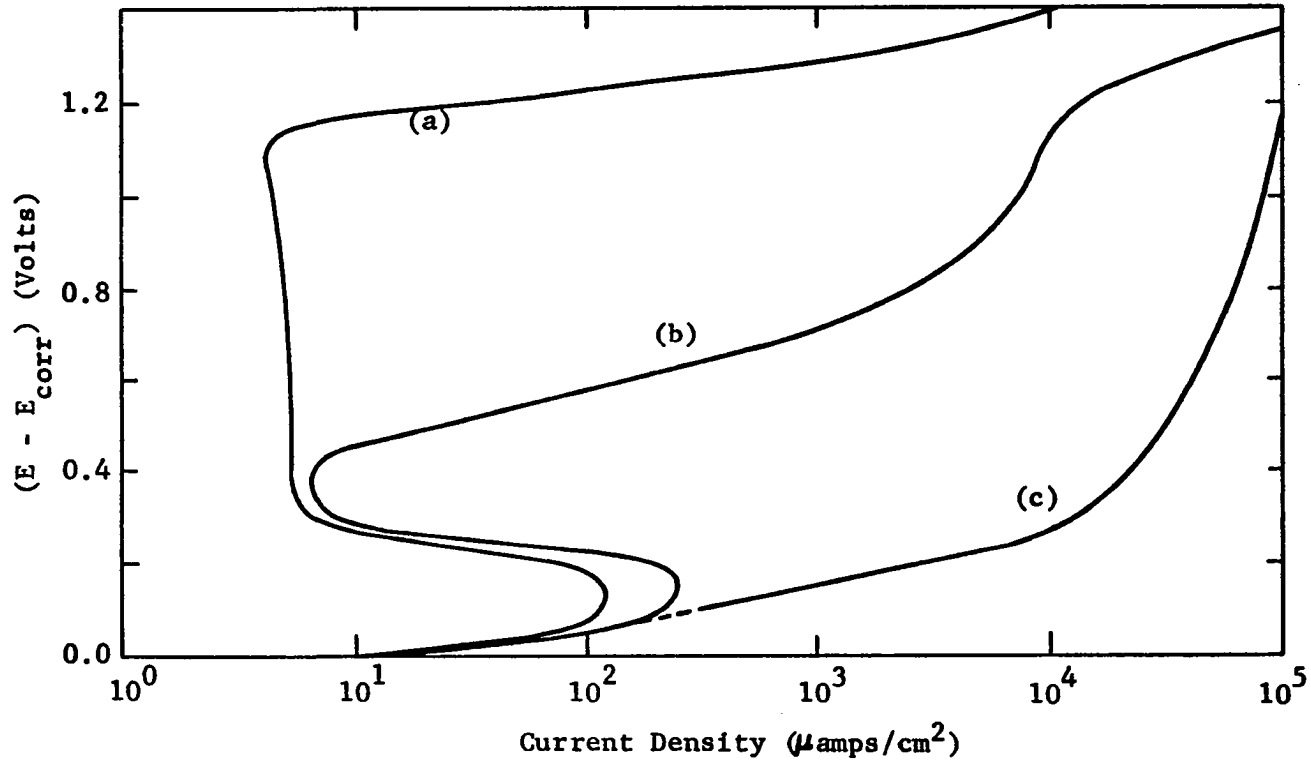

Fig. 4.3.--E-i Characteristics Showing: (a) Passivity, (b) Cumulative Processes Associated with Pitting and (c) Schematic Representation of a Completely Active Surface.

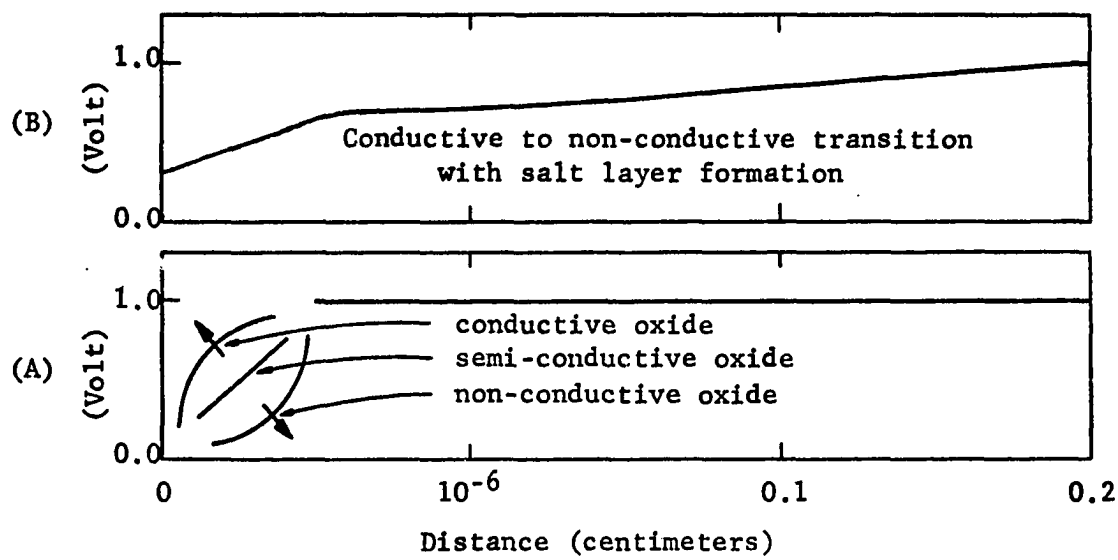

Fig. 4.4.--Schematic Potential-Distance Curves for (A) Passive Surface and (B) Active Surface--each Potentiostatically Controlled.

in such a case serves to suggest limitations on the active processes. Qualitatively, the current-potential dependency of curve (c) in Figure 4.3 decreases as the potential moves in the noble direction; rate control shifts from a charge-transfer mechanism to a diffusion mechanism in accord with the concept of superposition of partial processes. As current density increases, the concentration gradient in the interphase becomes more significant, particularly at long times, and the significance of iR-drop in the bulk electrolyte increases. For a completely active surface, as represented by curve (c), all points on the surface will exhibit nearly identical potentials. The features described above are combined to obtain the potential-distance curve shown in Figure 4.4(B) where the distance is measured from the metal surface.

Locally corroding surface. Suppose that equipotential loci are mapped over a passive and an active surface at equal potential increments as shown in Figure 4.5. Both surface types are potentiostatically controlled so that the potential of the metal bulk is, c.a., 1.0 volt positive with respect to a point 2.0 mm out into the electrolyte bulk. If the E-d (potential-distance) characteristics of the passive region of a pitting surface are in the similitude of the E-d characteristics of a completely passive surface and a corresponding similitude exists for the active areas, then it is of interest to follow what happens in the experimental sense as a pit initiates on a passive surface. Two limiting cases exist: the first and most likely situation is where the capillary continues to see only the passive surface after pit initiation, and the second is where the capillary sees only the active site or pit.

When potentiostatic control remains referenced to the passive surface, the newly formed pit acts as a current leak which would, if allowed, cause a reduction of the passive potential. The control circuit, however, increases the current to quickly compensate (2.5 μsec) so that the 1.0 volt equipotential line remains precisely at 2 mm, thus the passive areas retain identical potential gradients throughout the pit initiation process.

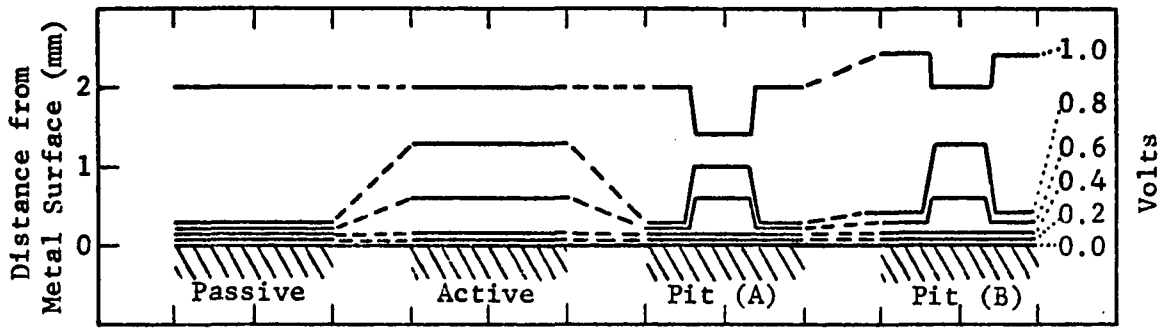

Fig. 4.5.--Schematic Equipotential Loci under Passive, Active and Pitting Modes with Potentiostatic Control. Pit (A) and Pit (B) are Limiting Cases of Passive and Active Control Derived by Merging Passive and Active Cases.

At the pit site the increased current must be accompanied by an appropriate change in the potential gradient and the effectual resistance, which is a combination of charge-transfer resistance and iR-drop. A special case extracted from the data to be presented in Chapter V will serve to establish the order of magnitude of various parameters.

Equation 2.1 is linearized [13] to the form $y = mx + b$ or specifically

$$\ln\left[\frac{i}{1-\exp nf\eta}\right] = \ln i_{corr} - \alpha nf\eta. \qquad \text{Eq. 4.1}$$

Curve (q) in Figure 5.4A provides several pairs of i and E (SCE) data between the corrosion potential and the passivation potential. Reference to Figure 5.4B indicates nearly direct E-i response characteristics over the potential range to partially justify the use of Equation 4.1. Conversion of E to η (the symbol for overvoltage, η, is used loosely to represent polarization potential, $E - E_{corr}$) and calculation of the left hand side of Equation 4.1 for corresponding i values allows a linear plot. The intercept gives i_{corr} = 128 $\mu A/cm^2$ which corresponds well with the value (78 $\mu A/cm^2$) estimated from published Tafel slopes (0.08 V/decade) [69] for nickel in 3.2 M HCl. If it is assumed that the active site current density is 4 A/cm^2 (see Table 5.4D) and charge-transfer is limiting during the very early stages of pit formation, the corresponding potential associated with the active site processes will be 0.2 V SCE. The effectual resistance , therefore, changes from 2.61×10^5 ohms on the passive surface to 0.141 ohms at the active site during the breakdown of an I = 5, r = 0, passive film in an I = 3.2, r = 1 electrolyte at E = +0.7 V SCE. Note that the active site potential is more noble than the passivation potential (+0.08 V SCE).

The inclusion of diffusive effects by the active site potential with passive site potentiostatic control tends to increase the potential required for the maintenance of the 4 A/cm^2 pit currents; therefore, the difference in potential between the passive and active sites is reduced, or, in other words, the active site potential is even more noble than with charge-transfer control only.

If potentiostatic control were referenced to the active site, an opposite response would occur in that the current leak would induce an increase in the active potential gradient, if it could, but the total current is forced to decrease to maintain the active site potential gradient.

It is of consequence to observe that the potential change over the passive surface is responsible for very little change in the magnitude of the current which means that virtually all observed current change is associated with active sites.

Discussion. Experimental measurements of currents and potentials over and near active pit sites has been reported by Rosenfeld and Danilov [57] and more recently by Isaacs [33]. Their observations are regarded as resulting from iR-drops in the electrolyte rather than strictly from potential differences between the active and passive surfaces.

An important factor in understanding localized corrosion is the magnitude of the potential difference between the active and passive sites. This is a point of controversy and estimates have ranged from near zero [77] to near one volt [49]. Thus far purely physical aspects of instrumental control have been applied to demonstrate a particular case where the potential difference could at most be 0.5 V. (This case was selected to enhance the magnitude of the potential difference.) Estimating the potential difference is not a simple matter, as will be further shown in the next section.

From the viewpoint of experimental technique, instrumental controls impose no qualitative complications as shown in Figure 4.5. Therefore, potentiostatic techniques can be beneficially applied to the investigation of the induction of localized corrosion.

Active Site Potential

Potentiostatic corrosion testing of passivable metals has been interpreted in terms of polarization theory as developed by Stern [68] and by Stern and Geary [67]. Greene [24] has discussed the problem of stability in terms of polarization theory and work performed by Franck. Briefly, three cases are possible in the superposition of an anodic

polarization curve and the corresponding cathodic process as shown in Figure 4.6. The letters A through E represent conditions at which anodic and cathodic processes have identical rates and, therefore, represent allowable states for an isolated corroding specimen.

In estimating the potential difference between the active and passive sites, there are two main arguments favoring a large difference. In terms of Figure 4.6, the active and passive sites could be at the potentials indicated by B and D, respectively. Thus, localized corrosion can be interpreted as a manifestation of system instability. The particular nickel alloy and electrolyte compositions used in this work all fall under case 1; therefore, active-passive site potential differences cannot be explained in this manner.

The second justification for a large potential difference is associated with chemically driven corrosion of an isolated specimen where the cathodic and anodic processes occur on the same surface. In this regard Pickering and Frankenthal [49] have argued that, for iron and stainless steel, hydrogen evolves from the pit sites even under anodic potentiostatic control, which implies local action inside the pit. Their work is further discussed in section B of Chapter V. The application of potentiostatic methods does, in effect, separate the anodic and cathodic sites and, thus, mitigates the possibility of large potential differences on the corroding surface, particularly at short times.

Induction Time

When pitting occurs it has been observed that a lag time exists [30, 61, 70, 71] between the imposition of a set of conditions conducive to pitting and the appearance of localized attack. This lag, or induction time, τ, has been observed when shifting the potential from the active side of the critical pitting potential to the noble side, and it has been observed on addition of an aggressive anion at a sufficiently noble constant potential. Both concepts are mentioned in the literature but little attention has been devoted to comparative methodology. It is intuitively apparent that differences must exist;

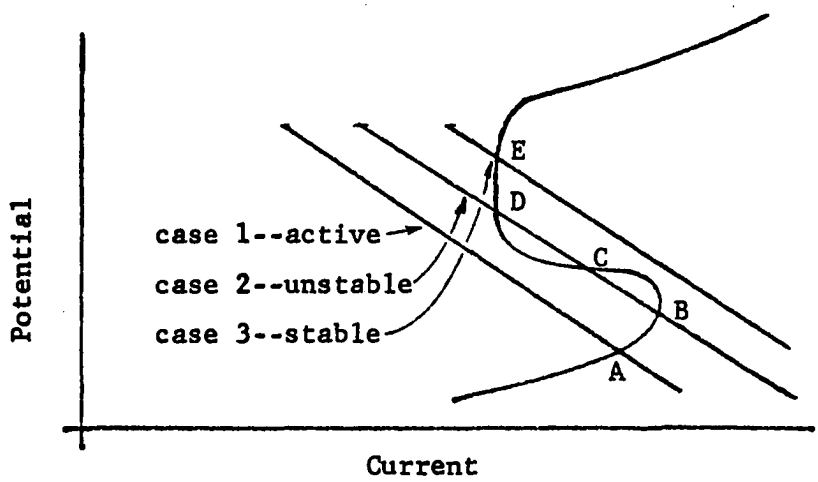

Fig. 4.6.--Superposition of Anodic and Cathodic Processes on a Common Surface. Active, Unstable and Stable Interactions are Shown [24].

for example, at constant composition, aggressive anions will be "in position" and likely a part of the passive film before activation processes commence, as opposed to the introduction of the aggressive anion after the passive film is formed.

Constant composition - τ_c. This method is based on the critical pitting potential concept, i.e., there exists some potential below which pitting will not occur and above which pitting will occur in a specified environment. The method requires the imposition of a potential shift, δE, and has the advantage of simplicity and ease of application. The disadvantage in some systems is that an apparent potential dependent interphase structure change occurs, as evidenced by the continuously changing index of refraction noted by Reddy and Rao [54, 55]; hence, the method does not produce a tidy induction time for only aggressive anion attack processes. It is true that the effects of interphase structure changes can be minimized by making δE approach zero, but this introduces long experimental times which tend to obscure the significance of the results. The tentative conclusion at this stage is that the extraneous effects associated with the potential shift limits its applicability and, therefore, holds little promise for present purposes.

Constant potential - τ_E. The induction time at constant potential lacks certain conveniences associated with τ_c, especially with regard to the physical manipulation aspect of experimentation. Flow cells have been used to simplify the introduction of the aggressive components with minimum electronic disturbance, but this, in turn, introduces a laminar boundary layer and diffusional effects which obscure the shorter induction time measurements. A particular advantage associated with τ_E is the capability, within certain concentration limits, e.g., $I = 0.1$, $r = 0$, to reduce the effects of a carrier anion. Note that a carrier anion exerts its own particular inhibiting or enhancement effects, and, in its presence, induction time is a superposition of anion contributions rather than a measure of the kinetics of the aggressive process alone. The use of pit resistant electrode material permits intermediate concentrations of aggressive

electrolytes without carrier anions, which allows some degree of experimental freedom. The objective is, therefore, to develop a suitable technique which avoids boundary-layer diffusion complications.

Experimental technique. The diffusion problem can be handled either by implementing a highly reproducible flow regime, such as the rotating disk [15, 20, 59] or by eliminating diffusion layers in a batch system. The latter is mechanically simple, but both electronic interruption and severe environmental disturbances are introduced. Specifically, for the batch scheme, the specimen would need to be passivated in one solution, removed, placed in the aggressive solution and re-polarized at the same potential. Despite the obvious handicaps, the advantage of mechanical simplicity prompted an estimate of the magnitudes of the handling effects. The procedure which evolved is outlined below with the suggestion that typical precautions used in polarization studies also be applied here.

1) Introduce the specimen into a polarization cell at the desired temperature and in a passivating electrolyte.
2) Initiate polarization at a potential slightly more noble than the highest passivation potential which will be encountered in the investigation. Hold this potential until the current is relatively constant with the objective of establishing a "reproducible" reference state through which all specimens will pass.
3) Adjust the potential to the value desired for the test and hold until the current is sufficiently constant.
4) Switch the potentiostat to standby and perform the following operations as quickly as possible (one minute should be sufficient with adequate preparation).
    a) Remove the specimen, rinse with distilled water and carefully blot the excess with soft, lint-free absorbent tissue.
    b) Place the specimen into a polarization cell which is identical in all respects except containing the aggressive electrolyte.

c) Reactivate the potentiostat at time $t = 0$ and monitor the i-t response from this point in time.

The two undesirable aspects of the batch method were tested experimentally by producing i-t curves for various combinations of potentiostat switching and out-of-cell exposure. Switching without specimen removal measures the effect of the switching operation alone and the difference between the switching effect and the combined switching and exposure effects suggests the magnitude of the latter. Response curves are shown in Figure 4.7 curves (a) through (f). As observed in the curves, the switching effect is the more significant of the disturbances and the magnitude varies with the potential. At this point there is justification only for concluding that the procedure outlined above introduces little more effect than would be introduced by simply switching the current off and on. At short times this effect tends to be small. A comparison of the induction time curves using the above technique with that obtained using a flow cell (see Figure 5.5D) indicates, however, that the switching operation causes no qualitative modifications of the nature of the i-t curve beyond those shown in Figure 4.7.

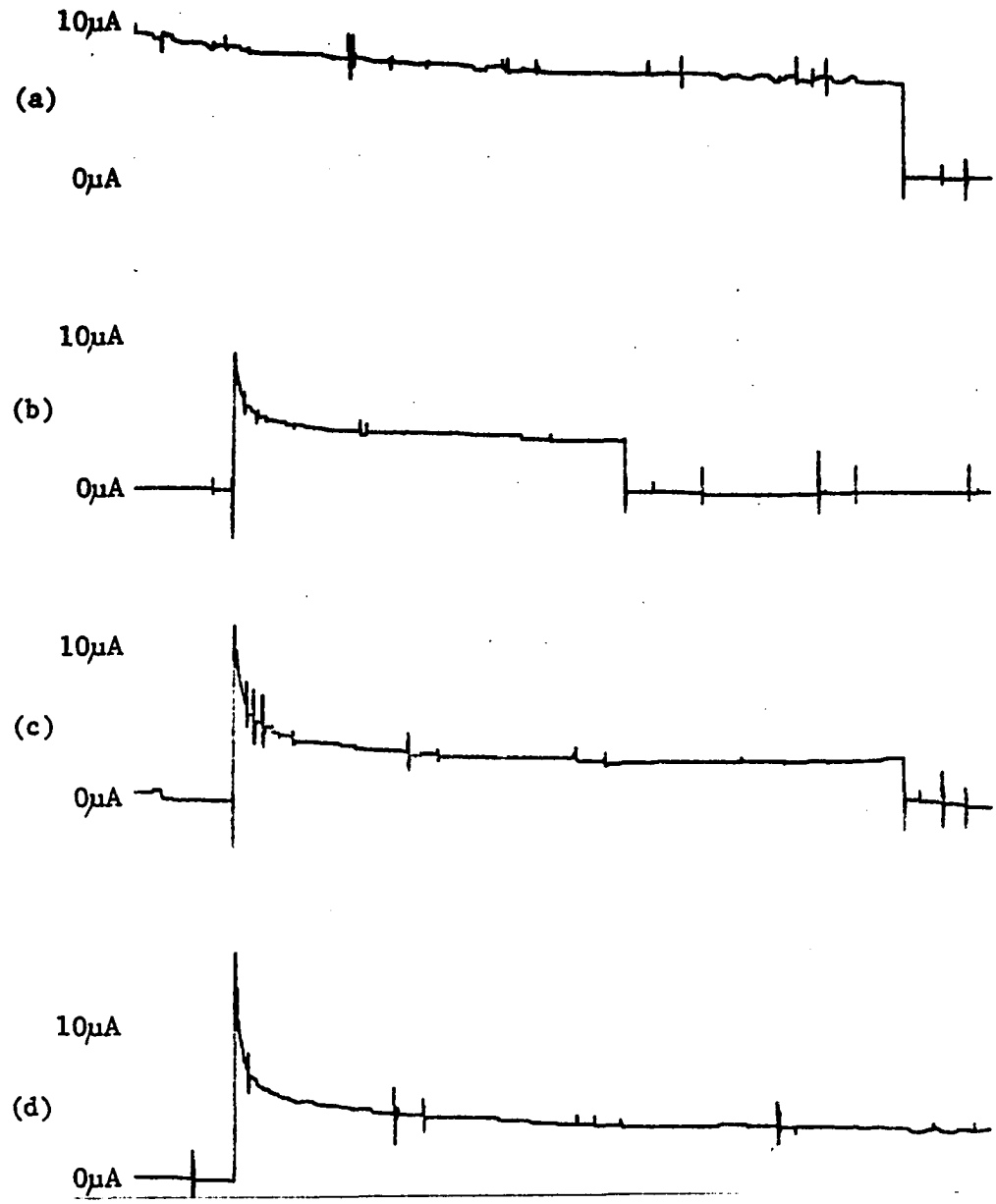

Fig. 4.7.--Current-Time Response Characteristics to Selected Disturbances of a Potentiostatically Controlled Anode at I = 0.1.
(a) Equilibrium Current at r = 0, E = +0.7 V.
(b) On Response After Off Only at r = 0, E = +0.7 V.
(c) On Response After Off, Rinse, Re-insertion to r = 0 Solution at E = +0.7 V.
(d) On Response After Off, Removal from r = 0 Solution, Rinse, Insertion to r = 1 Solution at E = +0.7 V.

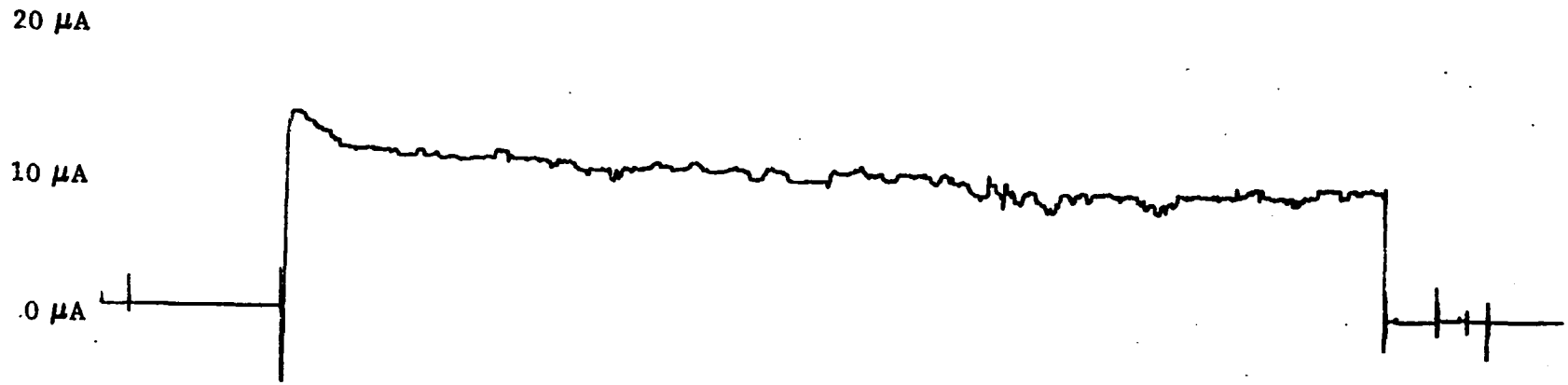

Fig. 4.7.--(e) On Response After Off Only for r = 0 Solution at E = +0.40 V.

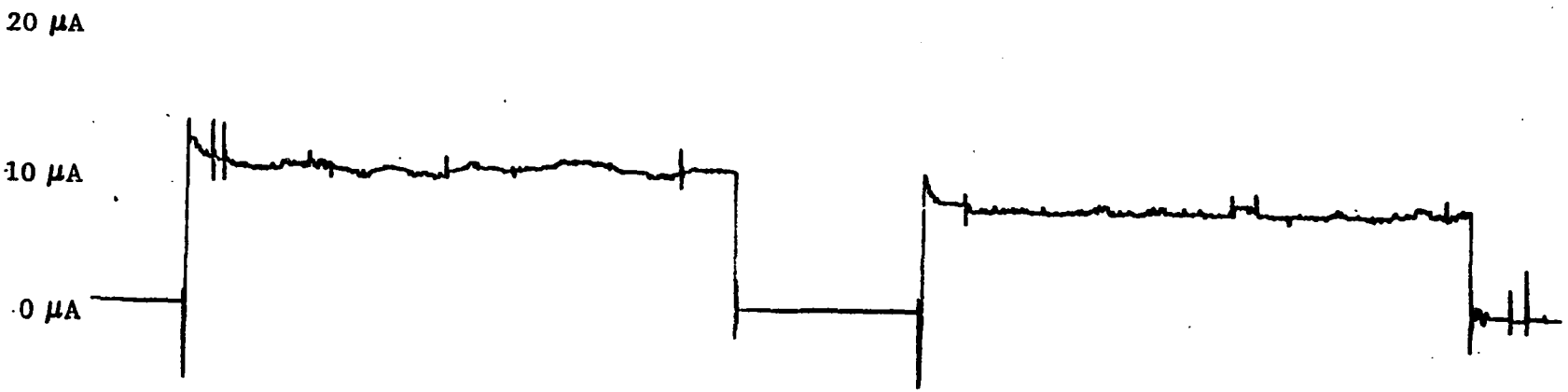

Fig. 4.7.--(f) On Response After Off Only for r = 0 Solution at E = +0.25 V (repeated once).

CHAPTER V

EXPERIMENTAL RESULTS AND ANALYSIS

Many facets must be brought together in the proper sequence to represent localized corrosion phenomena with adequate perspective, a task which is yet to be fully accomplished. The interdependence of the several aspects suggests that all of the data be considered collectively and as free of tangential considerations as is possible. To this end all data of this work are presented in the four sections of this chapter.

A. Polarization Curves

B. Potentiostatic-Response Curves

C. Attack Mode Photographs

D. Induction Time Curves

Each section is introduced with an index of the data included and a discussion of details about the methods of collection. Attention is drawn to particular implications of the data.

A. Polarization Curves

Table 5.1A indexes the various electrolyte compositions for which anodic polarization curves are available for Inconel X-750 at 30°C. The curves are presented in Figures 5.1A, 5.2A, 5.3A and 5.4A. The curves are used (1) to predict suitable conditions for examining induction times, (2) to show critical pitting potentials and (3) to indicate the relative order of magnitude of the driving force for the pitting process. These three points can be better understood in terms of an example. In Figure 5.1A, curve (a) is the combined response of the passive oxide film and the sulfate anion. Since no polarization curve for pure water is available, the precise magnitude of the sulfate effect is unknown. In the work that follows, reference to the sulfate

TABLE 5.1A--Index of Combinations of I and r for which Anodic Polarization Data are Available. ("A" designates the system for which H^+ is the only cation. "B" designates the system for which H^+ is constant at 1 M with Na^+ providing the difference. "*" indicates that scan reversal data are given.)

I	r				
	0	1/3	1	2	∞
0.1	A*	-	A*	-	A*
0.32	-	-	A	-	-
1.0	-	-	A	-	-
2.0	B	B	B	B	-
3.2	-	-	A	-	-
5.0	B	B	B	B	-

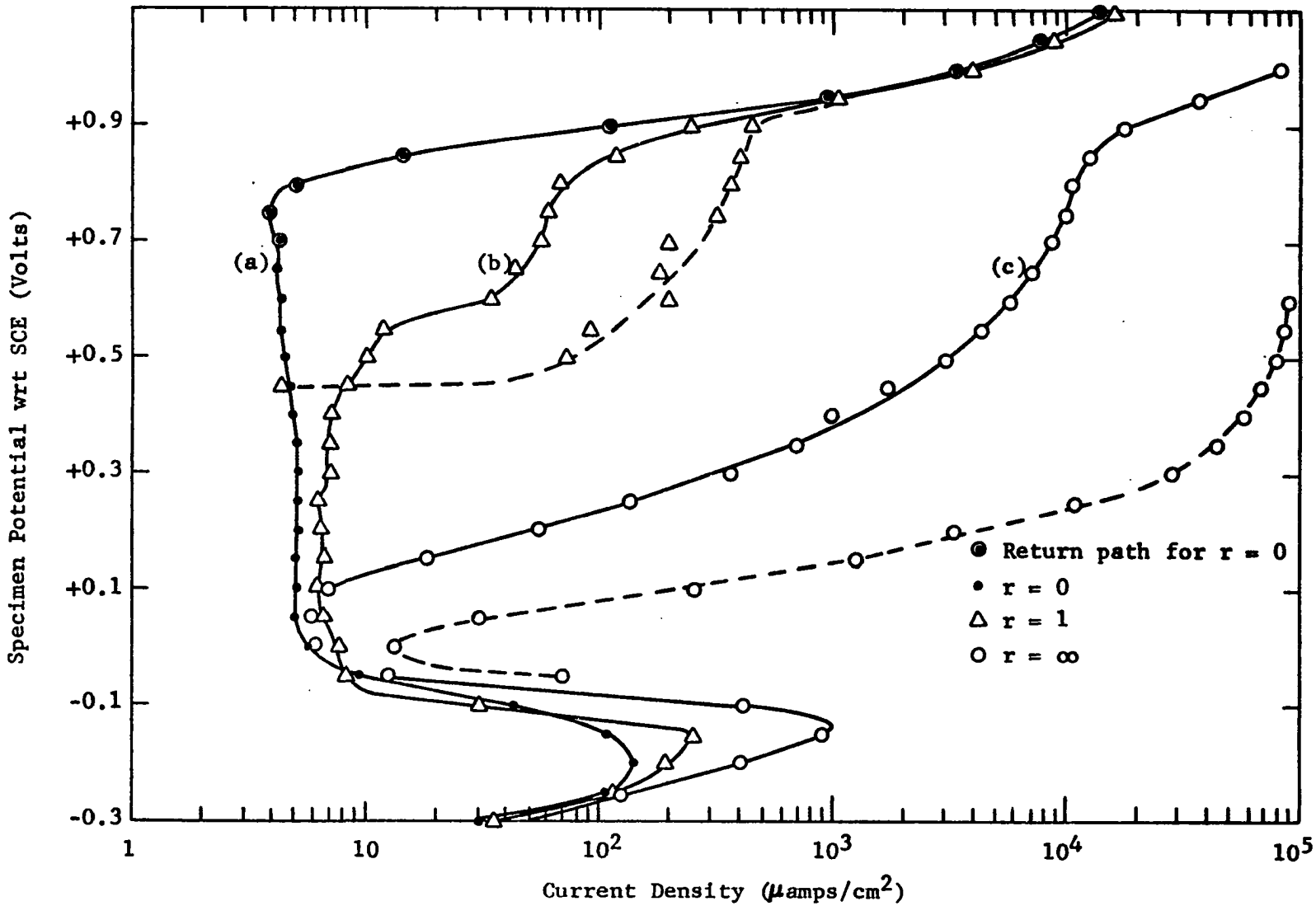

Fig. 5.1A.--Inconel X-750 Anodic Polarization Curves at 30°C, H_2 Atmosphere, HCl/H_2SO_4, I = 0.1.

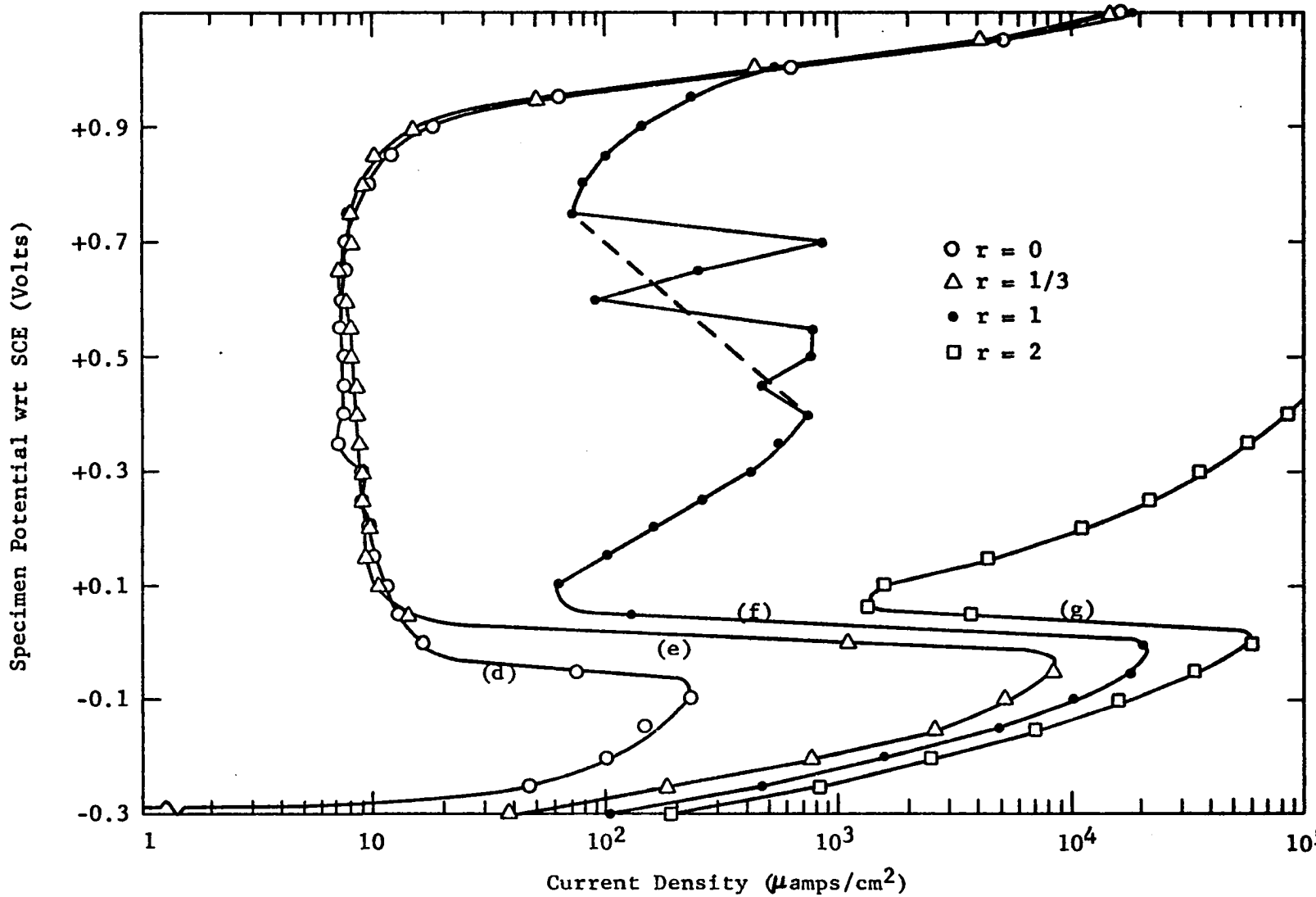

Fig. 5.2A.--Inconel X-750 Anodic Polarization Curves at 30°C, H_2 Atmosphere, Constant $[H^+]$, I = 2.

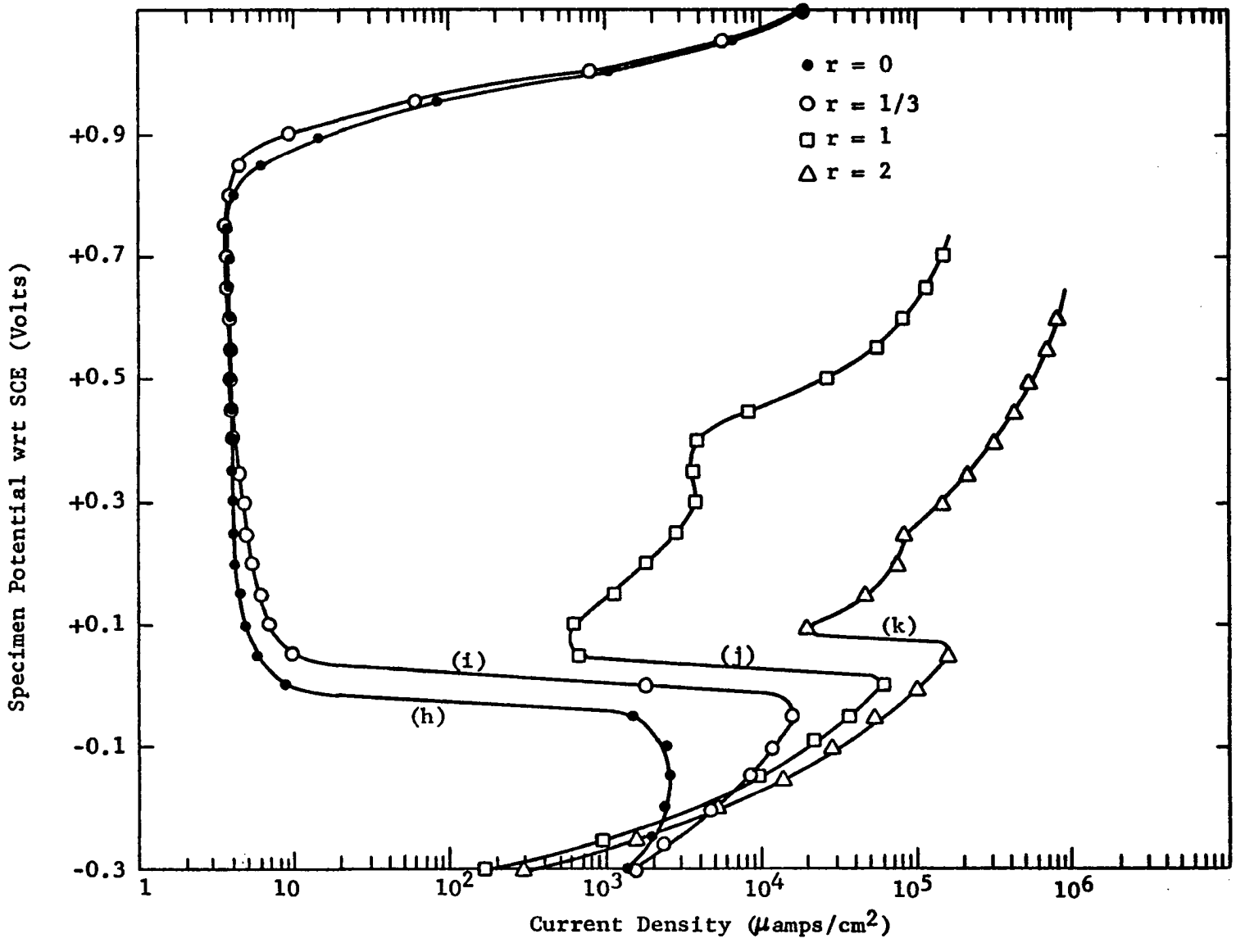

Fig. 5.3A.--Inconel X-750 Anodic Polarization Curves at 30°C, H_2 Atmosphere, Constant $[H^+]$, I = 5.

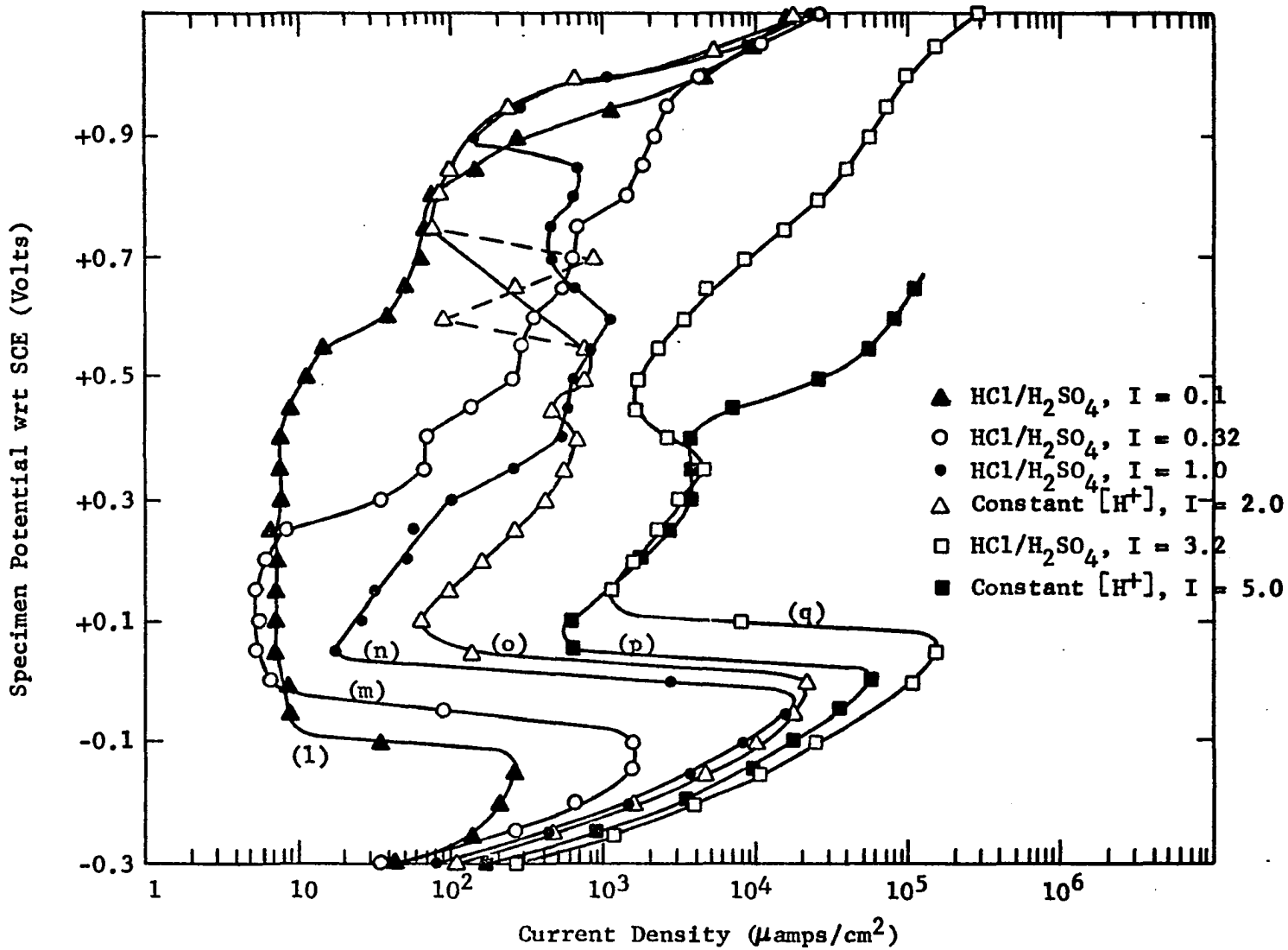

Fig. 5.4A.--Inconel X-750 Anodic Polarization Curves at 30°C, H_2 Atmosphere, r = 1.

effect will represent the combined sulfate and oxide for convenience of discussion. Therefore, curve (a) is the sulfate response at $r = 0$ and $I = 0.1$ and curve (c) is the chloride response at $r = \infty$ and $I = 0.1$. Curve (c) shows a critical pitting potential near +0.1 V SCE, therefore, it is likely that induction times will be observed in the potential range of +0.1 to +0.8 V SCE on changing electrolytes from $r = 0$ to $r = \infty$. On the basis of work reported elsewhere [61, 65, 70, 71] longer induction times are expected toward +0.1 V and very short induction times toward +0.8 V SCE. The differences in current levels between the two curves are assumed to indicate the reaction tendency. Curve (b), with equimolar chloride and sulfate concentrations ($r = 1$), will likely exhibit induction times between +0.5 and +0.8 V and the magnitudes of the induction times are expected to be proportionately longer than for the $r = \infty$ case at a given potential. Similar comparisons are used for curves generated at other ionic strengths.

Corrosion potentials for various I and r are given in Table 5.2A. All data were collected one (1) hour after immersion as a part of the polarization data acquisition and experimental conditions are as discussed previously.

For convenience, Table 5.3A is included to convert I and r values to chloride, sulfate, hydrogen and sodium ion concentration equivalents.

A major impression from the collective examination of the polarization curves is the competitiveness between anions for control of the active site interphase processes. Curves (a), (d) and (h) in Figures 5.1A, 5.2A and 5.3A, respectively, illustrate passivity as developed in a sulfate electrolyte. Curves (c), (g) and (k) in Figures 5.1A, 5.2A and 5.3A, respectively, illustrate rate control by the aggressive chloride ion at localized sites. At intermediate anion ratios, however, dominion of the localized interphase and, hence, the reaction rate appears to fluctuate as shown by curves (n) and (o) in Figure 5.4A. This characteristic is the focal point of work reported here.

Two additional characteristics, which can be noted now for future discussion, are (1) the hysteresis effects shown in curves (a), (b) and (c) in Figure 5.1A, and (2) the influence of potential

TABLE 5.2A--Corrosion Potentials of Inconel X-750, at 30°C for Various I and r. Electrolyte is Purged with Hydrogen and E_{corr} is Measured at 1 Hour from the Time of Immersion.

I	r	E_{corr} (V SCE)
0.1	0	-0.331
0.1	1	-0.336
0.1	1	-0.338
0.1	∞	-0.333
0.32	1	-0.329
0.5	1/3	-0.322
1.	1	-0.341
1.	1	-0.340
2.	0	-0.286
2.	1/3	-0.318
2.	1	-0.335
2.	1	-0.345
2.	2	-0.352
3.2	1	-0.345
5.	0	-0.372
5.	1/3	-0.371
5.	1	-0.348
5.	2	-0.350

and concentration on the domain of chloride control. Chloride control appears to follow the general rule that as the anion ratio increases, the chloride influence on corrosion rate increases and the potential range over which chloride dominates extends farther in the noble direction. This trend is particularly clear in Figure 5.2A.

TABLE 5.3A--I-r Equivalents in Ionic Molar Concentrations.

I	r	Cl^-	$SO_4^=$	H^+	Na^+
0.1	0	0.000	0.033	0.067	-
	1	.025	.025	.075	-
	3	.050	.017	.083	-
	7	.070	.010	.090	-
	∞	.100	.000	.100	-
0.32	1	0.080	0.080	0.240	-
	1.5	.107	.071	.249	-
	2	.128	.064	.256	-
	3	.160	.053	.267	-
	7	.224	.032	.288	-
1.0	1	0.250	0.250	0.750	-
2.0	0	0.00	0.67	1.00	0.33
	0.33	.20	.60	1.00	.40
	1	.50	.50	1.00	.50
	2	.80	.40	1.00	.60
3.2	1	0.8	0.8	2.4	-
5.0	0	0.0	1.67	1.0	2.33
	0.33	.5	1.5	1.0	2.5
	1	1.25	1.25	1.0	2.75
	2	2.0	1.0	1.0	3.0

B. Potentiostatic-Response Curves

It is proposed that the i-t response to successive small potential steps, such as those employed in potentiostatic polarization methods, provide an indicator of changes in the interphase structure. Data included to support this concept are i-t curves for four (4) combinations of ionic strength and anion rates as shown in Figures 5.1B through 5.4B. Data for the potentiostatic curves in section A were taken from the curves presented in this section and other similar curves by plotting the current at the end of each five (5) minute interval versus the potential maintained over the interval.

Examination of the curves reveals four (4) macro time scale features and one (1) micro time scale factor.

1) The current responds almost instantaneously to potential shifts to produce immediate steady-state i-t responses. This is observed usually for the first few intervals noble to the corrosion potential (see all four figures at -0.3V) and in the transpassive region under sulfate control (Figures 5.1B and 5.2B at 1.0 to 1.1V). This response is closely associated with the absence of hysteresis effects described in the previous section and, in that sense, is considered a reversible response.
2) The current makes no response or a very minimal response to the potential shift as is characteristically observed in the passive region. Note, this region was deleted in Figure 5.1B between 0.05 V and 0.8 V to facilitate data presentation. All responses in the deleted region are very similar to those immediately preceding and following the deletion. Non-sensitivity to electrical potential implies the chemical nature of the rate determining step or semi-conductive properties of a surface film.
3) The current increases quickly and decreases in a sweeping decay type curve as is characteristic near the passivation potential (see Figures 5.1B and 5.2B at -1.0 V to 0.0V). The current is inversely proportional to the square root of

time, which implies diffusion control. (Recall from the discussion of passivity in Chapter II the dipole rearrangement mechanism as suggested by Hoar [29].)

4) The current jumps and returns quickly to reassume an increasing mode as is characteristic of the region just noble to the critical pitting potential when chloride dominates interphase processes (see Figures 5.3B and 5.4B at 0.2 V to 0.3 V). In this case the increasing current is in part due to the increasing area of active dissolution, but the increasing slope from one section of the curve to another weakly suggests acceleration due to the potential increase. It is inferred that the initial current jump is associated with the acceleration of transport rates. In the limit as reactant concentrations in the interphase become large, the diffusion transport requirements become proportionately small and the short term peak disappears.

5) In addition to the long term i-t responses, there are also short term fluctuations which appear quite regularly where passivity is not in complete control [10, 35, 43, 49]. This behavior is particularly evident in the transition from chloride to sulfate control shown in Figure 5.2B at E = 0.65 to 0.5 V after the scan reversal. The implication is that relatively large areas are involved since molecular level transitions would, because of the large number participants, produce smoothed data; therefore, entire pits or intragranular surfaces are fluctuating between the active and passive states. Pickering and Frankenthal [49] suggested that intra-pit local action is the cause of fluctuations even though the external passive surface is potentiostatically fixed. Their work does not seem to apply in the present case as the potential and current fluctuations may be from some source other than corrosion processes. Specifically, they state that "near the bottom of the pit (within 50 μ), significantly larger potential changes and sharp transients are observed....Large

current transients are observed in phase with the potential transients." The impression is that the transient behavior is associated with the microprobe moving inside the 50 μ boundary as evidenced by two facts which seem out of place. (1) If the reported potential fluctuation of 400 mV is observable at 50 μ but not at, say, 100 μ, then an incredibly thick high-resistance layer must be postulated. (2) The surface was presumably potentiostated relative to a surface probe and the in-pit potential was monitored with the independent microprobe (potentiostatic control with respect to the microprobe invalidates the argument of in phase current and potential fluctuations and the surface layer resistance calculations). If the microprobe was independent, then the appearance of current fluctuations at all in the external circuit (referenced to the external passive surface) is contrary to in-pit local-action behavior, which the potential fluctuations represent by implication. The concurrent appearance of fluctuations with probe positions near the pit bottom may possibly be accounted for by interference at the probe tip such as by a micro bubble or reaction product precipitation at the orifice. Additional work is recommended in Chapter VII. Postelthwaite [51] suggested that rythmic hydrogel formation may account for current oscillations.

Figure 5.3B illustrates the i-t characteristics of the competitive anion interaction shown in curve (f) of Figure 5.2A. Note the response beginning 15 seconds prior to the 0.55 to 0.60 V shift and again three (3) minutes after the 0.70 V to 0.75 V shift. The approximately linear response shown possibly represents a uniform surface reaction rather than a single site nucleation and growth mechanism which would be logarithmic. The definite current level of 70 μA to 100 μA suggests the attainment of a well defined end-state associated with sulfate and oxide control.

Interpretation of response magnitudes should be done cautiously, since the current scale is not fixed; therefore, pen response must be evaluated in the context of what has gone before and that which comes after.

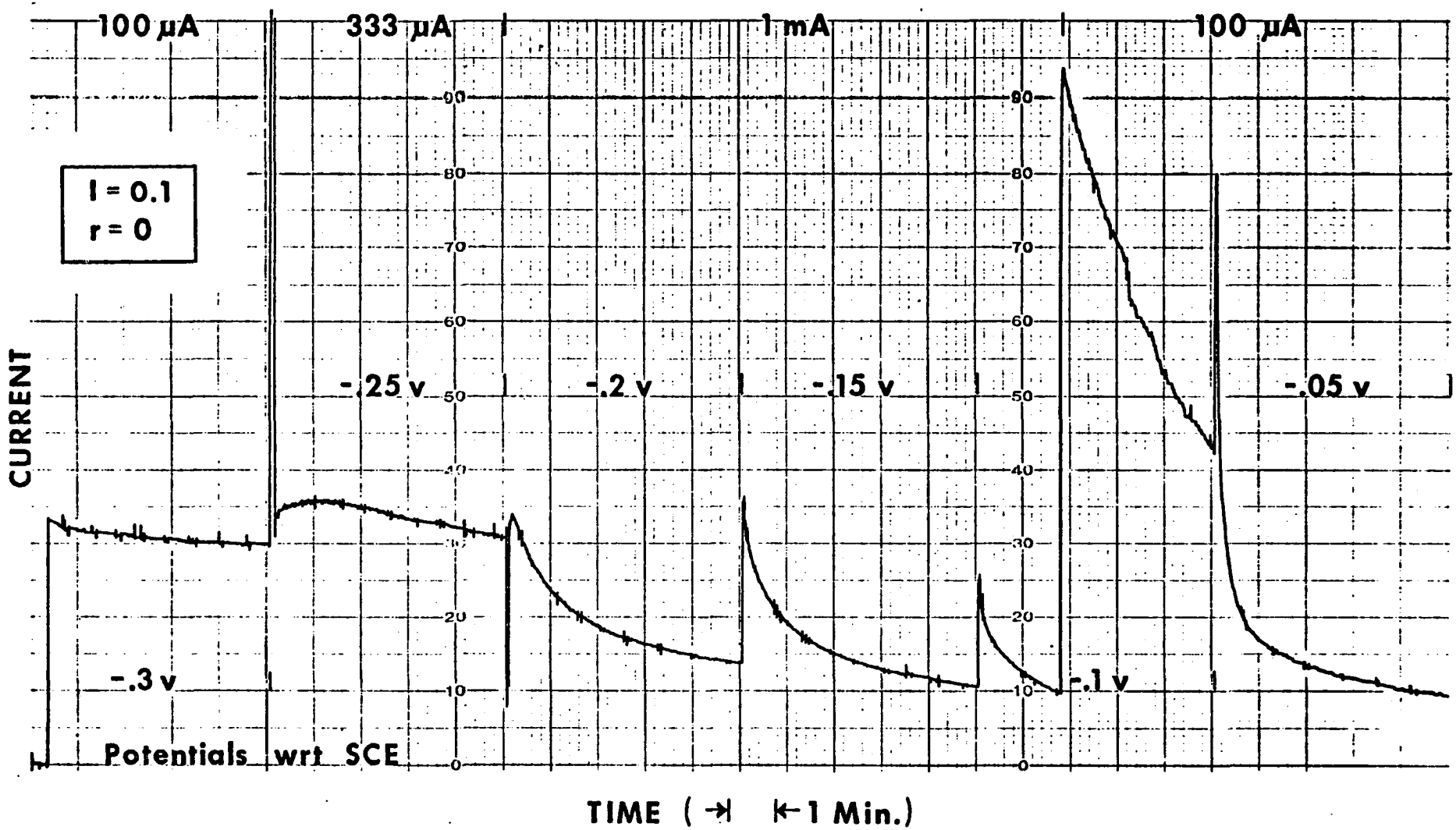

Fig. 5.1B.--Potentiostatic-Response Curves for I = 0.1, r = 0. (Current is read as a percentage of the full scale value shown at the top of the chart.) (part 1 of 4)

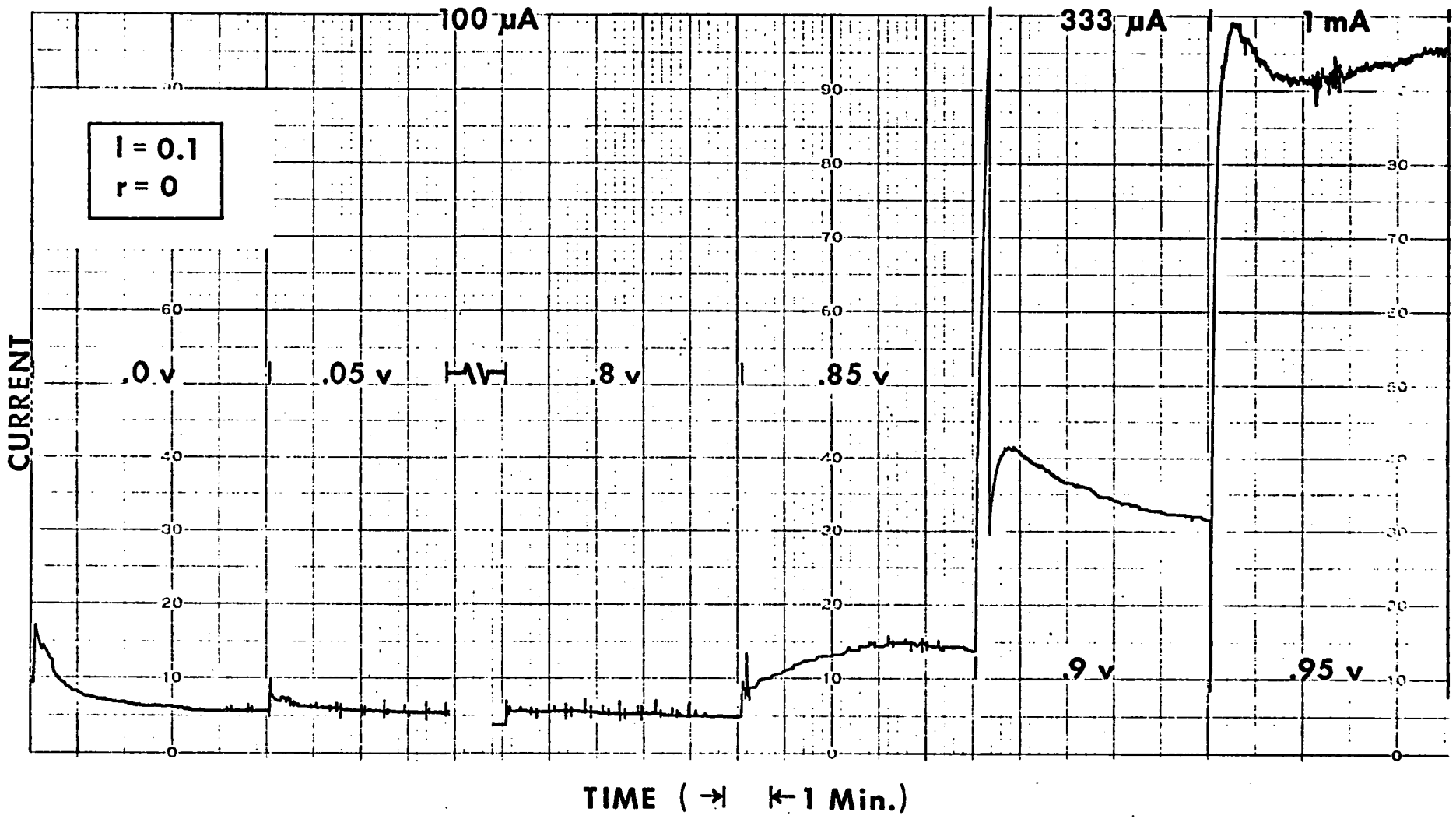

Fig. 5.1B.--(con't part 2 of 4)

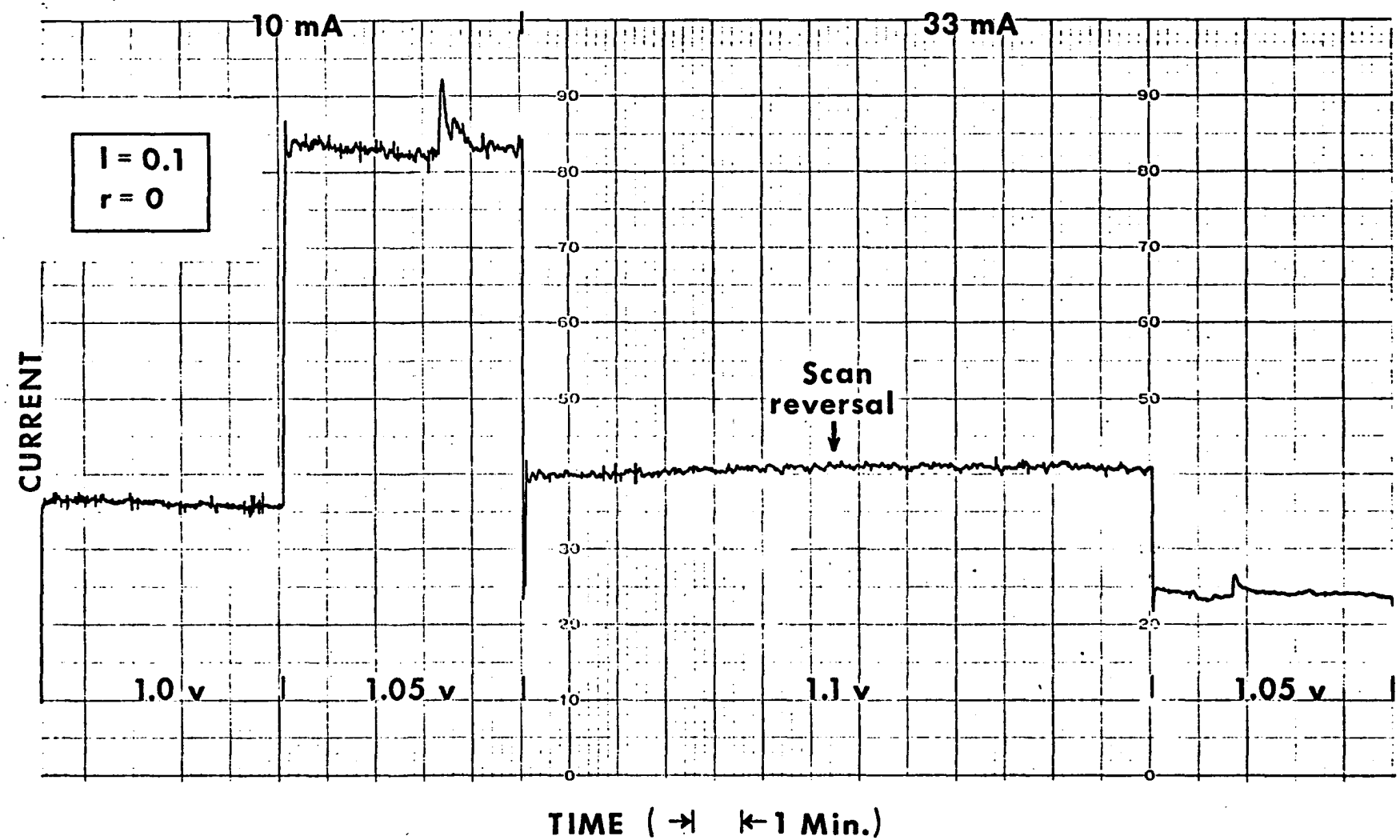

Fig. 5.1B.--(con't part 3 of 4)

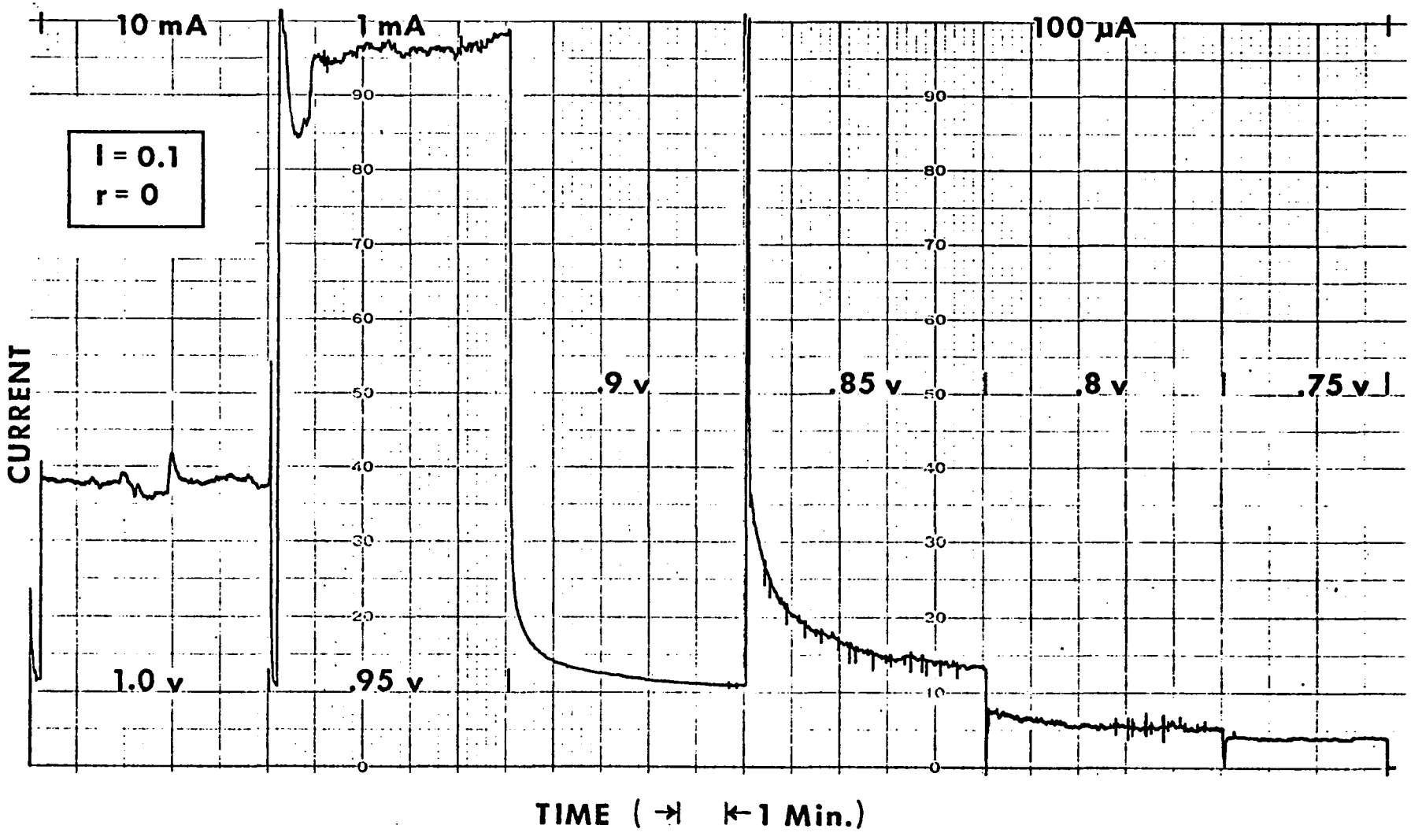

Fig. 5.1B.--(con't part 4 of 4)

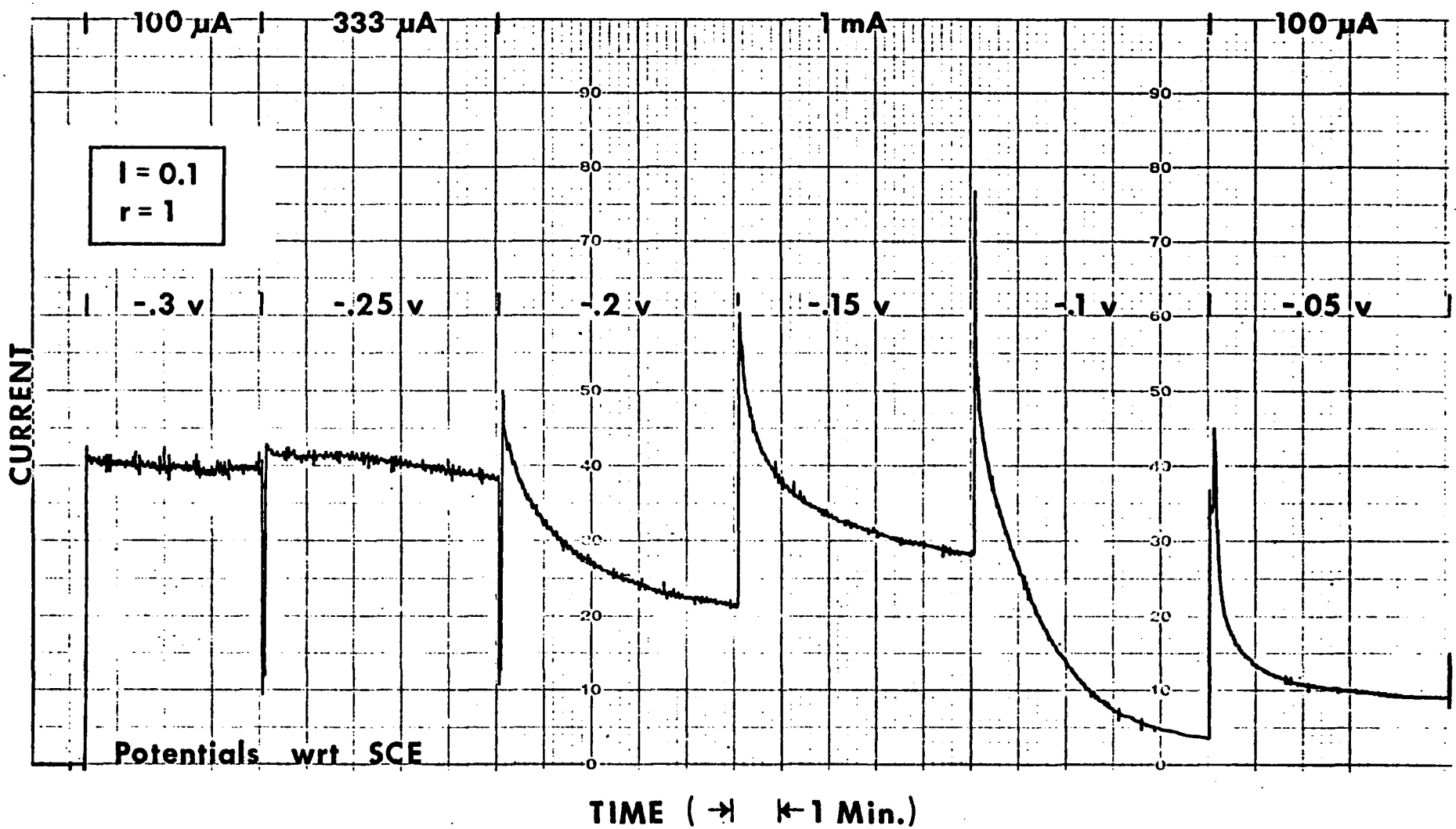

Fig. 5.2B.--Potentiostatic-Response Curves for I = 0.1, r = 1. (part 1 of 6)

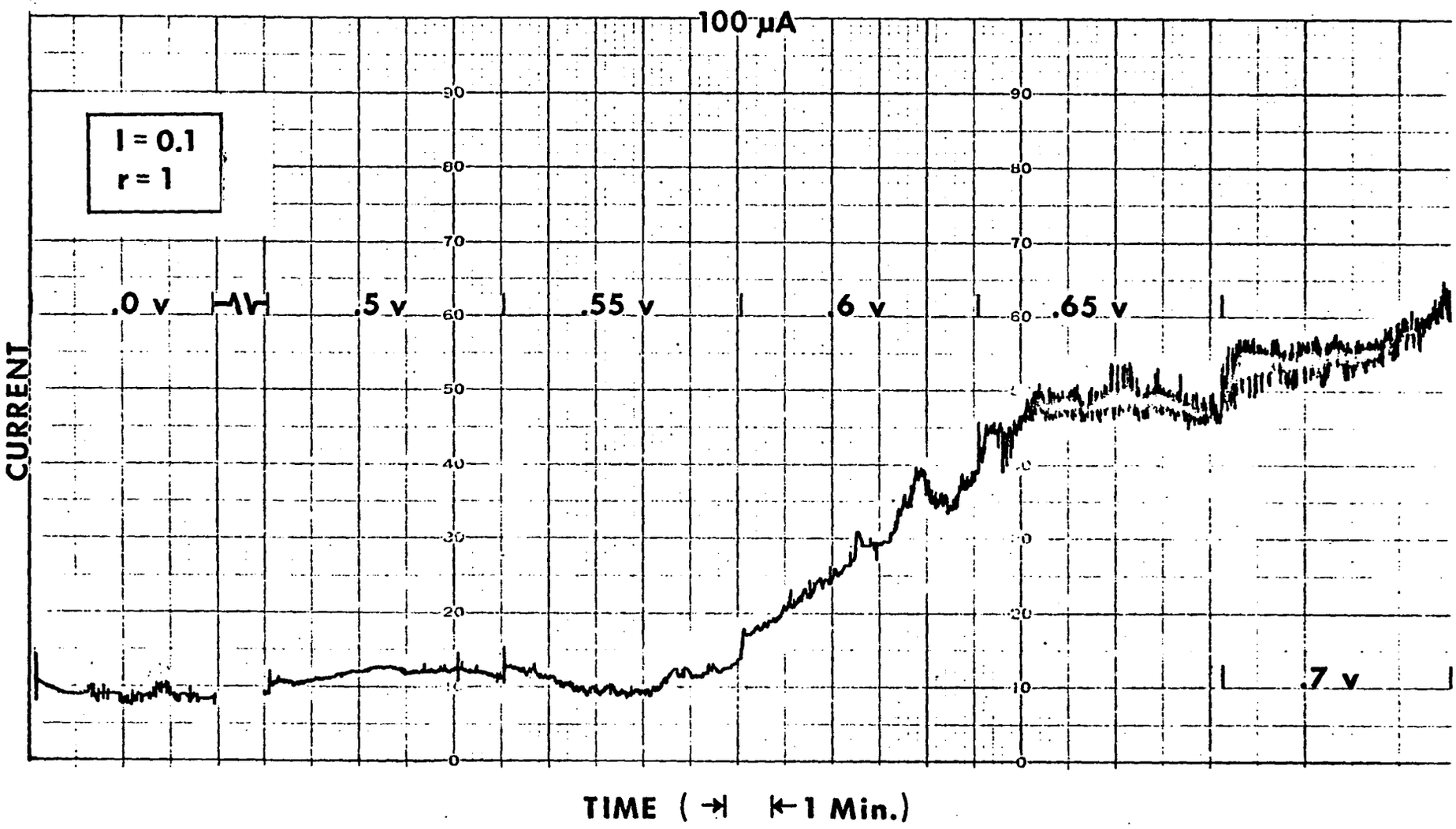

Fig. 5.2B.--(con't part 2 of 6)

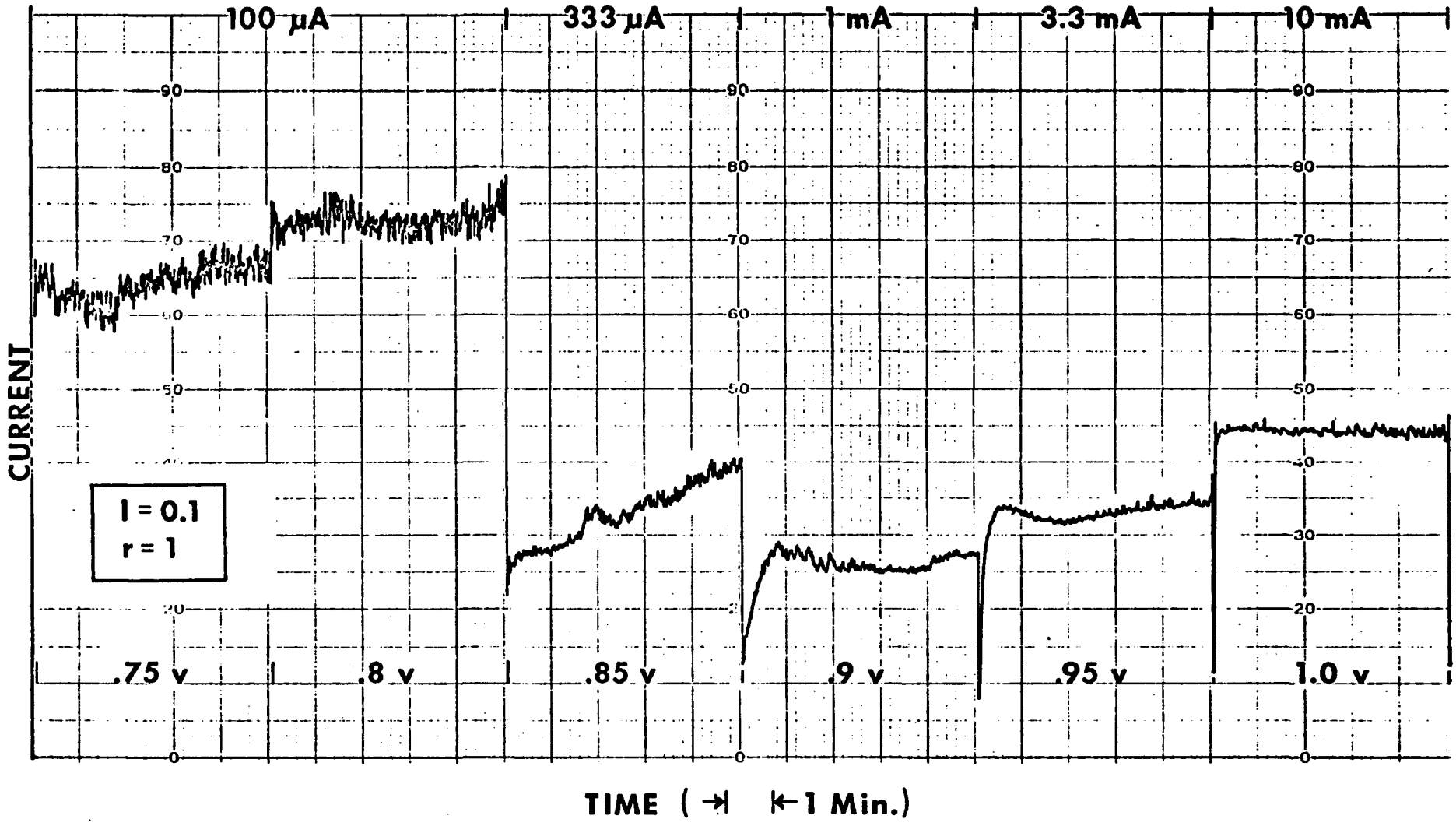

Fig. 5.2B.--(con't part 3 of 6)

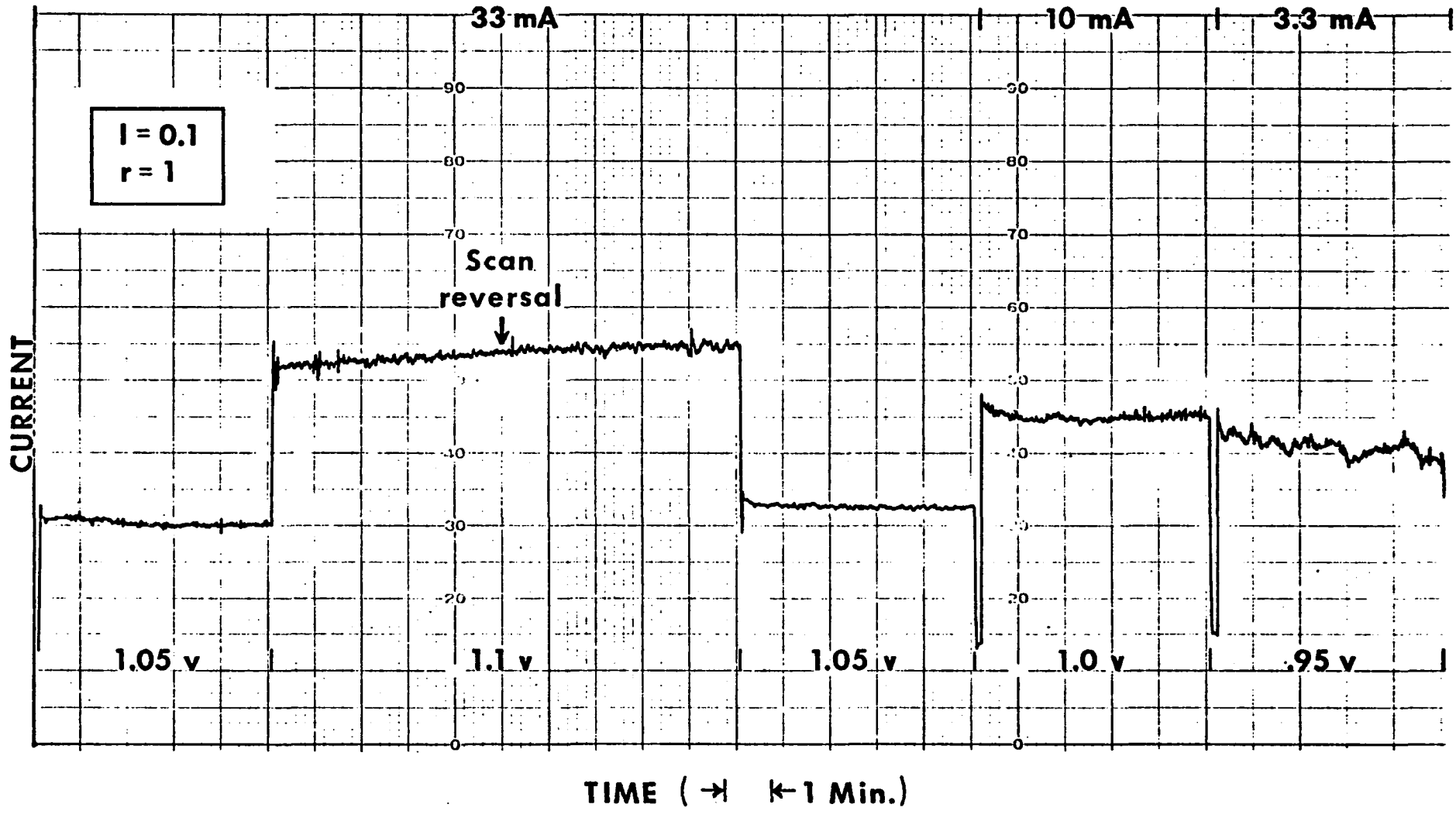

Fig. 5.2B.--(con't part 4 of 6)

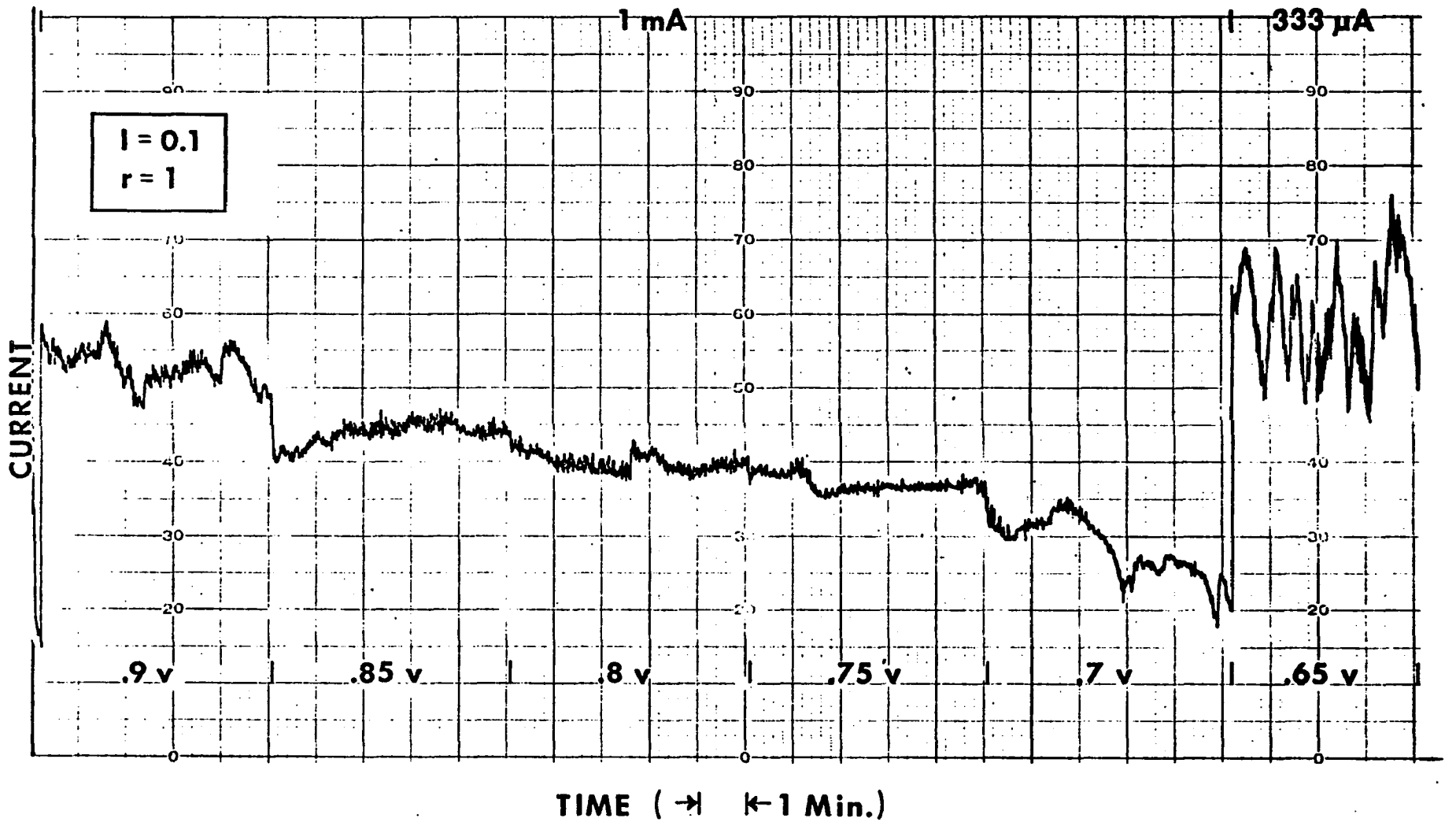

Fig. 5.2B.--(con't part 5 of 6)

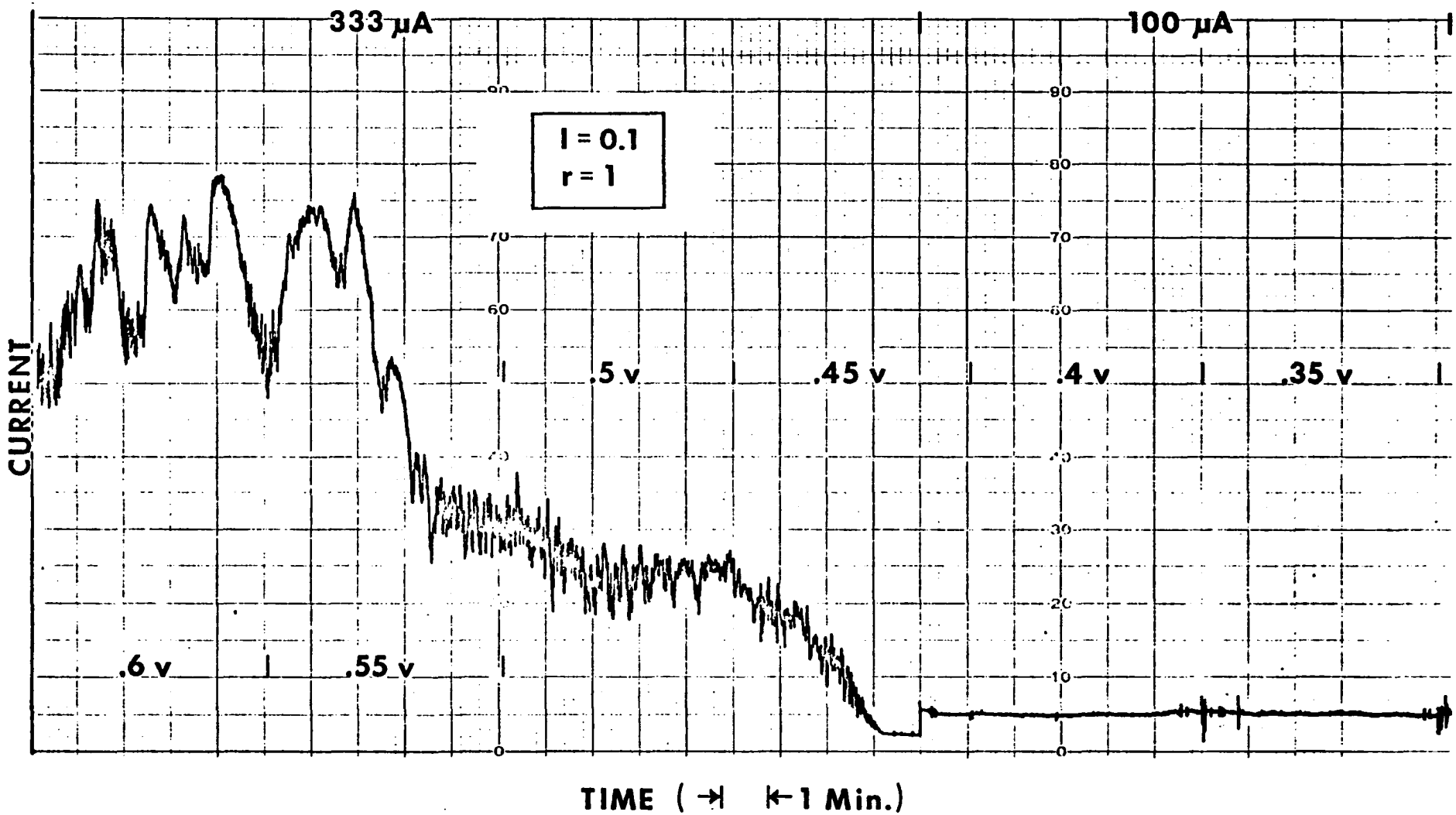

Fig. 5.2B.--(con't part 6 of 6)

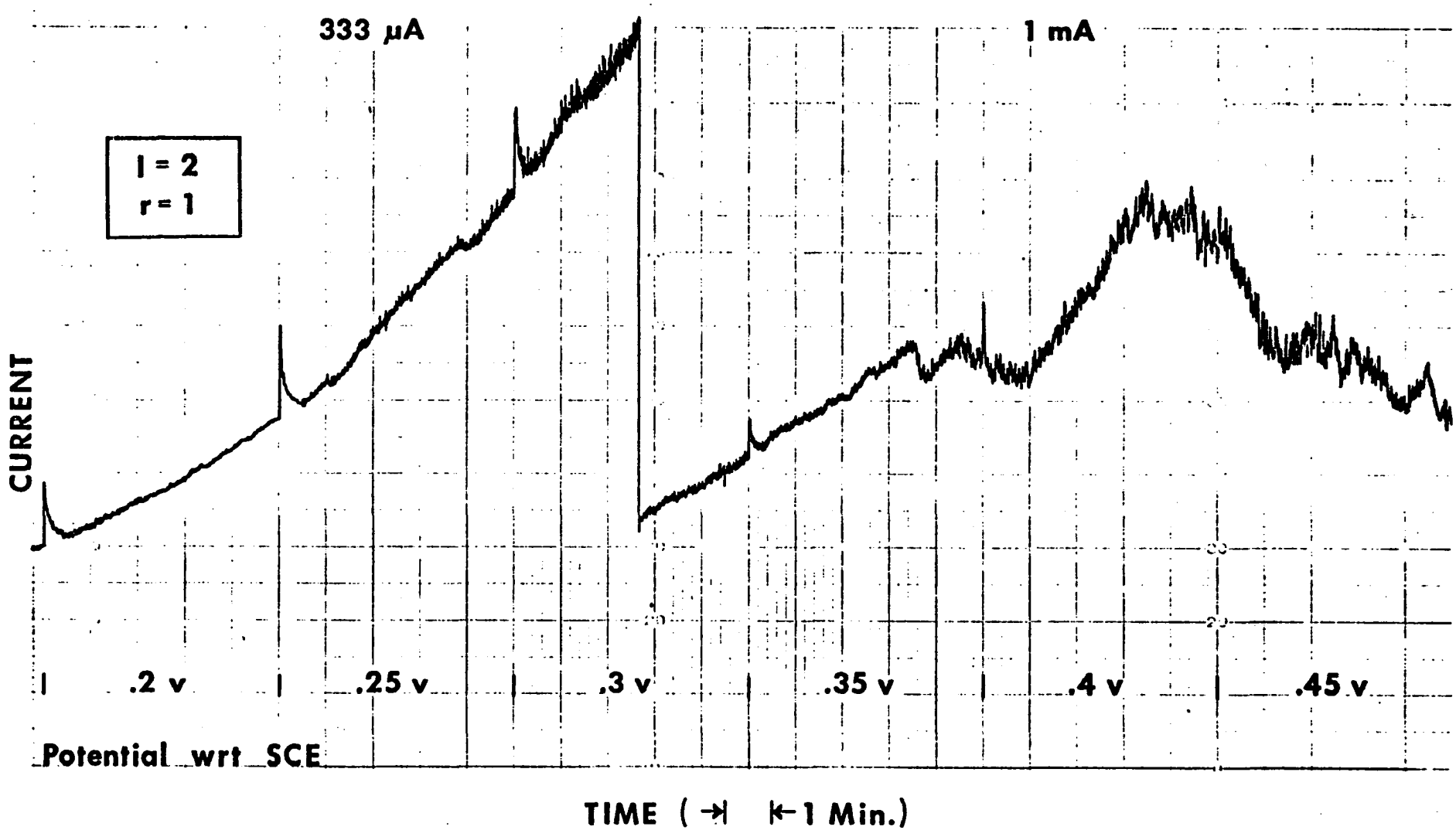

Fig. 5.3B.--Potentiostatic-Response Curves for I = 2, r = 1. (part 1 of 2)

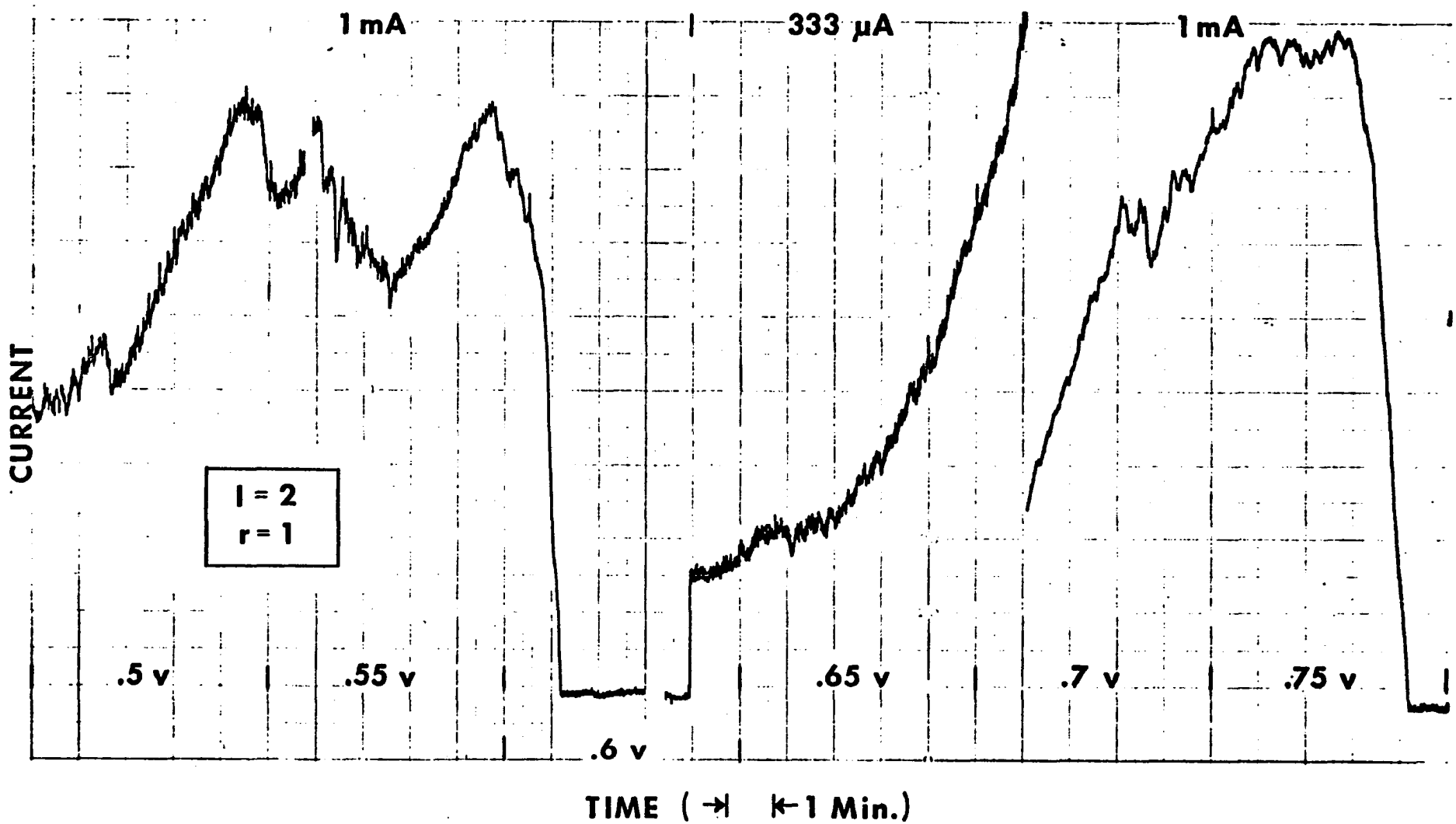

Fig. 5.3B.--(con't part 2 of 2)

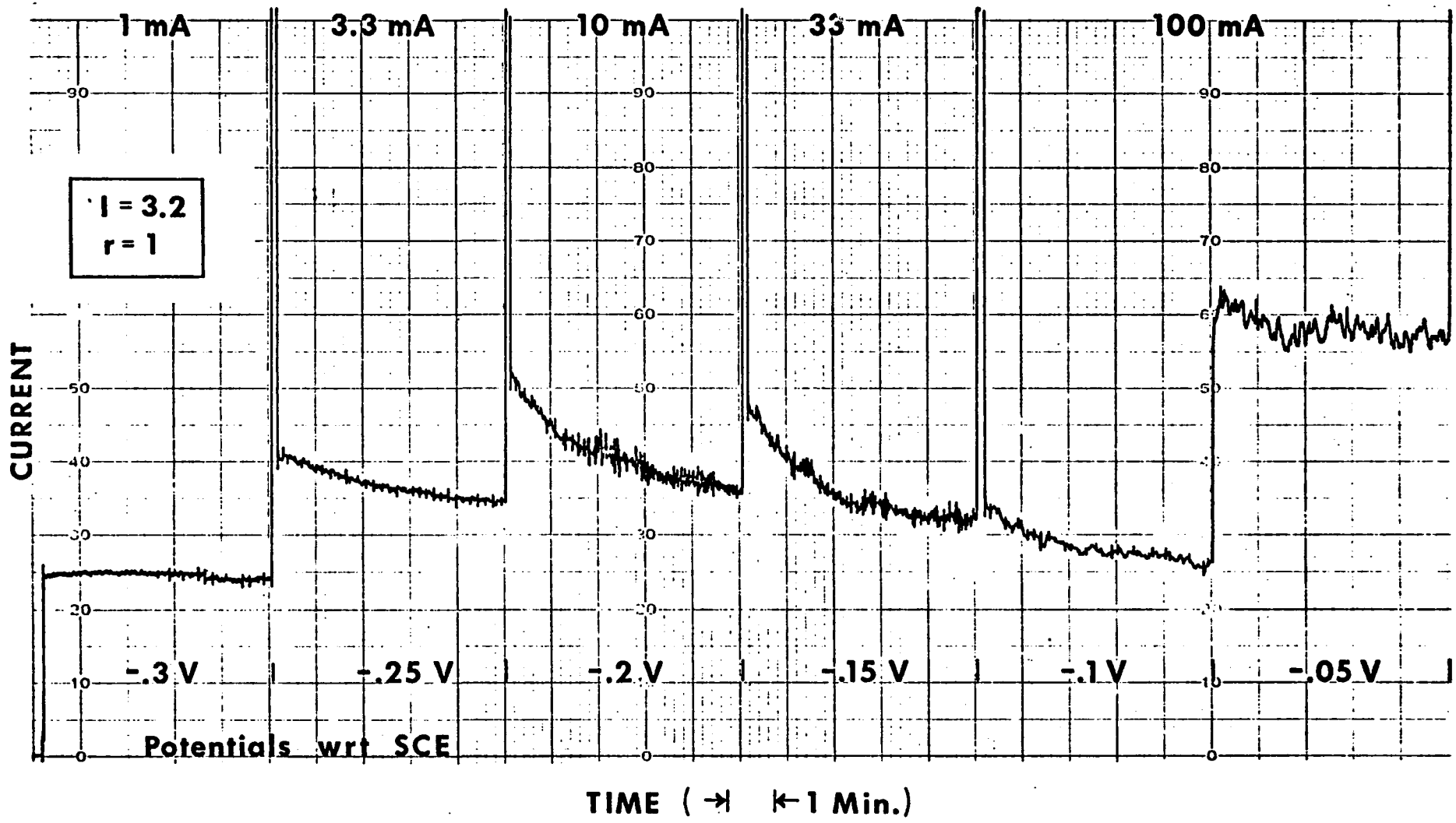

Fig. 5.4B.--Potentiostatic-Response Curves for I = 3.2, r = 1. (part 1 of 5)

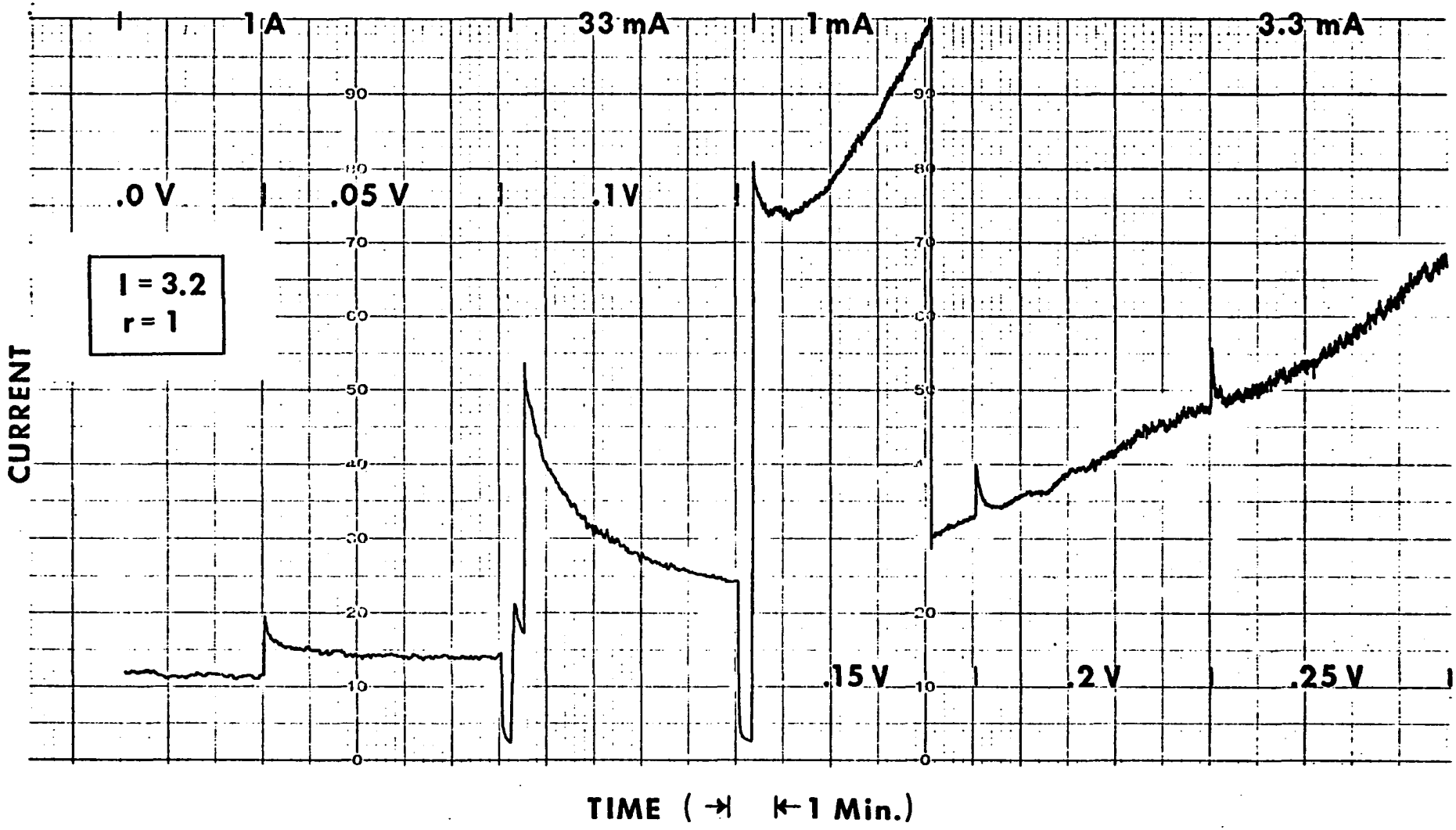

Fig. 5.4B.--(con't part 2 of 5)

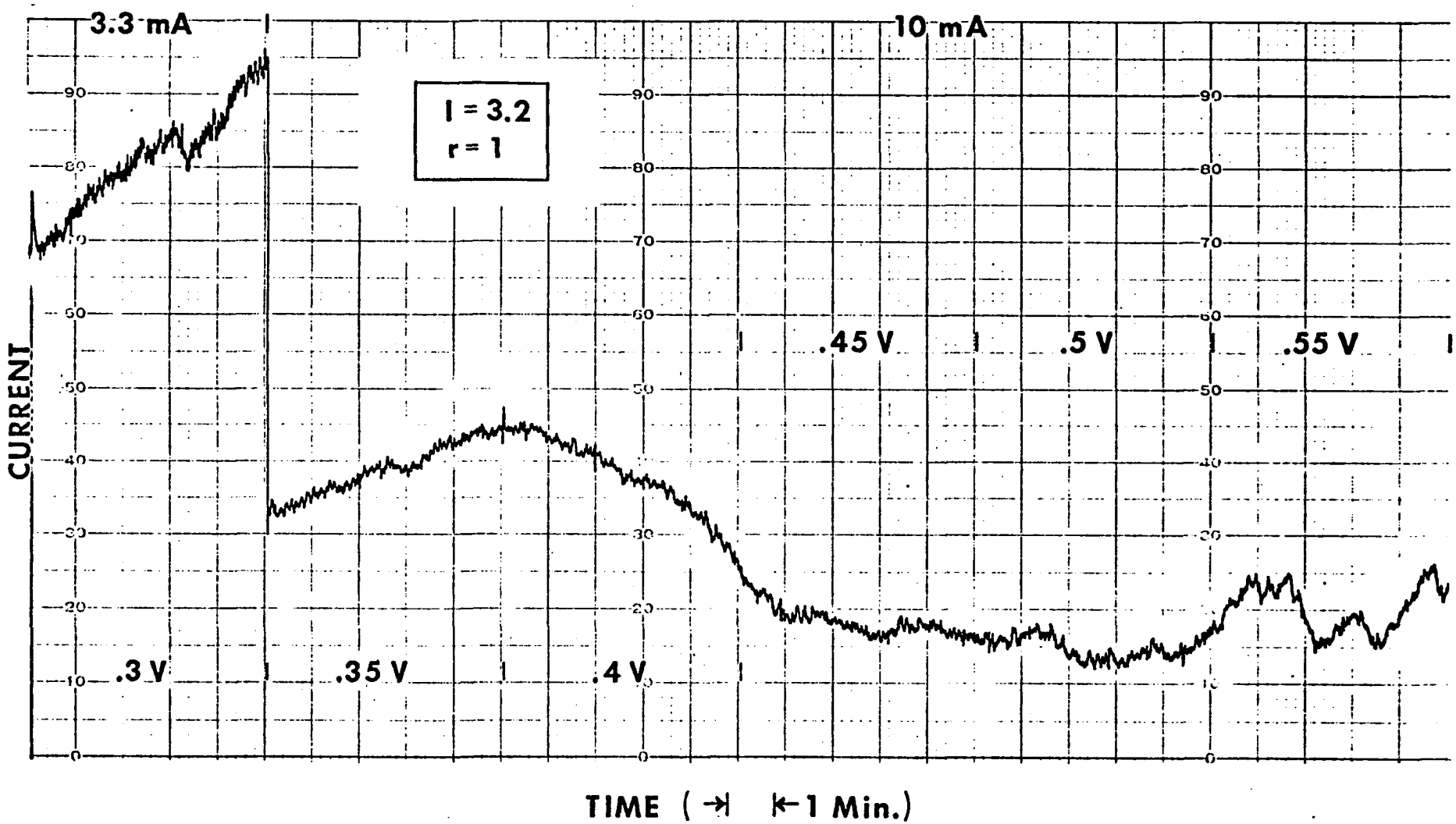

Fig. 5.4B.--(con't part 3 of 5)

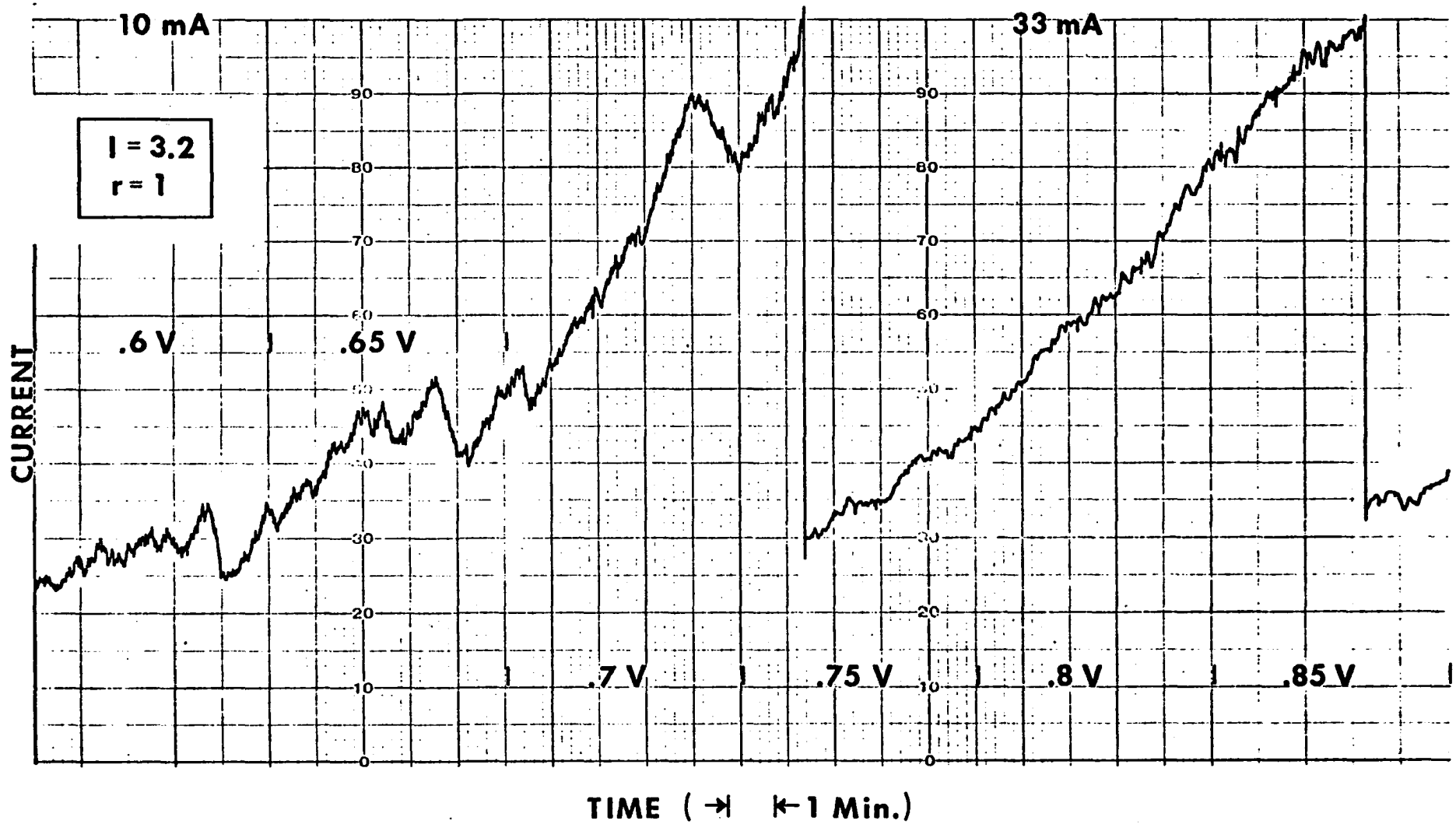

Fig. 5.4B.--(con't part 4 of 5)

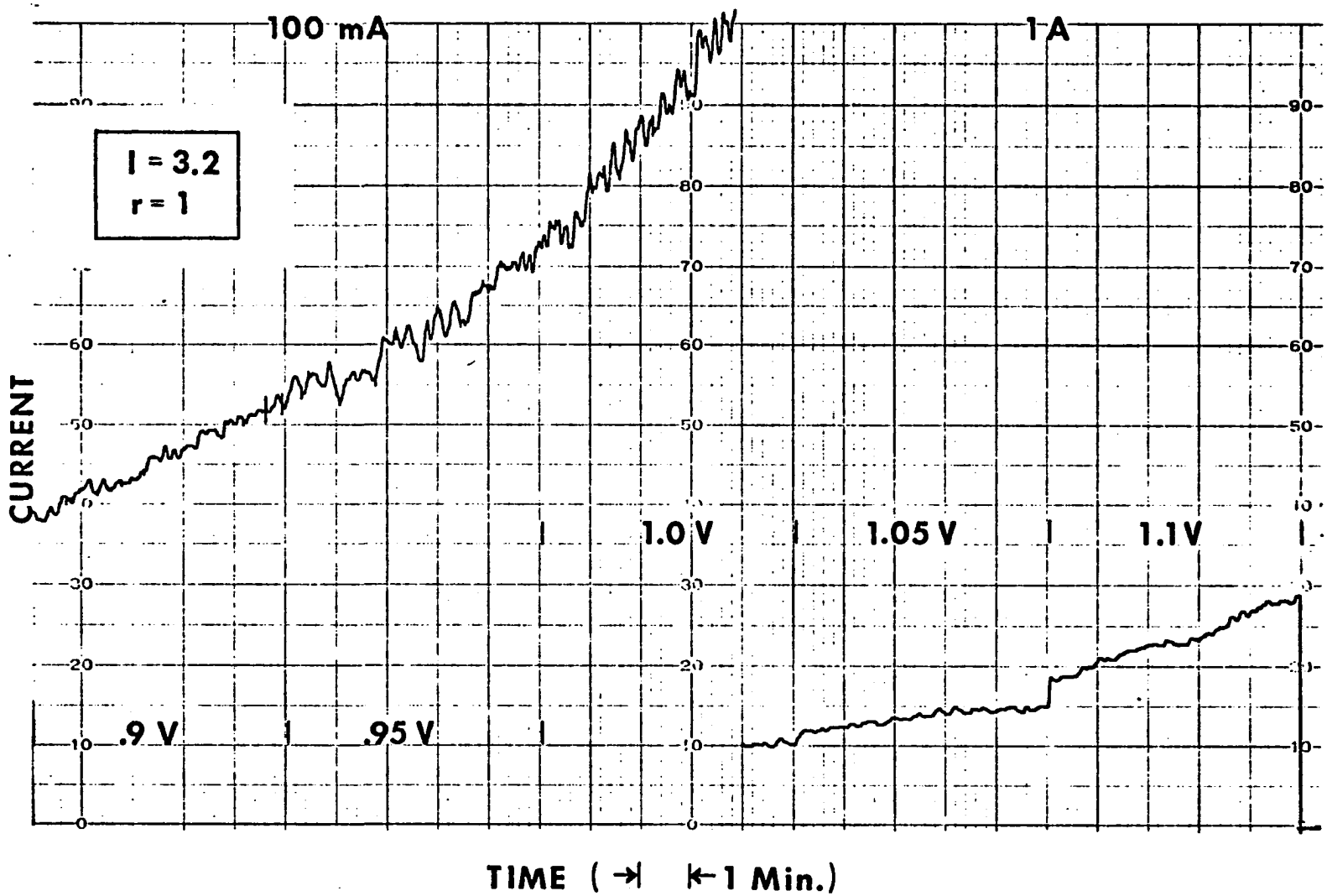

Fig. 5.4B.--(con't part 5 of 5)

C. Attack Mode Photographs

The purpose of these data are to illustrate the attack characteristics at various potentials with potentiostatic control. The data are all collected for $I = 2$ and anion ratios of 1 and 2. Reference to Figure 5.2A will serve to orient each case with respect to expected current magnitudes and known E-i and i-t characteristics. The method used to collect the data was generally to prepare and introduce specimens as described for polarization curves, except the potential was preset at the desired level and the specimen was polarized only at that potential for the desired duration. The specimen was immediately removed from the electrolyte, rinsed, dried, examined microscopically and photographed, all within 10 minutes. It is apparent, therefore, that these photographs do not represent the end condition encountered in producing the full polarization curve as shown in section A, as that would result in the accumulation of several attack types. The attempt here was to separate the modes by using a single potential only.

Figure 5.1C illustrates an intergranular attack mode at +1.1 V SCE, $I = 2$ and $r = 1$. Note that the surfaces carry fine scratches from surface preparation and that these do not provide particularly vulnerable sites. The attack for +1.1 V, $I = 2$ and $r = 0$ was identical in form and is, therefore, not shown. Reference to Figure 5.2A indicates that both $r = 1$ and $r = 0$ are represented by a common point in the reversible E-i region.

Figure 5.2C is at +0.7 V SCE, $I = 2$ and $r = 1$. Attack is a combination of grain etching (strong), intergranular (very faint) and pitting corrosion. It is interesting that the grain etch is particularly pronounced and suggests that crystallization rate control prevails. Mixed corrosion serves to emphasize the concept of anion competitiveness mentioned above.

Figure 5.3C is at +0.7 V SCE, $I = 2$ and $r = 2$. The attack shows pitting only and again abrasive marks are not particularly vulnerable. This particular specimen and that of Figure 5.2C were lightly polished using 0.3 μ alumina on a microcloth which accounts for the shape of the abrasive marks. Another specimen exposed to an identical electrolyte and a less noble potential (+0.3 V, $I = 2$, $r = 2$) gave

very similar results and was, therefore, not photographed.

Figures 5.4C and 5.5C are the cumulative effects of complete polarization scans in $\underline{N}$ HF and $\underline{N}$ H_3PO_4 respectively at 30°C. Both electrolytes produced intergranular attack and phosphoric acid also promoted etching. The implication is that HSO_4^-, $H_2PO_4^-$ and F^- have common or at least similar properties with regard to attack mode control.

The mere change in potential (the same specimen was used for both tests) as from Figure 5.1C to Figure 5.2C, the stepwise dependence on anion ratio as evidenced by similar attack modes at different ratios (as discussed under Figure 5.1C) and the stepwise dependence on potential as evidenced by similar attack modes at different potentials (as discussed under Figure 5.3C), all indicate the plausibility of interpreting rate determining processes in terms of active site interphase structure, where potential dependency enters the picture as Pourbaix [53] has shown by regulating thermodynamic stability.

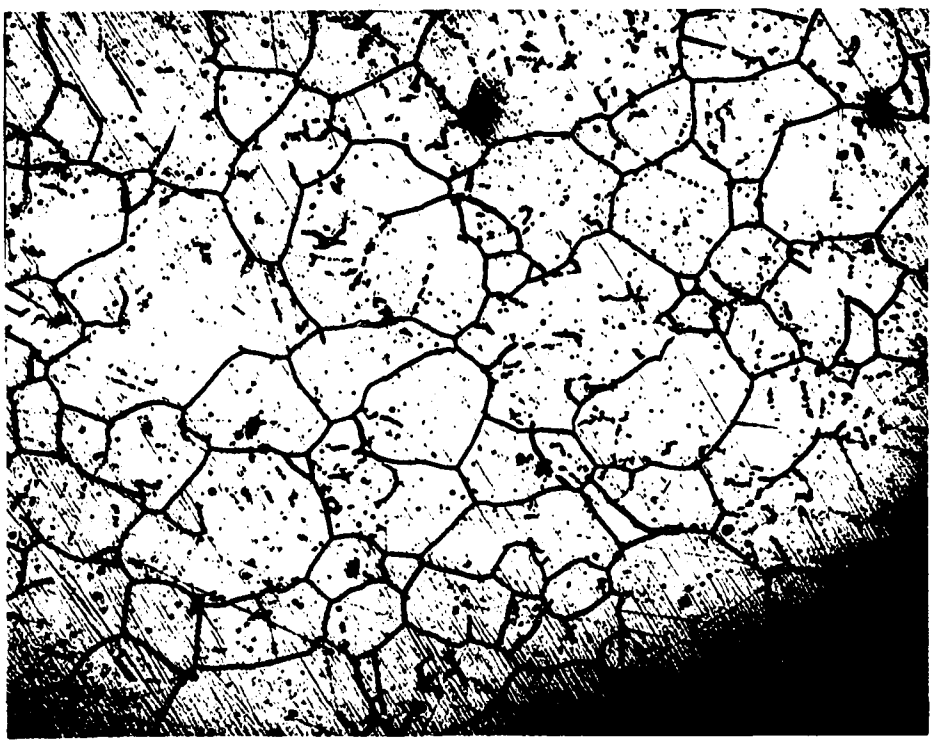

Fig. 5.1C.--Attack Mode at I = 2, r = 1, E = +1.1 V and at I = 2, r = 0, E = +1.1 V. 220X

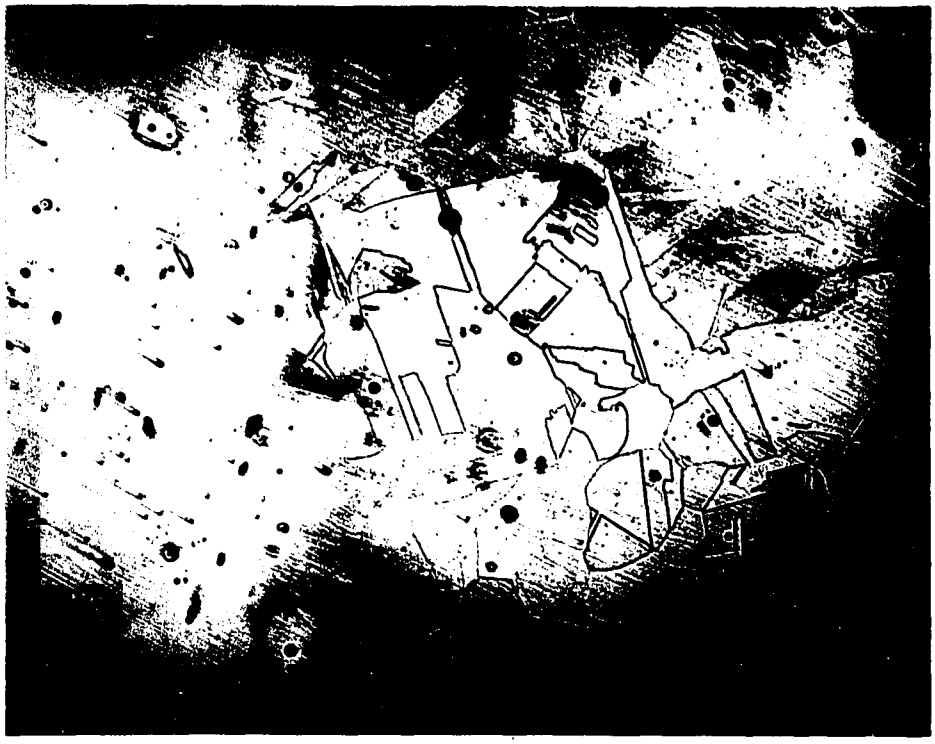

Fig. 5.2C.--Attack Mode at I = 2, r = 1, E = +0.7 V. 220X

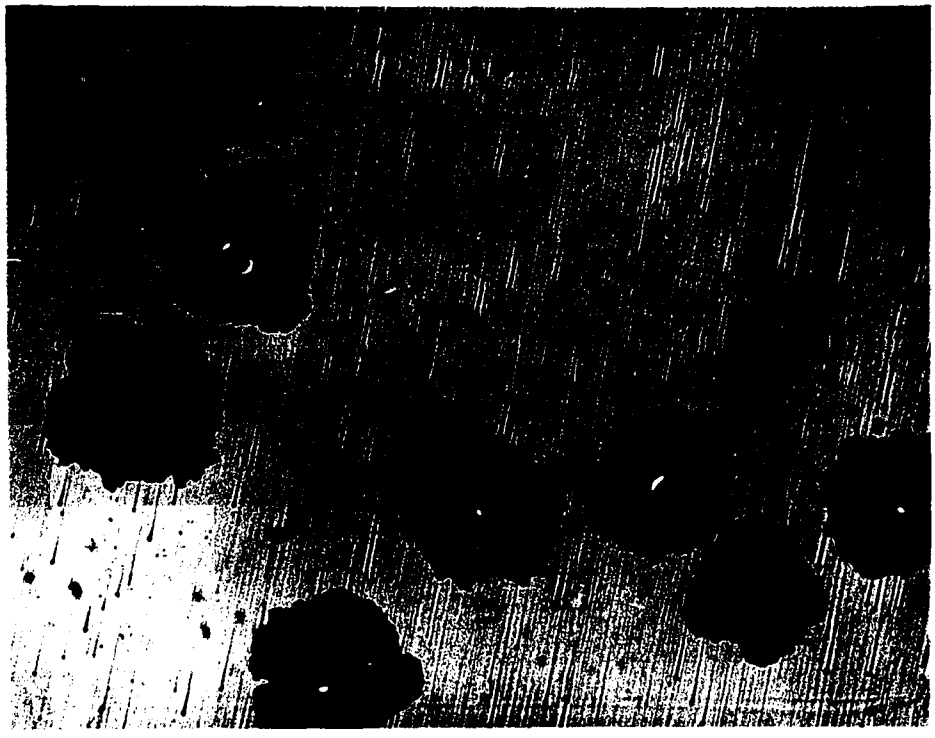

Fig. 5.3C.--Attack Mode at I = 2, r = 2, E = +0.7 V and at I = 2, r = 2, E = +0.3 V. 220X

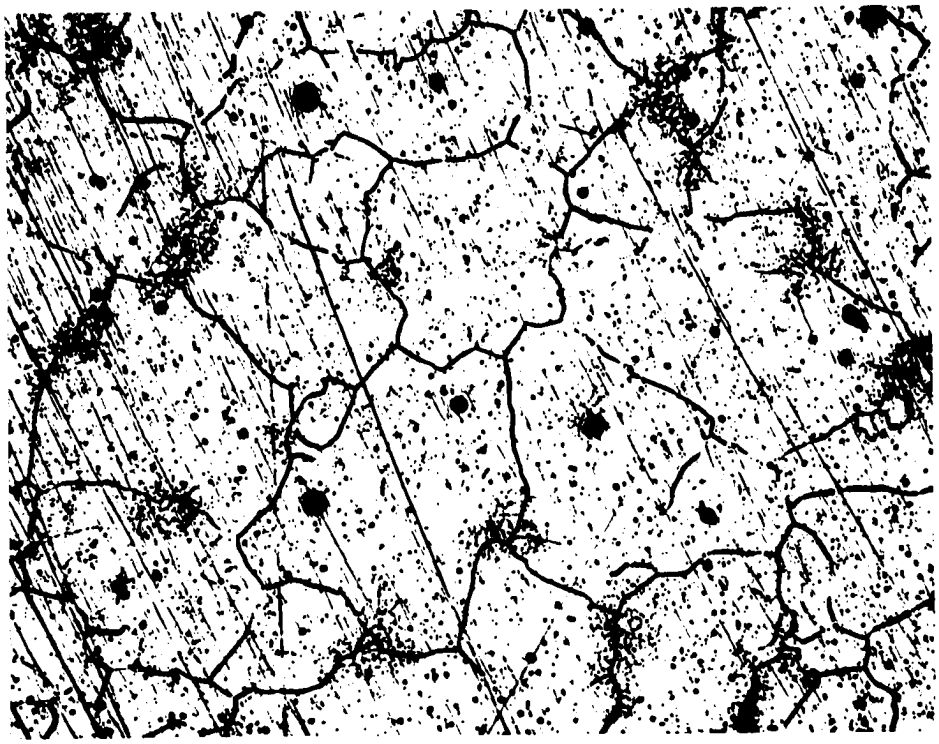

Fig. 5.4C.--Cumulative Attack over the Complete Anodic Polarization Curve in N HF. 220X

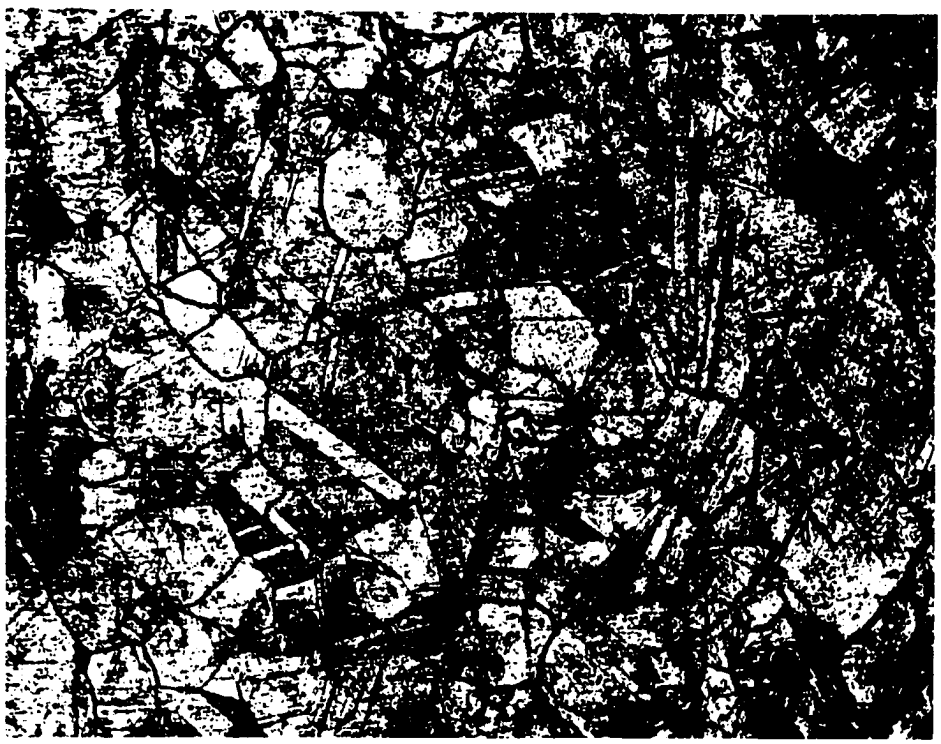

Fig. 5.5C.--Cumulative Attack over the Complete Anodic Polarization Curve in N H_3PO_4. 220X

D. Induction Time Curves

A description of the method used to collect current-time data for the analysis of induction times was given in Chapter IV. The available experimental data are indexed in Table 5.1D. Representative curves are shown in Figures 5.1D, 5.2D, 5.4D, 5.5D and 5.6D, and supplemental curves are presented in Appendix A. The curves are technically current-time curves from which induction times are measured, but since they are obtained after a particular sequence of operations which induce localized corrosion and are not general i-t curves, that fact will be noted by identifying them as induction time curves.

Two applications of induction time data are made in this work. The first is to test the applicability of the catalytic theory for the electrolyte-electrode system under study, and the second is to demonstrate the effect of potential on breakdown rates. The first point is pursued in this section and the second point is presented in Chapter VI.

Curve characteristics. Induction time was defined in Chapter III as the time between the imposition of an aggressive component and the appearance of the corresponding aggressive action as measured by an increased external current. A straight foreward example of the response encountered for Inconel X-750 is shown in Figure 5.1D. It was anticipated that the data would represent the breakdown process of passive films in aggressive electrolytes, but the analysis of this section will show that the interpretation of induction time data is dependent on further development of the concept of active site current densities.

In certain situations, difficulties are encountered in the current response as shown in Figure 5.2D. A source of the fluctuations shown can be argued in terms of the potentiostatic-response curves of section B. The latter represent current-time responses also, except the cumulative effects of preceding polarization are included and the equilibrium rather than kinetic aspect is emphasized by the incremented potential steps. Nevertheless, it is reasonable to assume that factors which gave rise to current-time fluctuations in the potentiostatic-response curves will also give rise to fluctuations in the induction time curves. A feature to note in Figure 5.2D, is the superposition of the competitive

TABLE 5.1D--Index of E, I and r at which Induction Times were Measured. (* designates a flow cell configuration.)

I	E (volts SCE)			
	r = 1	r = 3	r = 7	r = ∞
0.1	+0.70	+0.50 +0.60 +0.70	+0.40 +0.45 +0.50 +0.60 +0.70	+0.20 +0.25 +0.25 +0.35 +0.40
	r = 1.5	r = 2	r = 3	r = 7
0.32	+0.60 +0.70	+0.50 +0.60 +0.60 +0.70 +0.70*	+0.40 +0.50 +0.60 +0.70	+0.40 +0.40 +0.50 +0.60 +0.70 +0.70

TABLE 5.2D--Statistical Summary of Correlation Parameters for the Model $\ln t = b_o + b_1 \ln r$.

Number of cases	16			
F-level for inclusion	0.01			
F-level for deletion	0.005			
Tolerance level	0.001			
Multiple R	0.9679			
Std. error of Est.	0.5724			
Analysis of Variance	DF	Sum sqrs	Mean sq	F ratio
Regression	1	68.032	68.032	207.669
Residual	14	4.586	0.328	
Variables in Equation	Coefficient		Std. error	F to remove
Constant	b_o = 7.407			
Anion ratio	b_1 = -3.467		0.2406	207.669

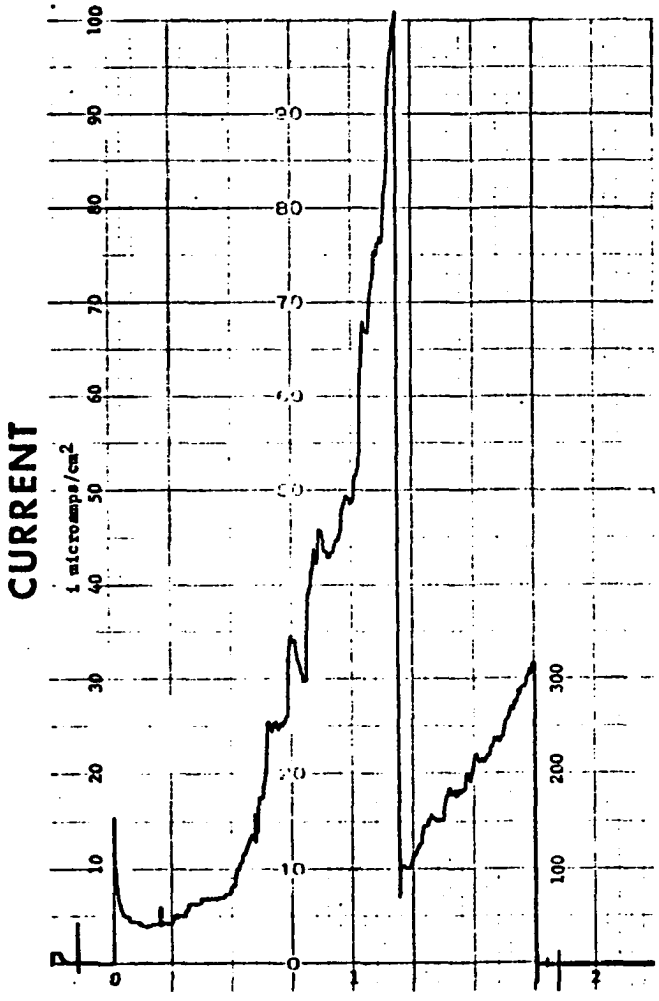

Fig. 5.1D.--Induction TimeCurve at I = 0.1, r = 3, E = +0.7 V.

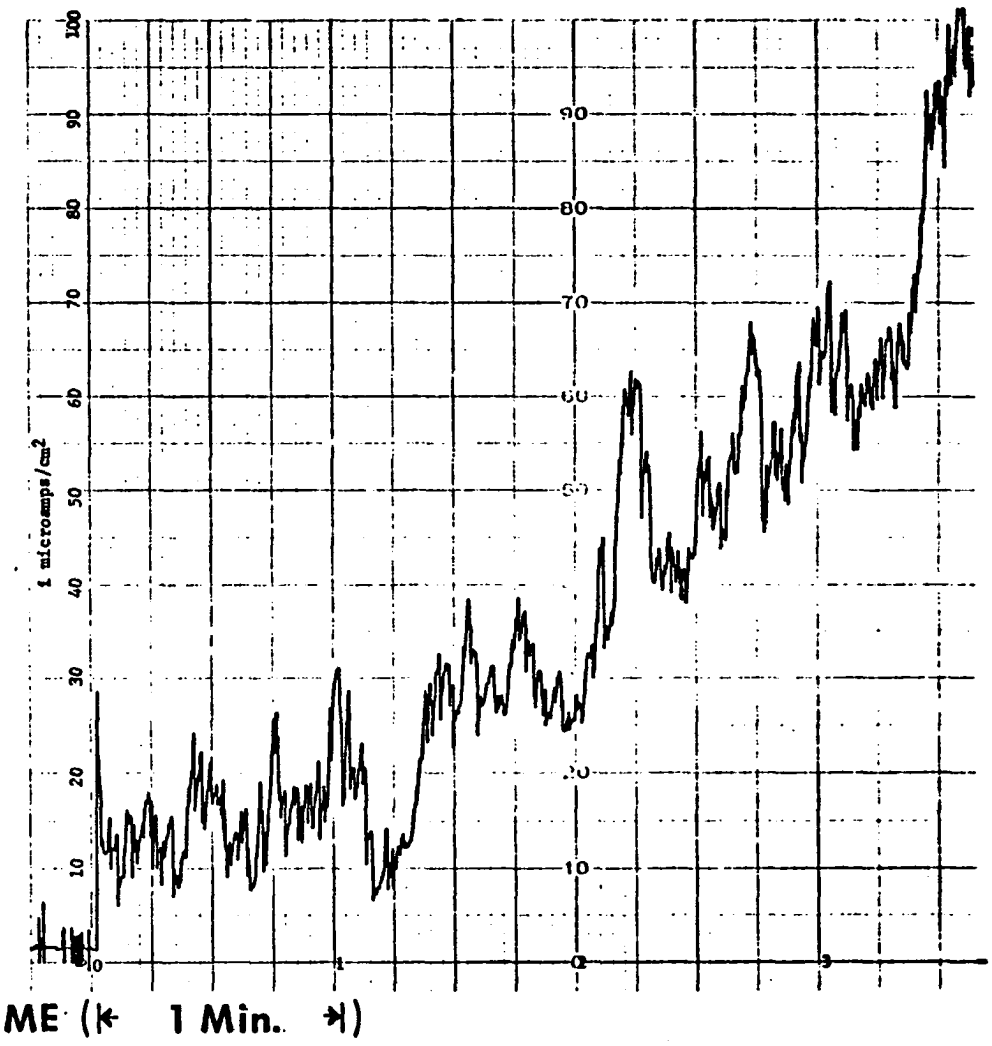

Fig. 5.2D.--Induction Time Curve at I = 0.1 r = 7, E = +0.4 V.

anion fluctuations on the increasing overall current. An attempt will be made to separate these two components.

One approach is to arbitrarily pick some current level, e.g., 100 μA, and temporarily re-define induction time as the time required to reach that limit. This has the undesirable feature of weighting the data with propagation effects, however, an analysis will serve as an orientation from which to view the curves.

The induction time curves will later be shown to be of the form

$$i = k\, t^2 \qquad \text{Eq. 5.1D.}$$

On the basis of work reported elsewhere [15, 30, 70, 71, 85], the time to 100 μA is expected to decrease as the potential becomes more noble (the discussion is limited to potentials between the critical pitting potential and the commencement of oxygen evolution). The time to 100 μA is also expected to decrease as the aggressiveness of the electrolyte increases. The functional combination of the latter two factors with Equation 5.1D, requires that

$$k = f(\eta, I, r)$$

Substitution of this function into Equation 5.1D, and taking logarithms gives

$$\ln t = b_o + b_1 \ln[f(\eta, I, r)] \qquad \text{Eq. 5.2D.}$$

An empirical correlation was obtained using linear regression techniques for the model described by Equation 5.2D, with $f(\eta, I, r) = r$. Correlation parameters are summarized in Table 5.2D, from which it appears that anion ratio is the principle independent variable.

An alternative method was sought to eliminate propagation effects to improve the evaluation of induction time. For this purpose some frequently used suppositions are useful.

1) The current density of an active site, i_a, does not increase as the total current increases; rather, the active area, A, increases.
2) The current density of the passive surface changes very little as active sites form, consequently, almost all of the external current increase is due to active site formation and growth.

3) The pit is geometrically approximated by a hemisphere, which implies that dissolution is radially uniform in rate from the initiation site.

The shape of the i-t curve can now be estimated for the early stages of pit formation. A simulation approach is used to emphasize the physical aspects of the analysis.

a) Suppose that the primary initiation act involves the removal of one metal atom which has a volume $\underline{V}$.

b) If the pit volume V is in a hemispherical shape, the radius and the surface area of the hemisphere are

$$r = \sqrt[3]{3V/2\pi}$$

$$A = 2\pi r^2$$

c) Using supposition (1) above, for sufficiently small δt, the current

$$\zeta = i_a A$$

where ζ designates the total current from the pit.

d) The actual number of charges transported during δt is

$$Q = k \zeta \delta t.$$

e) The number of atoms oxidized is Q/n, so with the transport of Q charges there is an associated change in pit volume of

$$\delta V = \underline{V} Q/n$$

f) By removing this volume as a thin hemispherical shell, if the previous pit radius was r_i, then the previous volume was

$$V_i = 2\pi r_i^3 /3$$

and the new total volume becomes

$$V_{i+1} = V_i + \delta V$$

from which the new pit radius becomes

$$r_{i+1} = \sqrt[3]{(3\delta V/2\pi) + r_i^3}.$$

A numerical solution of this scheme is shown graphically in Figure 5.3D, for different values of active site current density, i_a.

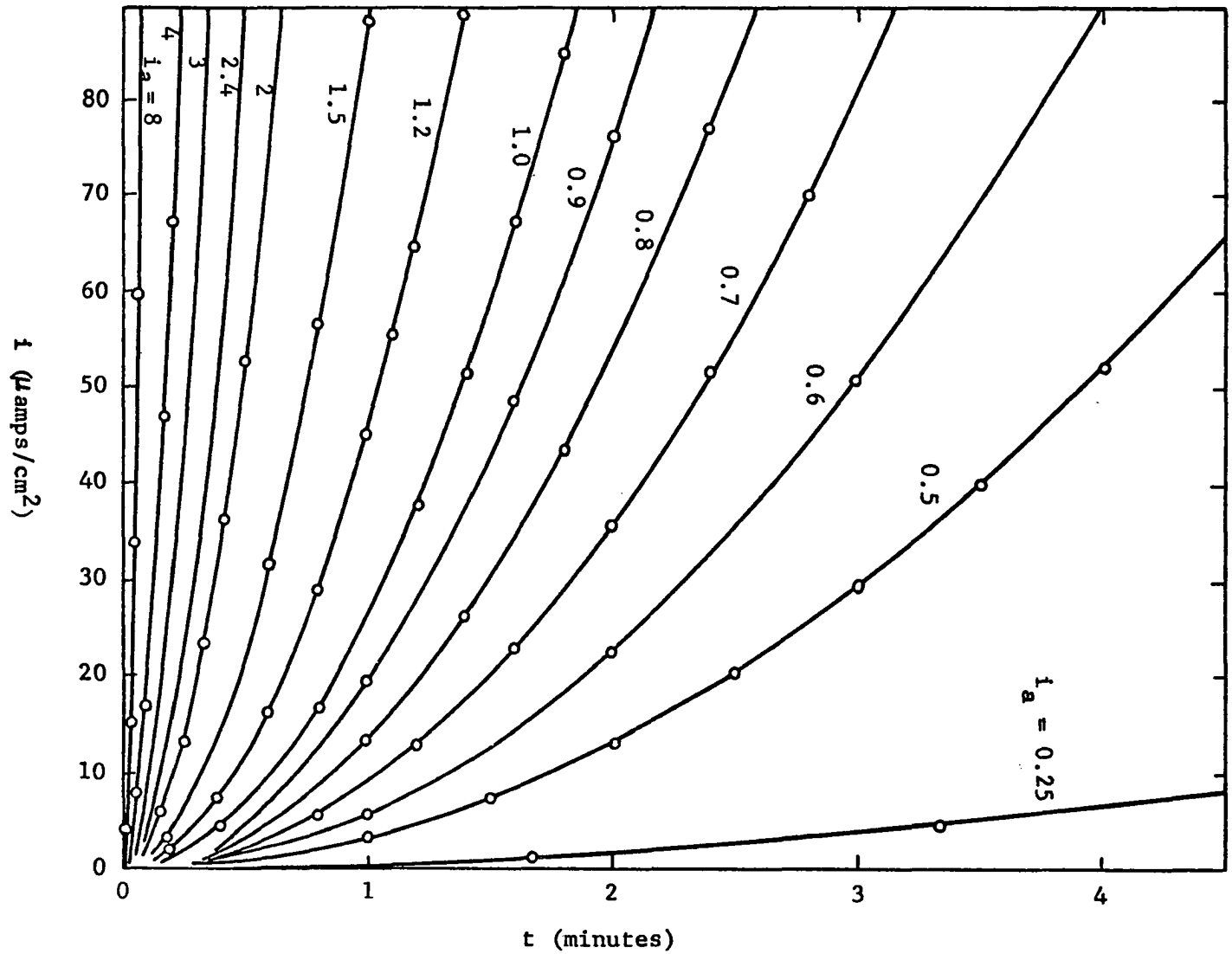

Fig. 5.3D.--Calculated i-t Curves for Various Active Site Current Densities.

The curves are analytically of the form given in Equation 5.1D ($i = k\ t^2$) which is in harmony with work of Schwenk [61]. The same result can be derived analytically:

A) At any time, t, the area of the pit, A, can be expressed in terms of the pit radius, R, as $A = 2\ \pi\ R^2$.

B) By supposition 1, above, the active site current density is constant, therefore, the total current from the pit, ζ, is

$$\zeta = i_a\ A = i_a\ 2\ \pi\ R^2. \qquad \text{Eq. 5.3D.}$$

C) Supposition 3, above, is expressed: (dR/dt) = constant or $R = ct$

D) Substitution of result 3) into result 2) gives the desired equation as $\zeta = i_a\ 2\ \pi\ c^2\ t^2$, which is equivalent to Equation 5.1D.

The shapes of the calculated i-t curves are similar to those obtained experimentally.

The application of Equation 5.3D, gives an important result. Pit diameters required to sustain a total pit current of 10 μA were calculated for various active site current densities. Table 5.3D, summarizes the results. The pit diameters range from 8 to 25 microns and are, therefore, microscopically visable when their current contribution is approximately equal to the total passive current contribution, at i_a values up to 10 $\mu A/cm^2$. It appears that induction time represents not only the lumped processes of pit initiation but also the propagation effects up to some few microns in diameter.

Application of the calculated i-t curves in Figure 5.3D provides a basis for estimating induction times with propagation effects removed. The method will be described by an example. Figure 5.4D shows a current increase beyond 11 minutes. The rising portion of the curve can be described by an $i = k\ t^2$ curve similar to one of those shown in Figure 5.3D. For the purposes of the example, if one pit is assumed responsible for the current increase, the calculated curve can be superimposed on the experimental curve. Since the calculated curves were established with time zero as the instant of localized film breakthrough, the time difference between the experimental zero time and the calculated

TABLE 5.3D.--Pit Diameters for Various Active Site Current Densities when the Total Pit Current Equals 10 Microamps.

i_a (Amps/cm^2)	Pit Diameter (cm)
10	0.80×10^{-3}
6	1.03×10^{-3}
4	1.26×10^{-3}
2	1.78×10^{-3}
1	2.52×10^{-3}

zero time represents the induction time with propagation effects removed and the curve slope indicates i_a. Data estimated by the application of this technique are summarized in Table 5.4D. An empirical correlation of induction time, τ, and active site current density, i_a, was obtained for the data of Table 5.4D according to the model

$$\log \tau = b_o + b_1 i_a.$$

A summary of the correlation parameters is given in Table 5.5D. The result simply says that at the 1 percent level of significance we can reject the hypothesis that there is no association between $\log \tau$ and i_a. Intuitively, one should expect the induction time to be inversely dependent on how fast the dissolution processes occur, as the data show. The assumption of the formation of a single pit is a weak point thus far and further work is recommended in Chapter VII.

Flow cell method. The induction time response at constant potential as measured with a flow cell is given in Figure 5.5D. Qualitatively, the current rises slowly at first but accelerates in a manner similar to those previously shown. Comparison with the batch method used in this work can be made from Figure 5.6D which employs identical I, r and E values. Qualitatively, there is no detrimental effect from electronic switching; however, the time to initiation suggests the influence of a boundary diffusion layer.

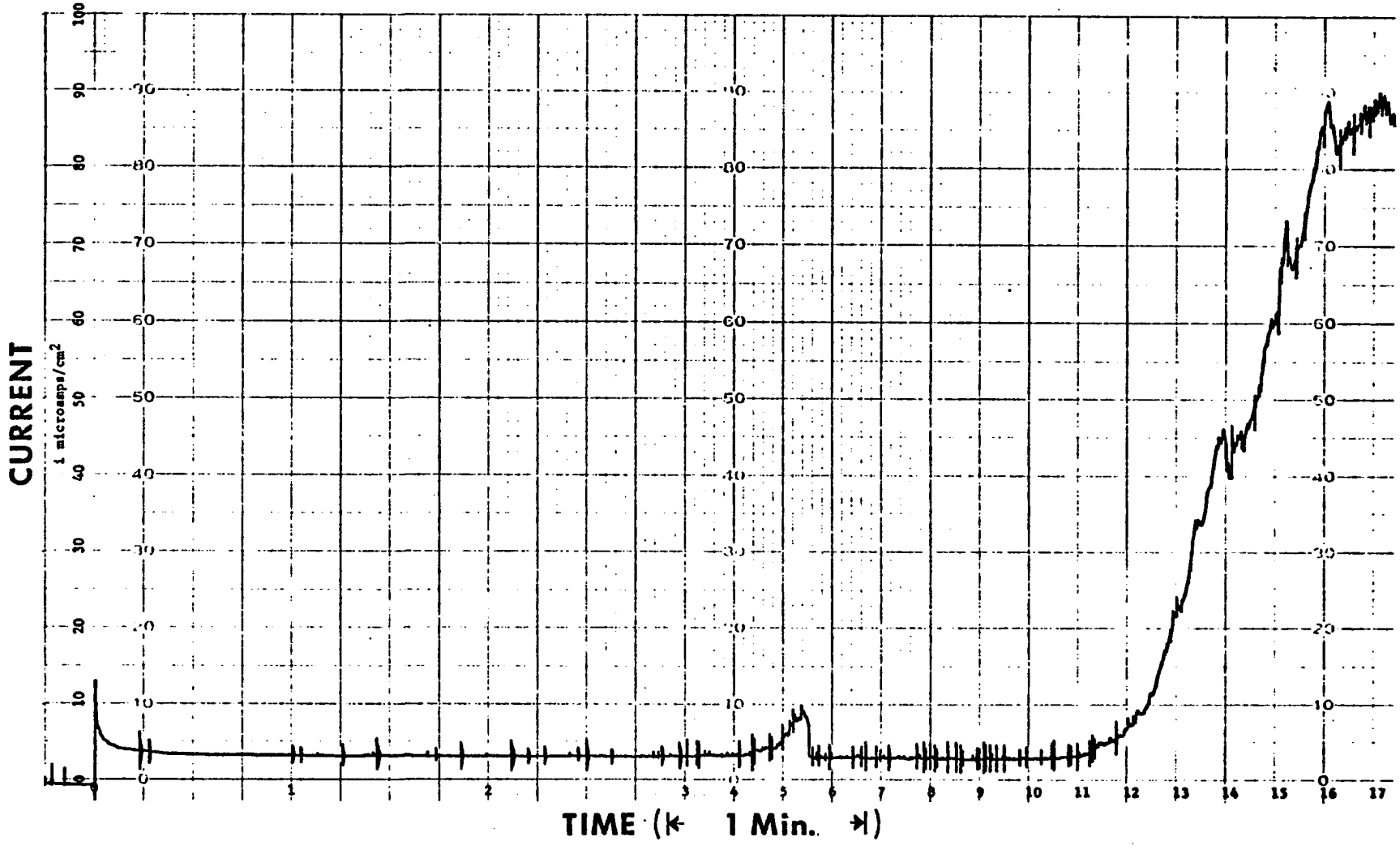

Fig. 5.4D.--Induction Time Curve at I = 0.32, r = 1.5, E = +0.7 V.

TABLE 5.4D--Induction Times and Active Site Current Densities for Experimental Curves with Propagation Effects Removed.

I	r	E (V)	i_a (A/cm^2)	τ (sec)	Cl^- (M)
0.1	1	+0.7	--	>1.15x10^4	0.025
0.1	3	+0.6	2	16	0.05
0.1	3	+0.7	1.5	11	.05
0.1	7	+0.6	4	3	.07
0.1	7	+0.7	3	4	.07
0.1	∞	+0.2	0.5	30	.1
0.1	∞	+0.25	0.6	75	.1
0.1	∞	+0.35	4	6	.1
0.1	∞	+0.4	4	1.5	.1
0.32	2	+0.5	1.2	30	.128
0.32	2	+0.6	1.2	12	.128
0.32	2	+0.7	1.2	35	.128
0.32	3	+0.4	4	4	.160
0.32	3	+0.5	3	5	.160
0.32	3	+0.6	3	12	.160
0.32	3	+0.7	3	9	.160

TABLE 5.5D--Statistical Summary of Correlation Parameters for the Model $\log \tau = b_o + b_1 i_a$.

Number of cases		15		
F-level for inclusion		0.01		
F-level for deletion		0.005		
Tolerance level		0.001		
Multiple R		0.8859		
Std. error of est.		0.2222		
Analysis of Variance:	DF	Sum Sqs	Mean Sq.	F ratio
Regression	1	2.341	2.341	47.406
Residual	13	0.642	0.049	
Variables in Equation:	Coefficient		Std. error	F to remove
Constant	b_o = 1.76107			
i_a	b_1 = -0.31354		0.04554	47.406

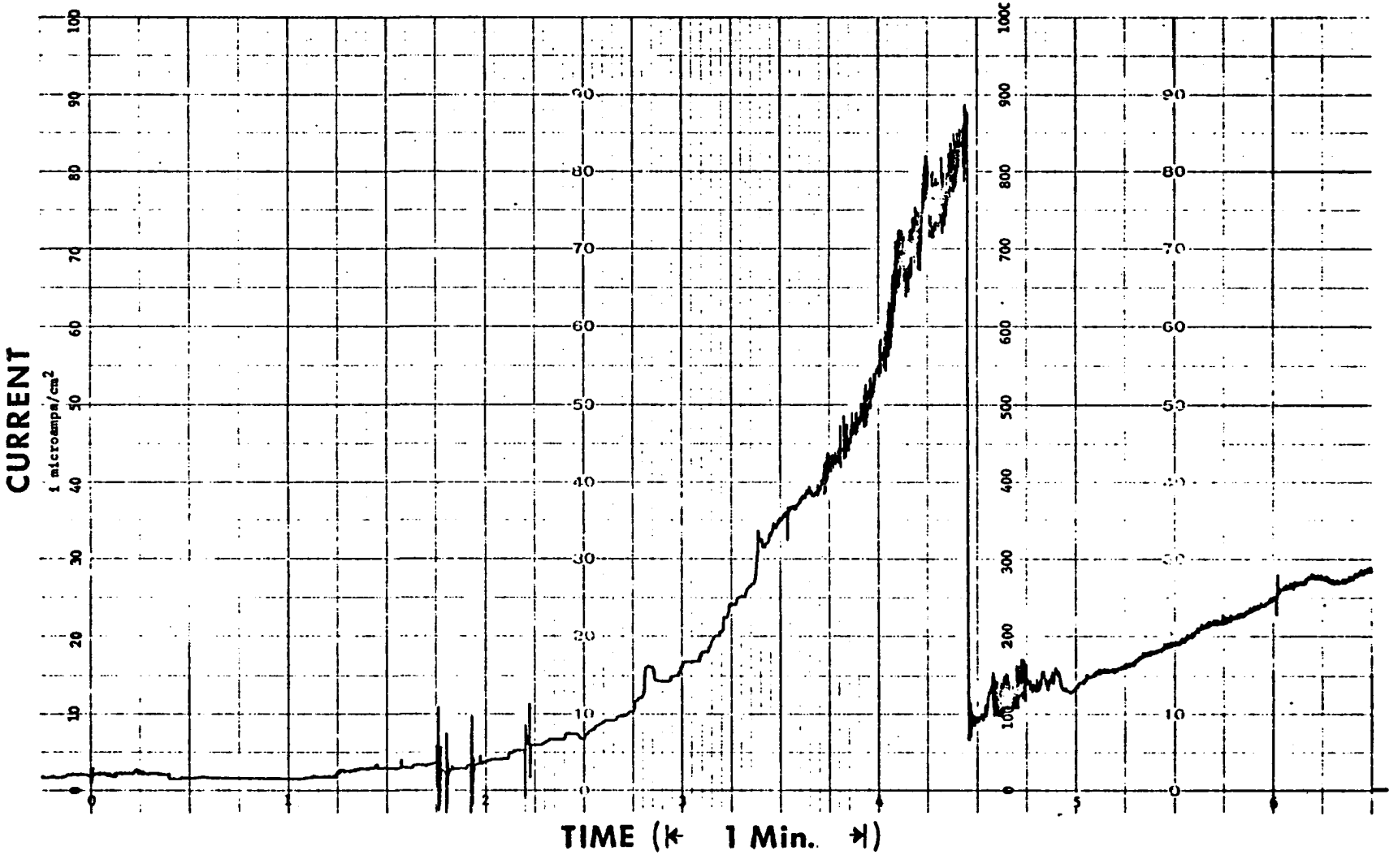

Fig. 5.5D.--Induction Time Curve for a Flow Cell at I = 0.32, r = 2, E = +0.7 V.

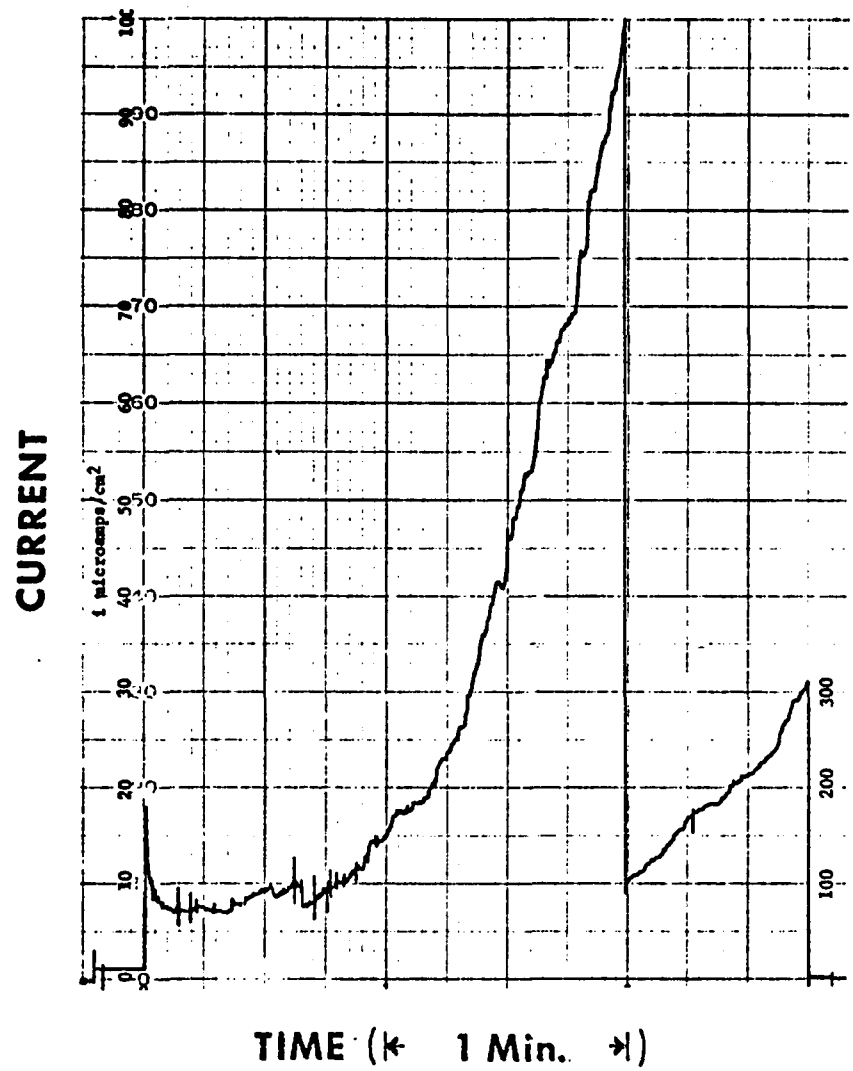

Fig. 5.6D.--Induction Time Curve at I = 0.32, r = 2, E = +0.7 V.

CHAPTER VI

DISCUSSION

Potential and i-t instability. The i-t fluctuations observed near +0.7 V SCE in Figure 5.4A, curves (n) and (o), cannot be satisfactorily explained in terms of the superposition of anodic and cathodic processes on a common surface. Two facts establish the basis for this conclusion. First, the system described in this work has the form shown as case 1 in Figure 4.6, which means that unstable passivity simply does not occur. Second, the potential difference between the active and passive sites has a maximum value of 0.5 V for the particular situation involving a large active site current density, but if the argument for anode-cathode superposition were correct, a potential difference of near one volt would be required. Detailed discussion of these factors is given in Chapter IV under subsections, Active Site Potential and Control Mechanics, respectively.

This situation creates the burden of explaining large current fluctuations in terms of small potential differences. Curve (c) in Figure 4.3, was hypothesized to represent the E-i response expected as if the entire surface were active without the superposition of passivity. (An equivalent interpretation of curve (c) is that it represents the active site current density, i_a.) In terms of Figure 4.3 the explanation is that the observed fluctuations at the active site are between curve (a) and curve (c) with a relatively small potential difference involved. Potentiostatic current-time curves were analyzed at different potentials to identify the nature of the potential dependency. Data for $I = 0.1$ and $r = 7$ are replotted in Figure 6.1 to show that the time to 100 μA tends to group and does not correspond directly with potential.

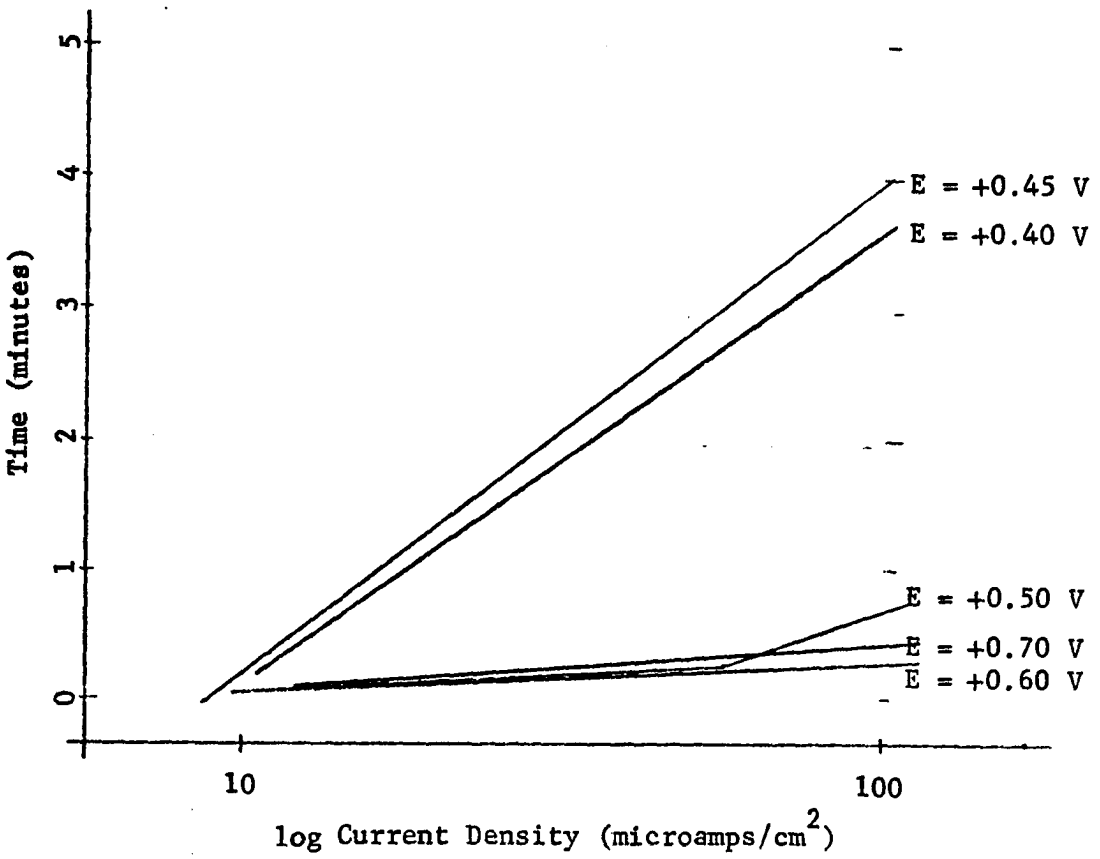

Fig. 6.1.--Current-Time Curves for I = 0.1, r = 7 and Various Potentials to Illustrate an Apparent Discontinuity in the Induction Time-Potential Relationship.

Postulate of active site structures. A basis for the apparent discontinuity in potential dependence shown in Figure 6.1 can be qualitatively established in terms of Pourbaix diagrams [53]. The nickel-water system has characteristic regions where specific species are thermodynamically stable, and at a given pH a particular specie may exist over a particular potential interval. Additional products will result from the inclusion of chloride ions with the establishment of new potential-pH product-stability-domains. The inclusion of an additional anion with the nickel-water system requires the construction of a concentration axis which creates three-dimensional stability domains. Even though the Pourbaix diagrams indicate only what is thermodynamically possible and cannot be used for direct kinetic interpretation, three-dimensional nickel-water-chloride-sulfate systems can be envisioned which would result in apparent potential discontinuity in terms of reaction product stability. The implication is that the apparent potential-induction time discontinuity shown in Figure 6.1 occurs because the active site structure involves a potential dependent transition.

Evidences of active site structures. Anion participation in the corrosion process is a major evidence pointing to active site structures. From the attack mode analysis in Chapter V, it was shown that at constant potential, an increase in the $Cl^-/SO_4^=$ ratio eliminated intergranular attack and grain etching but enhanced pitting. Since aqueous chloro-nickel complexes are unknown, specificity of attack implies that the anion is involved as a salt, e.g., $NiCl_2 \cdot (H_2O)_4$.

The potentiostatic-response curves shown in Chapter V also provide evidence of active site structures. Note that chloride attack is accompanied by hysteresis effects when the potential scan direction is reversed in the transpassive region and that sulfate has no hysteresis effects. Figures 5.1B and 5.2B are summarized in Figure 5.1A. One might argue that product accumulation is the cause of the hysteresis for the chloride system and that no product accumulation occurs for sulfate. However, since large local currents are associated with both attack modes and chloride salts tend to exhibit higher solubility than sulfate salts, it is concluded that product accumulation occurs for both. Consequently, simple mass accumulation is not by itself the important

factor, but rather the form or structure of the product regulates attack mode and rate. It is reasonable to expect a compact product layer to impose different conductive and diffusive requirements than an unconsolidated, highly solvated product. A conductive film would permit direct potential-current response, while the response of a capacitive film would be exponential.

Further evidence for active site structures is shown in the simultaneous examination of the polarization curves and the potentiostatic-response curves of Chapter V. Curves (e), (f) and (g) in Figure 5.2A demonstrate sulfate control, fluctuations between sulfate and chloride control and chloride control, respectively. Figure 5.3B (which corresponds to curve (f) in Figure 5.2A) illustrates the nature of the shift from chloride to sulfate control. Note that at +0.75 V the response continued as it had at +0.7 V until conditions became such that the transition occurred with no further change in potential. This is interpretable as a structure change with the establishment of a definite sulfate (oxide combined) controlled end-state. Nickel-chloride salts are typically labile [11]. No direct evidence is in hand on the various chemical compositions or structures of the active site films, however, it appears desirable to define them on both sides of the unstable region described here.

Vetter and Strehblow [77] analyzed the sharpness of the active-passive boundary in terms of electrolyte conductivity to conclude that "the pit surface cannot be an ordinary active metal surface not covered with a layer." They also reported electron microprobe analysis of pit surfaces to show chloride enrichment even though no product precipitation was possible in the pit.

Catalytic and Displacement Theories

A central point of the catalytic theory is the evaluation of τ, a matter which requires further work for Inconel X-750. In the discussion in Chapter III, $1/\tau$ was used as an estimate of the rate of lumped breakdown processes, and it was shown that the rate was proportional to the nth power of the chloride concentration which in turn was interp-

reted as the reaction order. The value of n was estimated to be 2.5 to 4.5 for austenitic stainless steel [30]. The application of two methods of estimating τ for Inconel X-750 led to values of n from 7.5 to 9.5 with the higher values associated with the removal of propagation effects. These large values of n are well out of the range for interpretation as reaction orders, hence, further investigation of kinetic parameters for Inconel X-750 must follow the separation of the overall initiation process into component parts.

Differences between the induction time behavior of the 18 chromium-8 nickel austenitic stainless steel and the Inconel X-750 is clearly evident. The stainless steel exhibited a sharply defined τ and the nickel alloy response ranged from a gradually accelerating anode current to an almost immediate large increase. A flow cell should be used cautiously as the superposition of a large active site current density on the mass transport through the boundary layer could plausibly produce a sharp response.

The catalytic theory is also based on the formation of the "initial transitional complex" which is described as $(M^{+m} \cdot x\ Cl^{-x})^{m-x}$ where x is 2.5-4.5. Nickel, the major constituent of Inconel X-750, is reported not to form any anionic chloro-complexes in aqueous solution even at the highest attainable chloride concentrations [11].

In either case mentioned above, there is reasonable doubt regarding the direct applicability of the catalytic theory for the present case.

The tenor of the displacement theory is toward the fundamental importance of structure, i.e., the displacement of a non-aggressive specie by an aggressive one and, as such, is largely in harmony with the present work. Here again, however, the suggestion is expressed for the formation of a "surface complex" between "chemico-adsorbed" aggressive anions and the metal. In the case of nickel and chloride, the improbability of a charged complex leads to difficulty in accounting for specificity of attack. The theory does not consider localized attack forms other than pitting such as intergranular corrosion or grain etching.

CHAPTER VII

CONCLUSIONS AND RECOMMENDATIONS

Eight specific points resulted from the work performed. Key points are emphasized with an asterisk (*).

1) Current-time instability was observed for intermediate chloride/sulfate ratios (see curve (f), Figure 5.2A).

2) Restrictions on the maximum allowable potential shift associated with the instability were evaluated (see Control Mechanics, Chapter IV).

*3) Potential limitations were shown to prevent the interpretation of the fluctuations as the superposition of cathodic and anodic processes on the same surface (see Active Site Potential, Chapter IV).

*4) Active site reaction-product-structures were postulated to account for the observed instability (see Chapter VI).

5) Anion participation in the corrosion processes and in the attack mode was cited as the first point of evidence for active site structures (see Chapter V, sections A, B and C).

6) A method was developed to obtain induction times without boundary-layer diffusion interference (see Chapter V, section D).

7) Induction time data demonstrated grouped potential responses to establish a second point of evidence for active site structures in terms of Pourbaix diagrams (see Chapter V, section D and Chapter VI).

8) Potentiostatic-response characteristics demonstrated a definite end-state in the transition from chloride to sulfate control of corrosion porcesses to establish a third point of evidence for the structure concept.

Some aspects have emerged which clearly need more work. Four suggestions are briefly summarized below.

A) The analysis of induction time was based on the concept of an active site current density. Further analysis of the induction time

in terms of the active site current density depends on the time-wise separation of the cumulative contributions of several active sites to the overall i-t curves. The separation would allow highly improved estimates of i_a and permit extrapolation to zero time as a means to estimate the active site current density at the time of induction. Knowledge of i_a at the time of passive film breakthrough for specific experimental conditions would provide a basis for the investigation of factors which govern the variance of the active site current density. (The analysis of i_a based on developed pits includes the effects of product accumulation and precipitation.) Microscopical studies [28] have been conducted toward this end, but the experimental limitations are those of magnification of the total surface in-situ and monitoring all of the active sites simultaneously.

Techniques developed for the measurement of induction time in this work can provide an approximately reproducible surface, i.e., a reference state. Application of the technique should permit at least a precursory evaluation of the total surface via motion pictures. An experiment of this type would also provide at least a basis for evaluating propagation characteristics and observing local corrosion site interactions, i.e., whether the formation of subsequent sites affects previously formed sites.

B) Further analysis of the potential difference between the passive and active surface is also possible. The author devised a system on which the simultaneous evolution of hydrogen and pitting on consolidated areas of a single, electrically isolated specimen [47] was observed. The experimental arrangement is conducive to the measurement of potentials at several points very near the surface without interference or shielding from the associated probes and electrodes [9, 86]. Basically a non-driven specimen is oriented in a potential gradient which induces consolidated local cell action. The observed distribution of pits suggests that the potential gradient regulates pit frequency, but the uniformity of size suggests the active site current density is independent of potential. The system provides a convenient arrangement for the measurement of potentials over the surface.

C) The appearance of intergranular attack is not normally associated with a solution treated alloy. Further work to define the composition at the grain boundaries using an electron microprobe would be of interest. Reversion to pure nickel for the examination of the high noble potential regions of attack, particularly with regard to attack mode, should be fruitful in characterizing the nature of anionic participation. The absence of compositional effects on the part of the metal spacimen reduces the likelihood that anion participation is non-specific.

D) Hydrogen bubbles on the surface of an anode (generated by cathodic polarization) have been observed to influence pit formation [47] and solid bodies pressed against an anode are generally recognized to stimulate localized corrosion (crevice). Preliminary work showed that pits formed only at visable bubbles and not at sites where bubbles are presumably submicroscopic. Particular patterns and frequencies of pit formation can be forced using these artifices to ascertain the existence of critical active areas (an upper limit of anode to cathode or a maximum closeness of initiation sites) or critical bubble size. Such limits would prove useful in assessing the theory of local anode-cathode action inside of pits as accounting for i-t fluctuations. It was also shown that cathodic reactivity, as measured by the ability to evolve hydrogen, and anodic reactivity, as measured by the formation of pits, is not directly related, i.e., hydrogen formation sites were not more susceptible to pit formation than other areas.

REFERENCES

(1) Anderson, T. N., and H. Eyring, "Principles of Electrode Kinetics," Physical Chemistry, an Advanced Treatise, Vol. IX-A, Chapter 3, Academic Press, Inc., New York, 1970.

(2) Bianchi, G., A. Cerquetti, F. Mazza, and S. Torchio, U. R. Evans International Conference on Localized Corrosion, Preprint 28 (1971), "Pitting Corrosion of Austenitic Stainless Steel and Properties of Surface Oxide Films."

(3) Bockris, J. O'M., and A. K. N. Reddy, Modern Electrochemistry, Vol. 2, Plenum Press, New York, 1970.

(4) Bockris, J. O'M., A. K. N. Reddy, and B. Rao, J. Electrochem. Soc., 113, 1133 (1966), "An Ellipsometric Determination of the Mechanism of Passivity of Nickel."

(5) Bohni, H., and H. H. Uhlig, Corr. Sci., 9, 353 (1969), "Effects of Alloyed Re on the Critical Pitting Potentials of 18%Cr--10%Ni Stainless Steels."

(6) Brennert, S., Iron and Steel Inst. J., 135, 101 (1937), "Methods for Testing the Resistance of Stainless Steels to Local Corrosive Attack."

(7) Brown, B. F., C. T. Fujii, and E. P. Dahlberg, J. Electrochem. Soc., 116, 218 (1969), "Methods for Studying the Solution Chemistry Within Stress Corrosion Cracks."

(8) Butler, J. N., Ionic Equilibria, Addison--Wesley Company, Inc., Reading, Massachusetts, 1964.

(9) Compton, K. G., Mat. Res. & Stds., 10, 13 (1970), "The Use of Reference Electrodes in Corrosion Studies."

(10) Coriou, H., A. Monnier, G. Pinard-Legry, and G. Plante, U. R. Evans International Conference on Localized Corrosion, Preprint 19 (1971), "Electrochemical Study of Pit Growth on Stainless Steel in an Oxidizing Medium."

(11) Cotton, F. A., and G. Wilkinson, Advanced Inorganic Chemistry, Interscience Publishers, John Wiley & Sons, 1962.

(12) Dean, S. W., Jr., W. D. France, Jr., and S. J. Ketcham, Symposium on State of the Art in Corrosion Testing Methods, ASTM Annual Meeting, Toronto, Electrochemical Methods of Testing, 1970.

(13) Delahay, P., Double Layer and Electrode Kinetics, Interscience Publishers, John Wiley & Sons, Inc., New York, 1965.

(14) Devanathan, M. A. V., B. V. K. S. R. A. Tilak, Proc. Roy. Soc., Ser. A, 290, 527, "On the Specific Adsorption of Anions in the Electric Double Layer."

(15) Ebersbach, U., K. Schwabe, and P. Konig, Electrochim. Acta, 14, 773 (1969), "Zur Kinetik Der Anodischen Passivierung von Eisen, Kobalt und Nickel-II. Untersuchungen Uber Die Passivierung von Nickel in Schwefelsaure und Perchlorsaure mit Der Rotierenden Scheibenelektrode."

(16) France, W. D., Jr., J. Electrochem. Soc., 114, 818 (1967), "A Specimen Holder for Precise Electrochemical Polarization Measurements on Metal Sheets and Foils."

(17) France, W. D., Jr., H. L. Craig, Jr., J. J. Demo, Jr., D. L. Graver, E. G. Haney, and S. J. Ketcham, "The Reproducibility of Potentiostatic and Potentiodynamic Anodic Polarization Measurements," An ASTM G-1/XI Interlaboratory Testing Program, 1967.

(18) France, W. D., Jr., and N. D. Greene, Corrosion, 26, 1 (1970), "Comparison of Chemically and Electrolytically Induced Pitting Corrosion."

(19) Frankenthal, R., J. Electrochem. Soc., 114, 542 (1967), "On Passivity of Iron-Chromium Alloys."

(20) Franz, F., P. Novak, U. R. Evans International Conference on Localized Corrosion, Preprint 44 (1971), "Pitting Corrosion of Rotating Electrodes."

(21) Fujii, C. T., U. R. Evans International Conference on Localized Corrosion, Preprint 55 (1971), "A Review: Macro-Cells for the Study of Solution Chemistry and Electrochemistry in Localized Corrosion."

(22) Greene, N. D., W. D. France, Jr., and B. E. Wilde, Corrosion, 21, 275 (1965), "Electrode Mounting for Potentiostatic Anodic Polarization Studies."

(23) Greene, N. D., Experimental Electrode Kinetics, Renesselaer Polytechnic Institute, Troy, N. Y., 1965.

(24) Greene, N. D., Corrosion, 18, 136t (1962), "Predicting Behavior of Corrosion Resistant Alloys."

(25) Greene, N. D., and R. B. Leonard, Electrochim. Acta, 9, 45 (1964), "Comparison of Potentiostatic Anodic Polarization Methods."

(26) Handbook of Chemistry and Physics, Chemical Rubber Publishing Co., Cleveland, 1963.

(27) Harned, H. S., and B. B. Owen, The Physical Chemistry of Electrolytic Solutions, 3rd Ed., Reinhold Publishing Corp., New York, 1958.

(28) Hisamatsu, Y., T. Yoshii, and Y. Matsumura, U. R. Evans International Conference on Localized Corrosion, Preprint 21 (1971), "Electrochemical and Microscopial Study of Pitting Corrosion of Austenitic Stainless Steel."

(29) Hoar, T. P., Corr. Sci., 7, 341 (1967), "The Production and Breakdown of the Passivity of Metals."

(30) Hoar, T. P., and W. R. Jacob, Nature, 216, 1299 (1967), "Breakdown of Passivity of Stainless Steel by Halide Ions."

(31) Horvarth, J., and H. H. Uhlig, J. Electrochem. Soc., 115, 791 (1968), "Critical Potentials for Pitting Corrosion of Ni, Cr-Ni, Cr-Fe and Related Stainless Steels."

(32) Huntington Alloy Products Division Manual, Section 3, 1964.

(33) Isaacs, H. S., U. R. Evans International Conference on Localized Corrosion, Preprint 56 (1971), "Surface Potential Scanning of Stainless Steel During Pitting Corrosion."

(34) Ives, M. B., U. R. Evans International Conference on Localized Corrosion, Preprint 8 (1971), "Etch Pitting-Theory and Observation."

(35) Jones, D. A., and N. D. Greene, Corrosion, 25, 367 (1969), "Electrochemical Detection of Localized Corrosion."

(36) Jones, G., and B. C. Bradshaw, J. Am. Chem. Soc., 55, 1780 (1933), "The Measurement of the Conductance of Electrolytes."

(37) Kielland, J., J. Am. Chem. Soc., 59, 1675 (1937), "Individual Activity Coefficients of Ions in Aqueous Solutions."

(38) Kolotyrkin, J. M., J. Electrochem. Soc., 108, 209 (1961), "Effects of Anions on the Dissolution Kinetics of Metals."

(39) Kolotyrkin, J. M., Corrosion, 19, 261t (1963), "Pitting Corrosion of Metals."

(40) Leckie, H. P., J. Electrochem. Soc., 117, 1152 (1970), "A Contribution to the Applicability of Critical Pitting Potentials."

(41) Leckie, H. P., and H. H. Uhlig, J. Electrochem. Soc., 113, 1262 (1966), "Environmental Factors Affecting the Critical Potential for Pitting in 18-8 Stainless Steel.

(42) Legault, R. A., S. Mori, and H. P. Leckie, Corrosion, 26, 121 (1970), "An Electrochemical-Statistical Study of the Effect of Chemical Environment on the Corrosion Behavior of Mild Steel."

(43) Morris, P. E., and R. C. Scarberry, Corrosion, 26, 169 (1970), "Anodic Polarization Measurements of Active-Passive Nickel Alloys by Rapid-Scan Potentiostatic Techniques."

(44) Mueller, W. A., Corrosion, 25, 473 (1969), "Theoretical Considerations in the Measurements of Polarization and Corrosion Potential Curves."

(45) Nathan, C. C., and C. L. Dulaney, U. R. Evans International Conference on Localized Corrosion, Preprint 54 (1971), "Localized Corrosion as a Statistical Phenomenon."

(46) Parsons, R., Trans. Faraday Soc., 47, 1332 (1951), "General Equations for the Kinetics of Electrode Processes."

(47) Pascoe, R. F., Unpublished Data.

(48) Possal, N., and C. Liu, Electrochim. Acta, 16, 1987 (1971), "Determination of Critical Pitting Potentials of Stainless Steels in Aqueous Chloride Environments."

(49) Pickering, H. W., and R. P. Frankenthal, U. R. Evans International Conference on Localized Corrosion, Preprint 12 (1971), "Mechanism of Pit and Crevice Propagation on Iron and Stainless Steels."

(50) Piron, D. L., E. P. Koutsoukos, and Ken Nobe, Corrosion, 25, 151 (1969), "Corrosion Behavior of Nickel and Inconel in Acidic Chloride Solutions."

(51) Postelthwaite, J., R. A. Brierley, and M. J. Walmsley, U. R. Evans International Conference on Localized Corrosion, Preprint 20 (1971), "Pitting at Elevated Temperatures."

(52) Pourbaix, M., et al., Corr. Sci., 3, 239 (1963), "Potentiokinetic and Corrosimetric Investigations of the Corrosion Behavior of Alloy Steels."

(53) Pourbaix, M., Atlas of Electrochemical Equilibria in Aqueous Solutions, Translated from the French by James A. Franklin, Pergamon Press, CEBELCOR, 1966.

(54) Reddy, A. K. N., and B. Rao, Can. J. Chem., 47, 2693 (1969), "The Mechanism of Passivation of Nickel as Determined by an Automatic Recording Ellipsometer."

(55) Reddy, A. K. N., and B. Rao, Can. J. Chem., 47, 2687 (1969), "The Mechanism of Formation of Pre-Passive Films on Nickel: A Chrono-ellipsometric Study."

(56) Riggs, O. L., Jr., Corrosion, 25, 130 (1969), "Discussion: Role of the Anion in Passive Layer Formation."

(57) Rosenfeld, I. L., and I. S. Danilov, Corr. Sci., 7, 129 (1967), "Electrochemical Aspects of Pitting Corrosion."

(58) Sato, N., Electrochim. Acta, 16, 1683 (1971), "A Theory for Breakdown of Anodic Oxide Films on Metals."

(59) Sato, N., T. Nakagawa, K. Kudo, and M. Sakashita, U. R. Evans International Conference on Localized Corrosion, Preprint 26 (1971), "Chloride-Pitting Dissolution of Rotating Stainless Steel Electrodes in Acid Solution."

(60) Schwabe, K., Electrochim. Acta, 12, 67 (1967), "Aziditat Konzentrierter Electrolytlosungen."

(61) Schwenk, W., Corrosion, 20, 129t (1964), "Theory of Stainless Steel Pitting."

(62) Siejka, J., and C. Cherki, J. Electrochem. Soc., 119, 991 (1972), "A Study of Passivity Phenomena by Using O^{18} Tracer Techniques."

(63) Smialowska, S., U. R. Evans International Conference on Localized Corrosion, Preprint 18 (1971), "Review: The Pitting of Iron-Chromium-Nickel Alloys."

(64) Smialowska, S., and M. Czachor, U. R. Evans International Conference on Localized Corrosion, Preprint 24 (1971), "The Analysis of Electrochemical Methods for the Determination of Characteristic Potentials of Pitting Corrosion."

(65) Smialowska, S., Corrosion, 27, 233 (1971), "Review of Literature on Pitting Corrosion Published Since 1960."

(66) Smialowska, S., and M. Czachor, Br. Corr. J., 4, 138 (1969), "Electrochemical Investigation of the Nucleation and Propagation of Pits in Fe, Cr Alloys."

(67) Stern, M., and A. L. Geary, J. Electrochem. Soc., 104, 56 (1957), "A Theoretical Analysis of the Shape of Polarization Curves."

(68) Stern, M., J. Electrochem Soc., 104, 645 (1957), "Electrochemical Polarization."

(69) Stern, M., and E. D. Weisert, Proc. Amer. Soc. Test. Mat., 59, 1280 (1959), "Experimental Observations on the Relation Between Polarization Resistance and Corrosion Rate."

(70) Stolica, N. D., Corr. Sci., 9, 205 (1969), "Pitting Corrosion on Fe-Cr Alloys."

(71) Stolica, N. D., Corr. Sci., 9, 455 (1969), "Pitting Corrosion on Fe-Cr and Fe-Cr-Ni Alloys."

(72) Streicher, M. A., J. Electrochem. Soc., 103, 375 (1956), "Pitting Corrosion of 18Cr-8Ni Stainless Steel."

(73) Tomashov, N. D., G. P. Chernova, and O. N. Marcova, U. R. Evans International Conference on Localized Corrosion, Preprint 13A (1971), "Investigation of Pitting Repassivation on 18Cr-14Ni Steels Additionally Alloyed with V, Si, Mo or Re."

(74) Trout, B. L. and R. D. Daniels, Corrosion, 28, 331 (1972), "Potentiostatic Polarization of Inconel X-750."

(75) Vermilyea, D. A., J. Electrochem. Soc., 118, 529 (1971), "Concerning the Critical Pitting Potential."

(76) Vetter, K. J., Electrochim. Acta, 16, 1923 (1971), "General Kinetics of Passive Layers on Metals."

(77) Vetter, K. J., and H. H. Strehblow, U. R. Evans International Conference on Localized Corrosion, Preprint 10 (1971), "Pitting Corrosion in an Early Stage and its Theoretical Implications."

(78) Vetter, K. J., Electrochemical Kinetics, Academic Press, Inc., New York, 1967, Translated by Scripta Technica, Inc. from Electrochemische Kinetik, Springer-Verlag, Berlin, 1961.

(79) Vetter, K. J., J. Electrochem. Soc., 110, 597 (1963), "A General Thermodynamic Theory of the Potential of Passive Electrodes and its Influence on Passive Corrosion."

(80) Wallwork, G. R., and B. Harris, U. R. Evans International Conference on Localized Corrosion, Preprint 15 (1971), "Localized Corrosion in Mild Steel."

(81) Wilde, B. E., and E. Williams, Electrochim. Acta, 16, 1971 (1971), "Use of Current/Voltage Curves for the Study of Localized Corrosion and Passivity Breakdown on Stainless Steels in Chloride Media."

(82) Wilde, B. E., U. R. Evans International Conference on Localized Corrosion, Preprint 23 (1971), "On Pitting and Protection Potentials: Their Uses and Possible Misuses for Predicting Localized Corrosion Resistance of Stainless Alloys in Halide Media."

(83) Wilde, B. E., and E. Williams, J. Electrochem. Soc., 117, 775 (1970), "On the Correspondence between Electrochemical and Chemical Accelerated Pitting Corrosion Tests."

(84) Wranglen, G., U. R. Evans International Conference on Localized Corrosion, Preprint 34 (1971), "Active Sulfides and the Pitting Corrosion of Carbon Steels."

(85) Yahalom, J., and I. Weisshauss, U. R. Evans International Conference on Localized Corrosion, Preprint 30 (1971), "Observation of Nickel Oxide Film in Pits caused by Chloride Ions."

(86) Yeager, E., and J. Kuta, "Techniques for the Study of Electrode Processes," Physical Chemistry, An Advanced Treatise, Vol. IX-A, Chapter 4, Academic Press, Inc., New York, 1970.

APPENDICES

A. Supplementary Induction Time Curves

B. Significance of the Transfer Coefficient

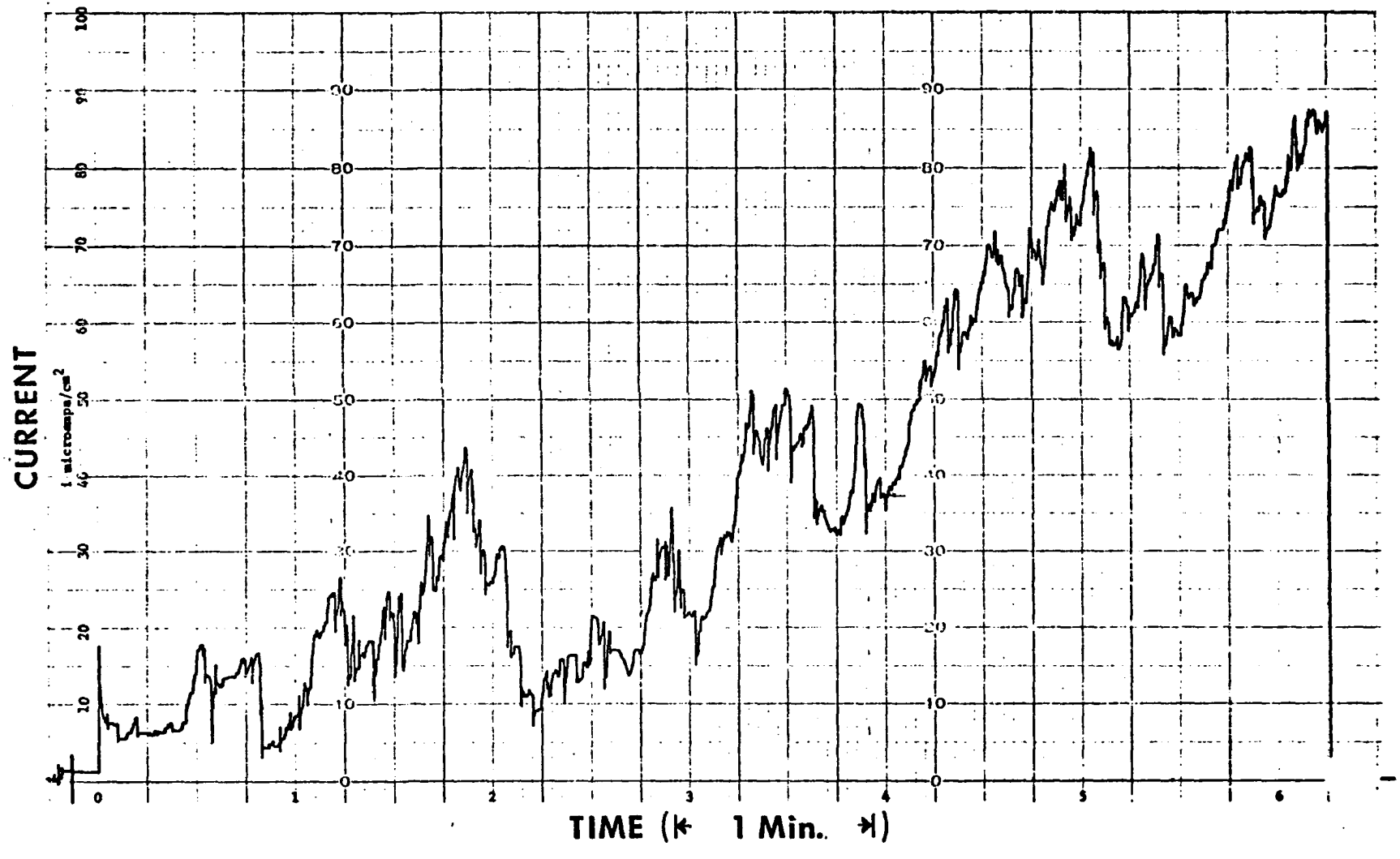

Fig. A.1.--Induction Time Curve at I = 0.1, r = 3, E = +0.5 V.

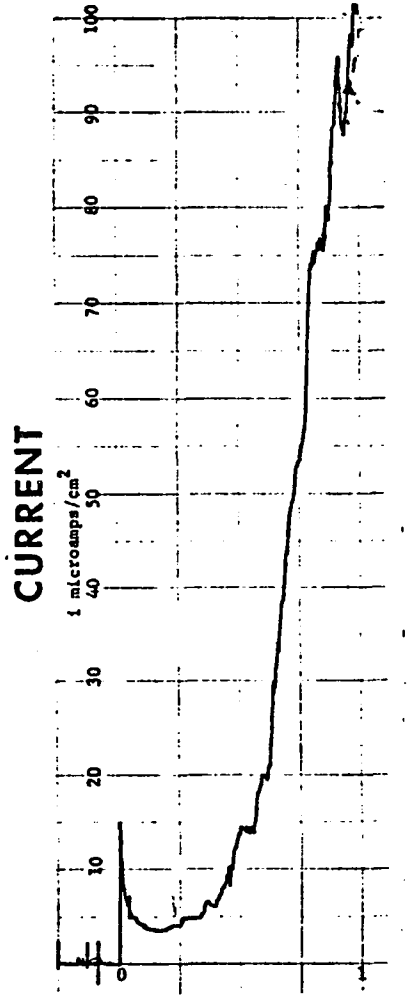

Fig. A.2.--Induction Time Curve at
I = 0.1, r = 3, E = +0.6 V.

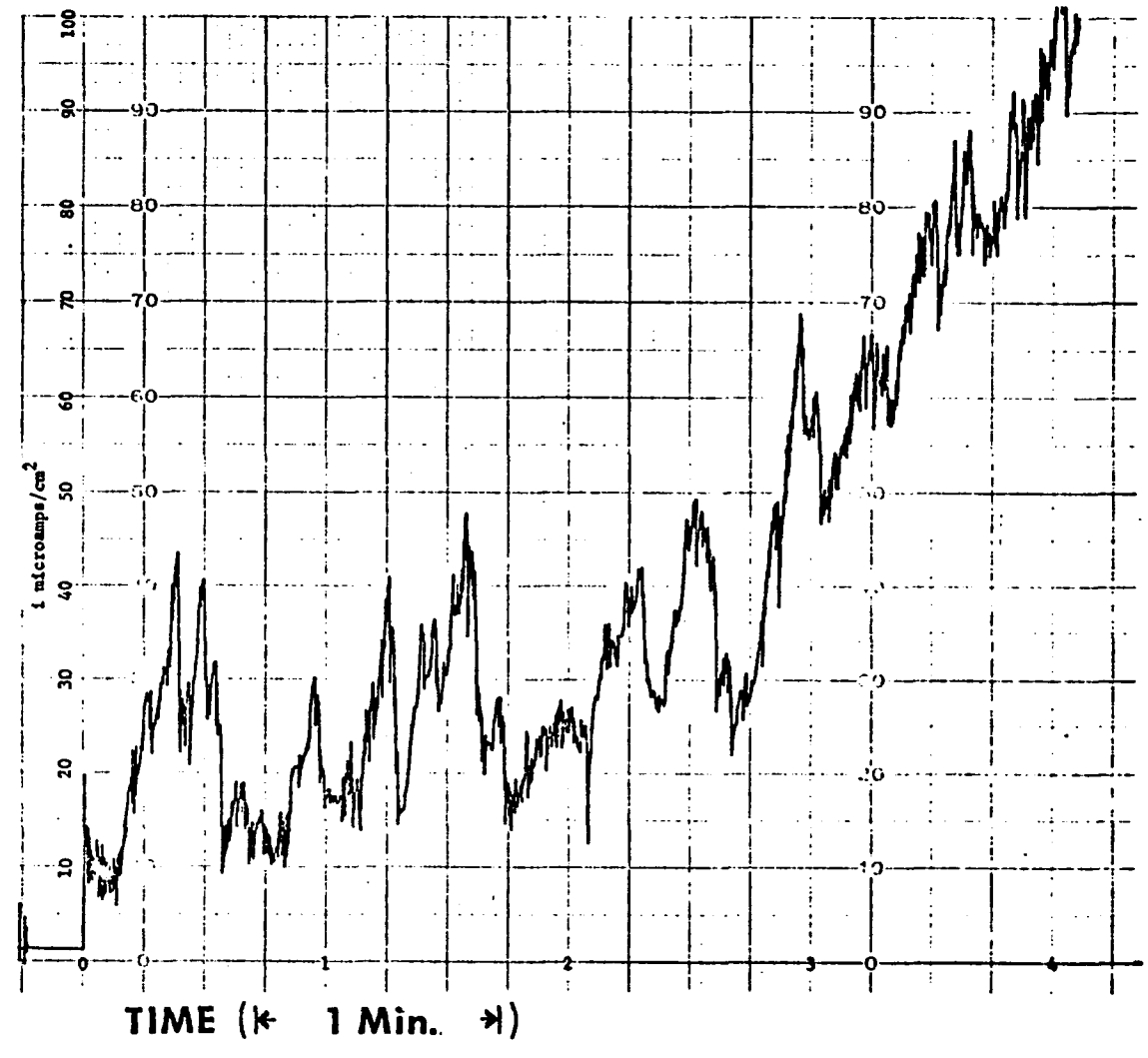

Fig. A.3.--Induction Time Curve at
I = 0.1, r = 7, E = +0.45 V.

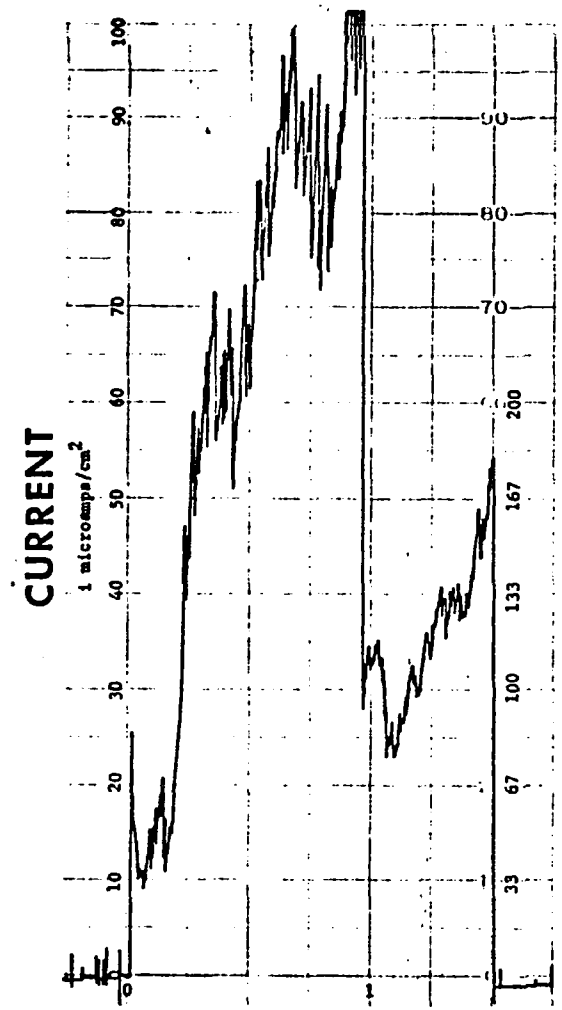

Fig. A.4.--Induction Time Curve at I = 0.1, r = 7, E = +0.5 V.

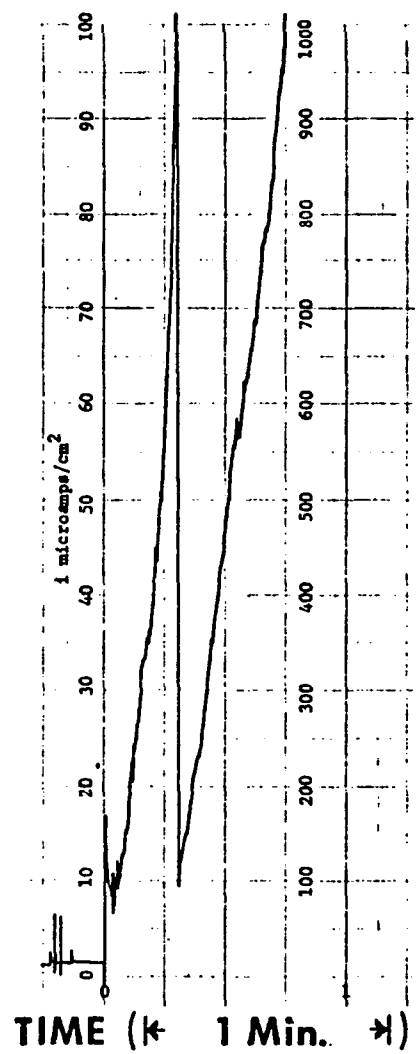

Fig. A.5.--Induction Time Curve at I = 0.1, r = 7, E = +0.6 V.

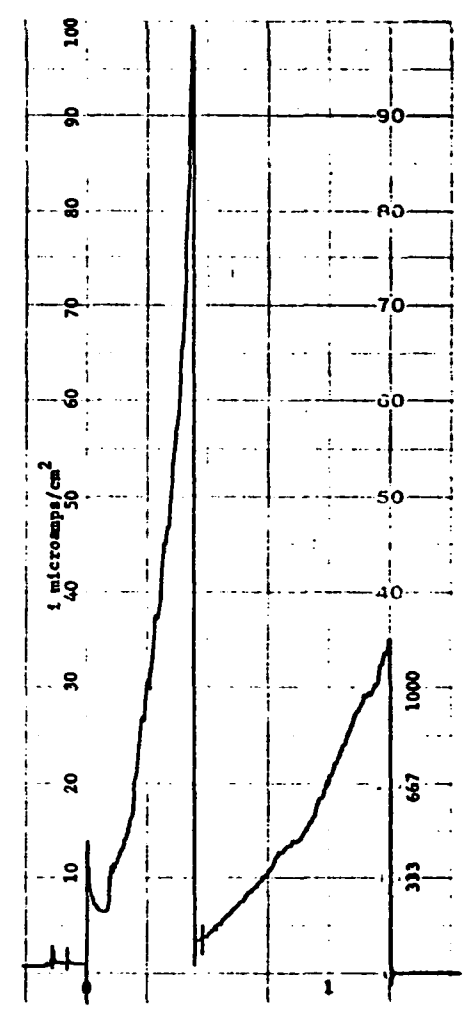

Fig. A.6.--Induction Time Curve at I = 0.1, r = 7, E = +0.7 V.

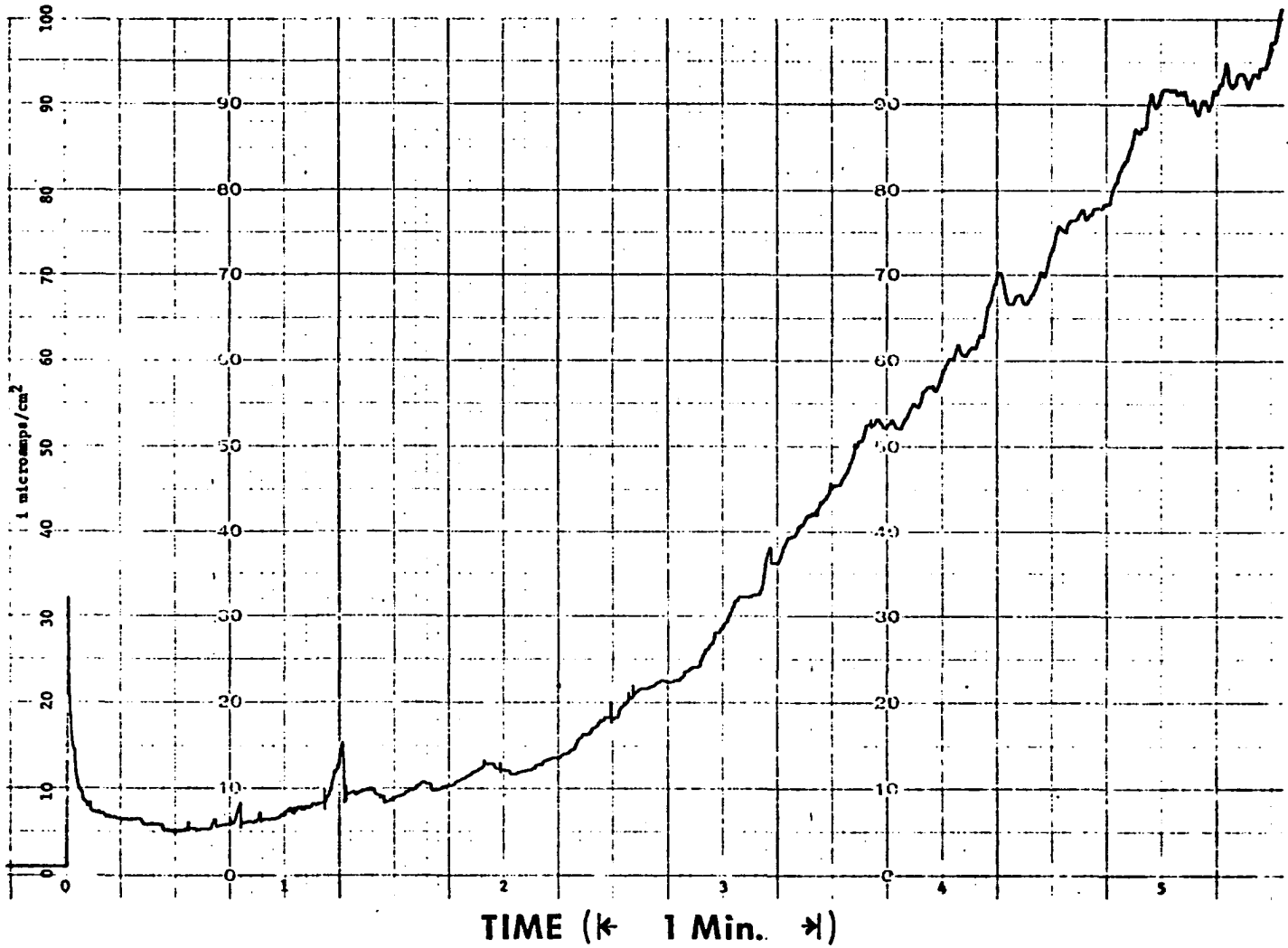

Fig. A.7.--Induction Time Curve at I = 0.1, r = ∞, E = +0.2 V.

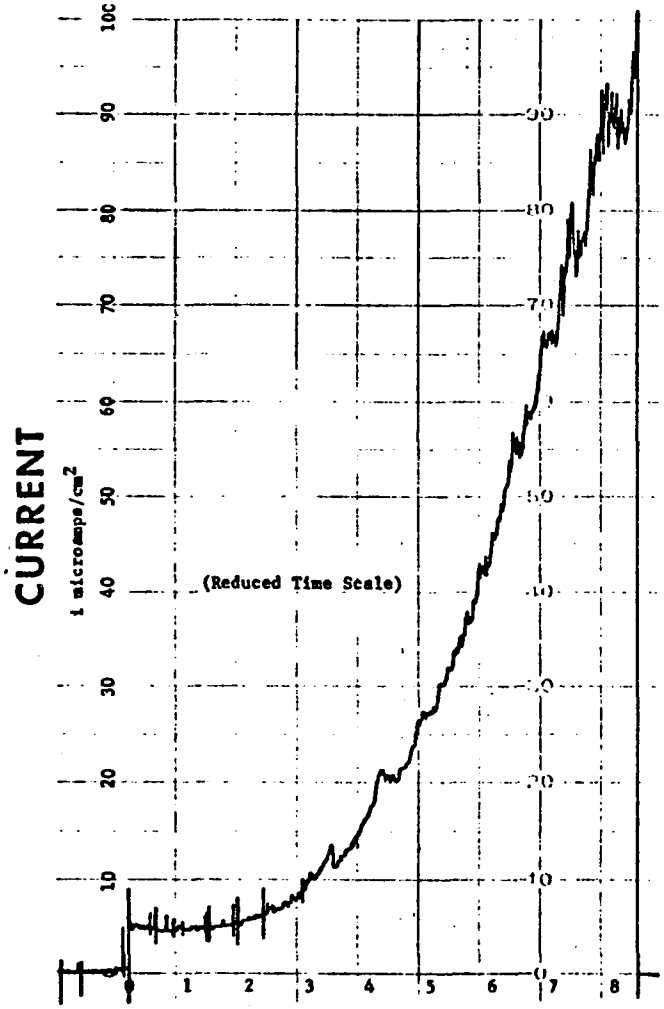

Fig. A.8.--Induction Time Curve at I = 0.1, r = ∞, E = +0.25 V.

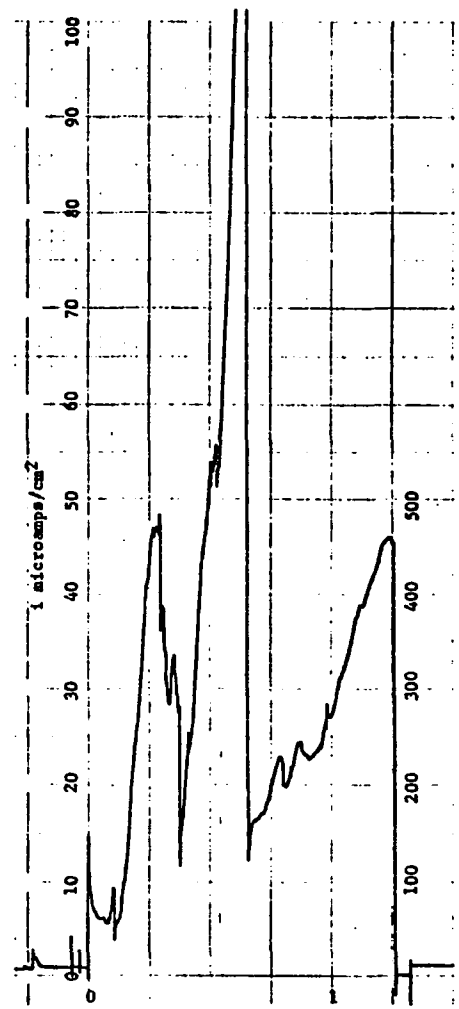

Fig. A.9.--Induction Time Curve at I = 0.1, r = ∞, E = +0.35 V.

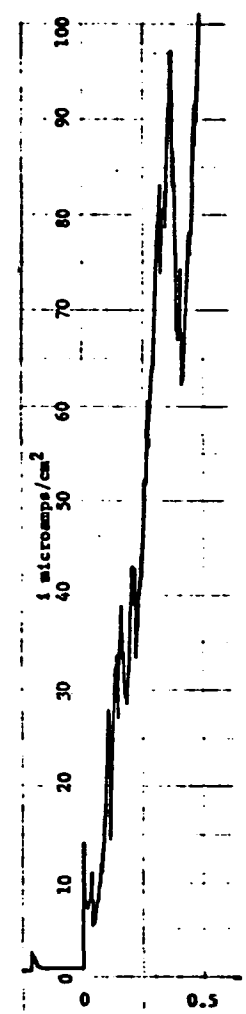

Fig. A.10.--Induction Time Curve at I = 0.1, r = ∞, E = +0.4 V.

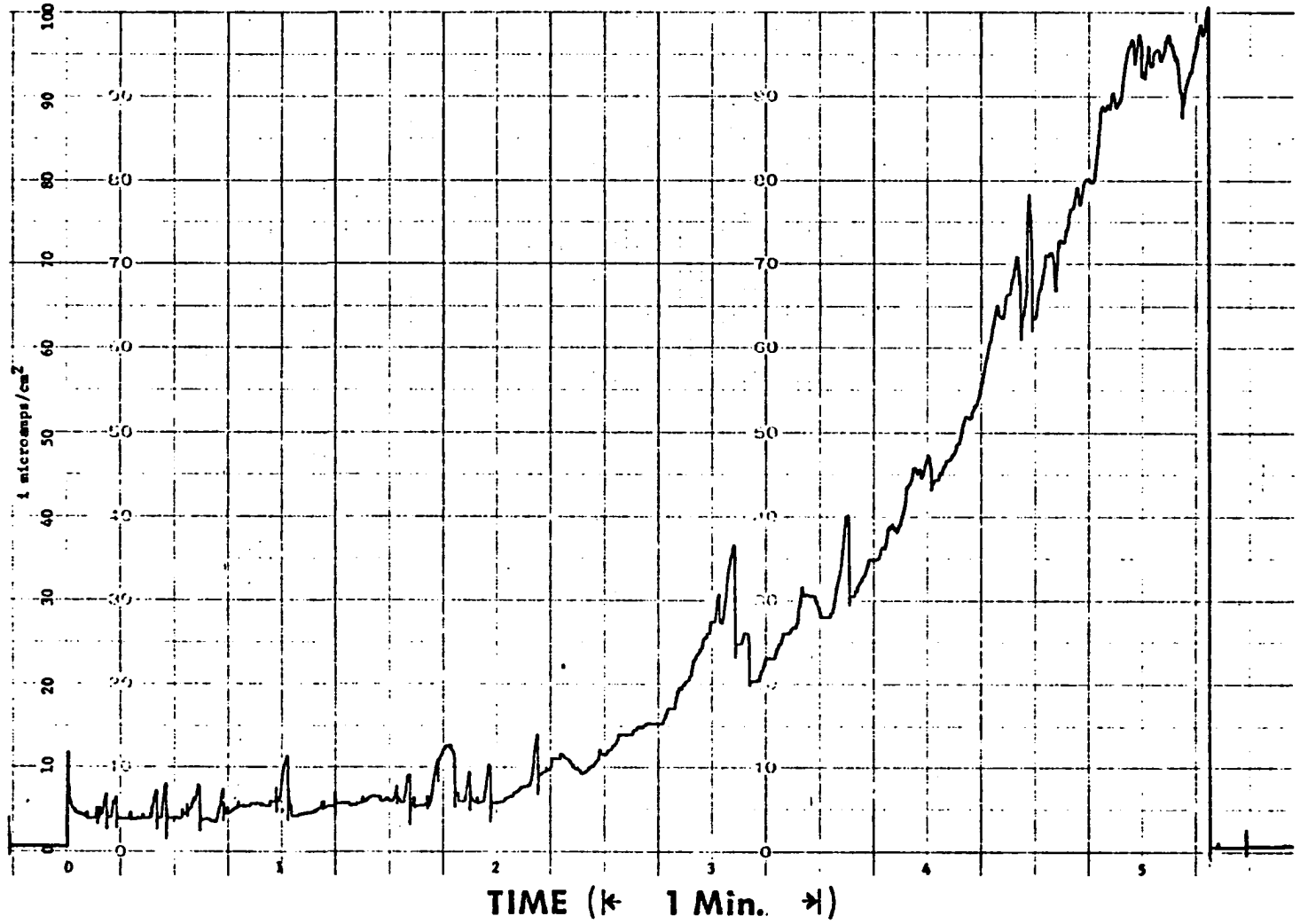

Fig. A.11.--Induction Time Curve at I = 0.1, r = ∞, E = +0.25 V.

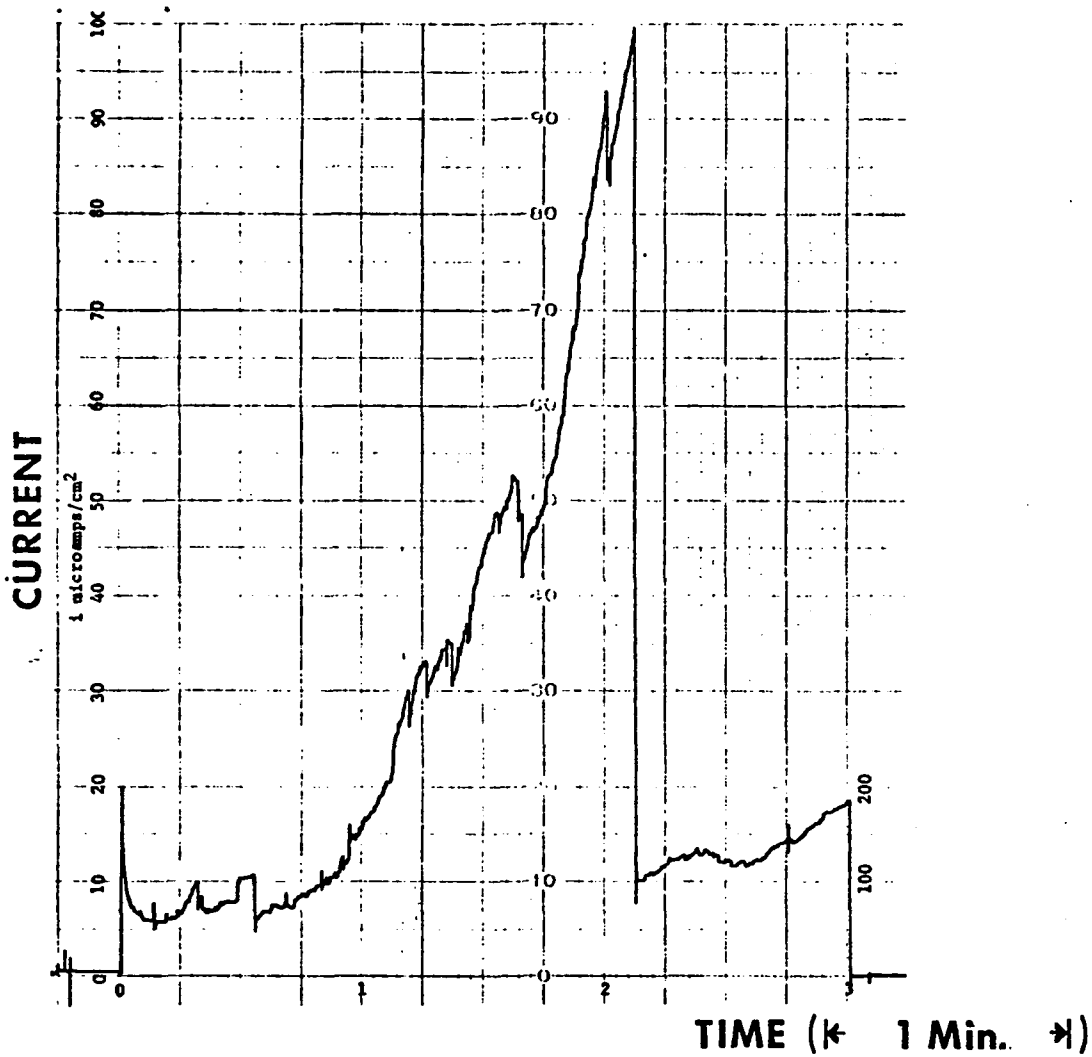

Fig. A.12.--Induction Time Curve at
I = 0.32, r = 2, E = +0.5 V.

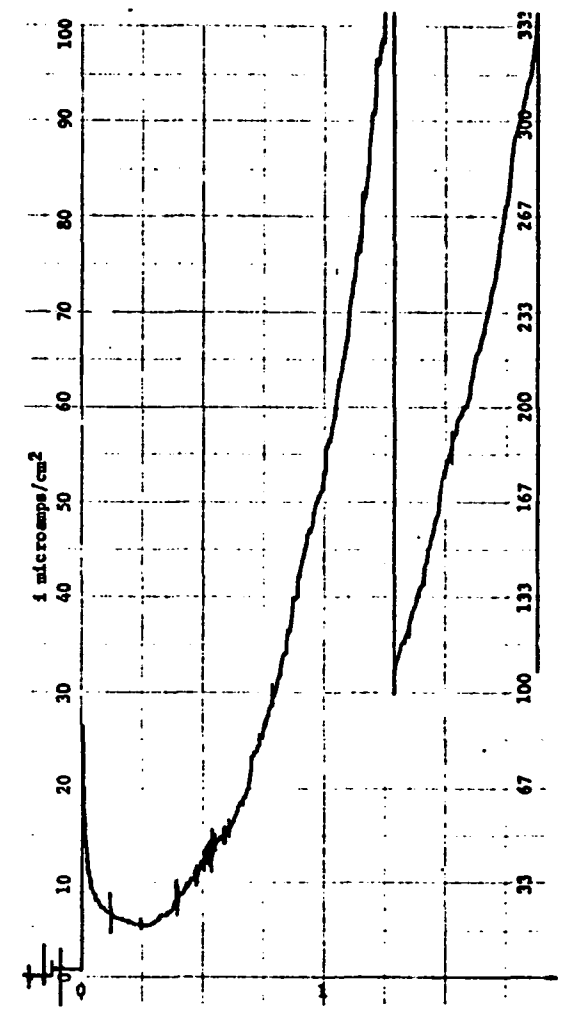

Fig. A.12.--Induction Time Curve at
I = 0.32, r = 2, E = +0.6 V
(micropolished).

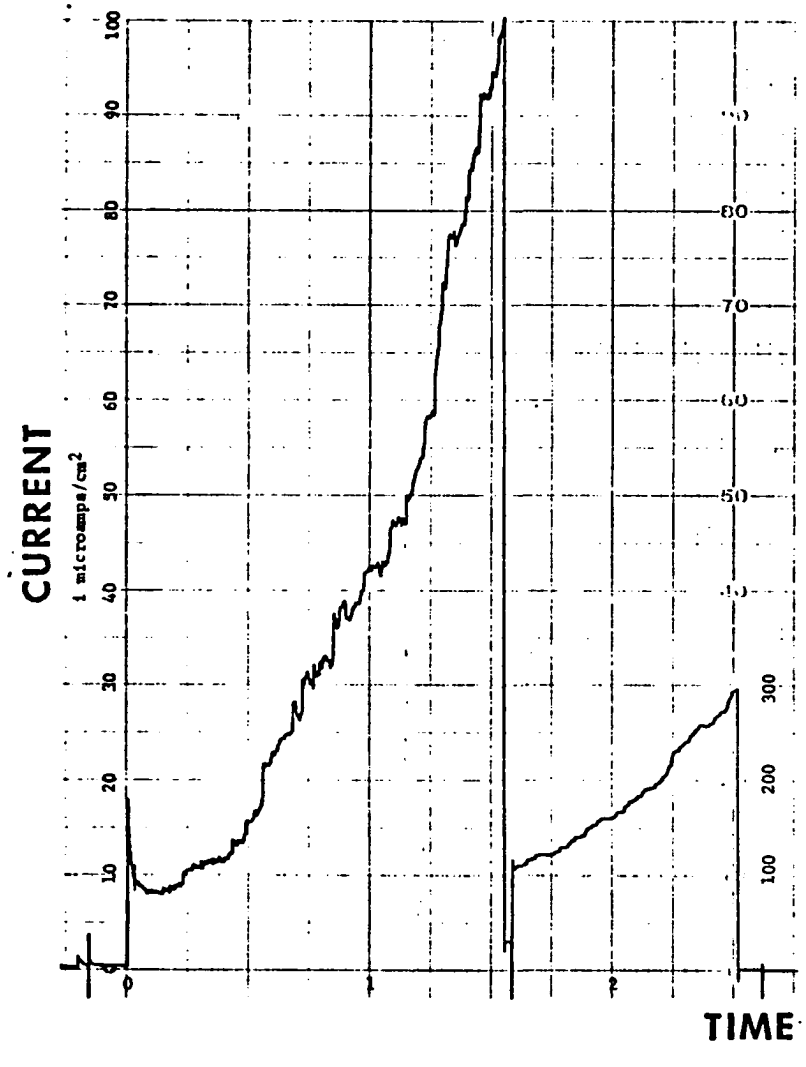

Fig. A.14.--Induction Time Curve at
I = 0.32, r = 2, E = +0.6 V.

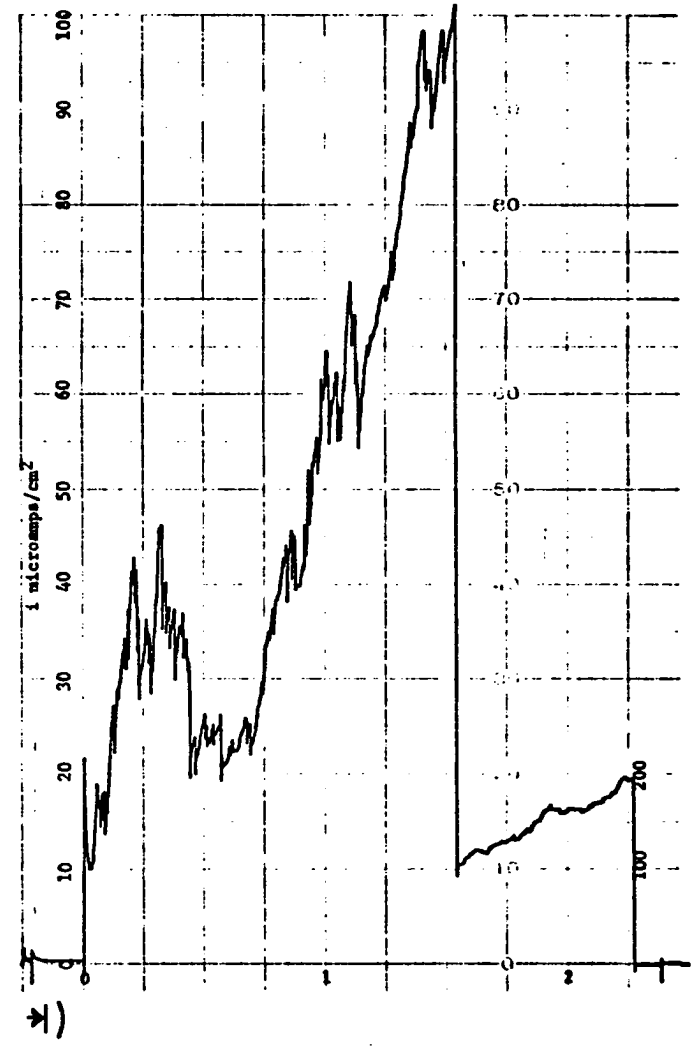

Fig. A.15.--Induction Time Curve at
I = 0.32, r = 3, E = +0.4 V.

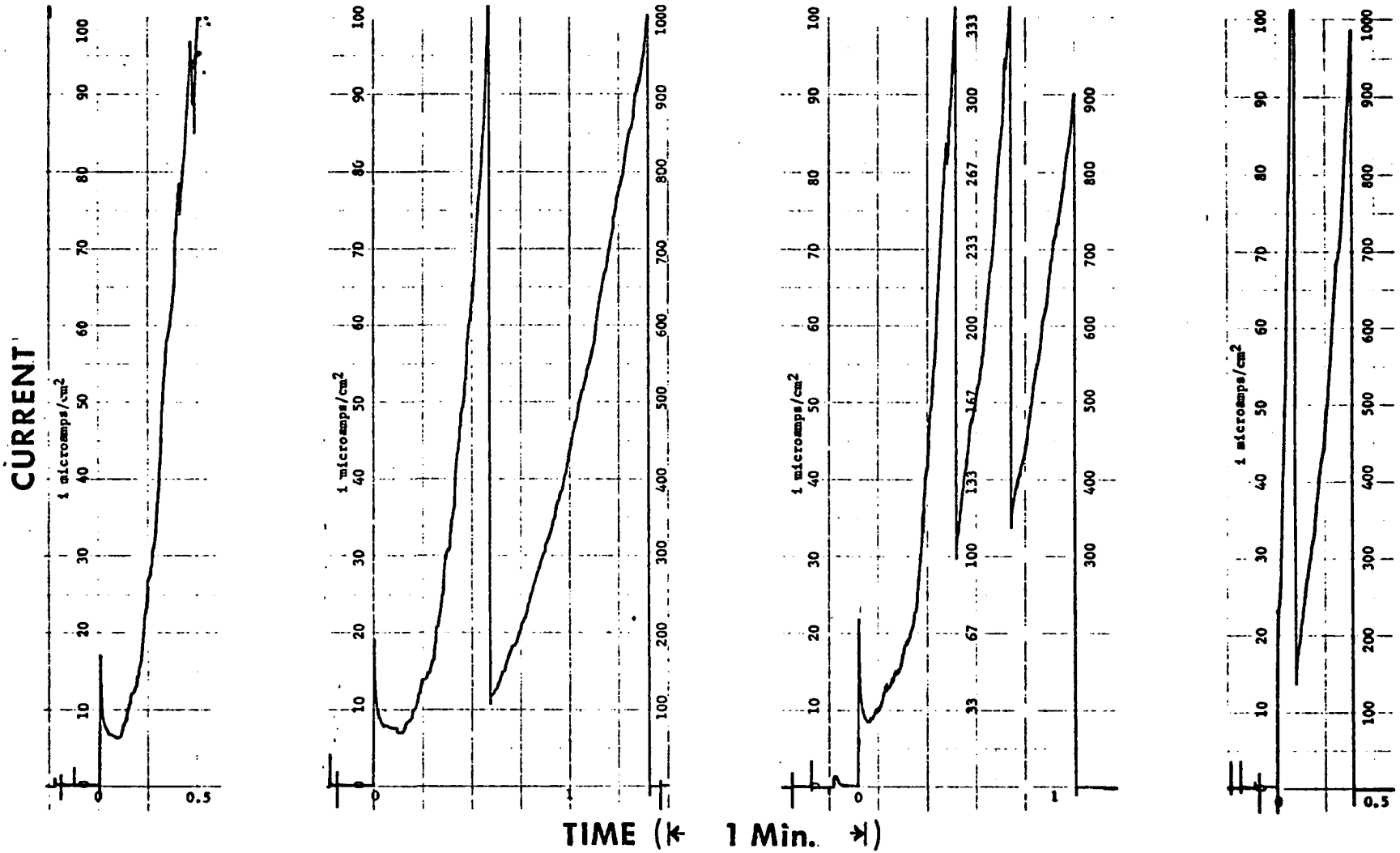

Fig. A.16.--
I = 0.32
r = 3
E = +0.5 V.

Fig. A.17.--
I = 0.32
r = 3
E = +0.6 V.

Fig. A.18.--
I = 0.32
r = 3
E = +0.7 V.

Fig. A.19.--
I = 0.32
r = 7
E = +0.6 V.

APPENDIX B

SIGNIFICANCE OF THE TRANSFER COEFFICIENT

The transfer coefficient, α, has been defined [3, 13, 45] to relate the chemical and electrical aspects of charge transfer. This can be understood by comparing the electrochemical reaction rate constant to the frequently encountered chemical reaction rate constant, k', where

$$k' = k \exp(-E_a/RT) \qquad \text{Equation B.1}$$

and the activation energy, E_a, is arbitrarily defined in terms of the enthalpy for the reaction, ΔH_r. Since ΔH_r is virtually temperature independent E_a is also temperature independent, therefore, reaction rates are frequently regulated by regulating the temperature for the reaction.

In an electrochemical reaction temperature is frequently held constant and the reaction rate is regulated by varying the electric potential, or in terms of Equation B.1, the activation energy is regulated. The discussion which follows illustrates the conditions for which α is a measure of the change of activation energy associated with the change in electric field strength across the plane of charge transfer.

Figure B.1, shows potential energy curves for the ejection of a metal atom to form a metal ion as represented by Reaction B.1:

$$(M\text{-}M) + m\ H_2O \rightarrow M\ (ne^-) + (M^{+n} - m\ H_2O) \qquad \text{Reaction B.1}$$

Curve a results if the metal atom presses too close to the other metal atoms in the crystal lattice or if it pulls too far away so the metal-metal bond is stretched. The valley of curve a is the position of a surface atom at the minimum potential energy. A similar curve b can be used to represent the hydrated metal ion, which is repulsed as it attempts to approach too near the metal surface.

By assuming that the resulting potential energy curve represents the potential energy-distance path for the metal-metal ion transition, a basis is established from which to evaluate the effect of electrical

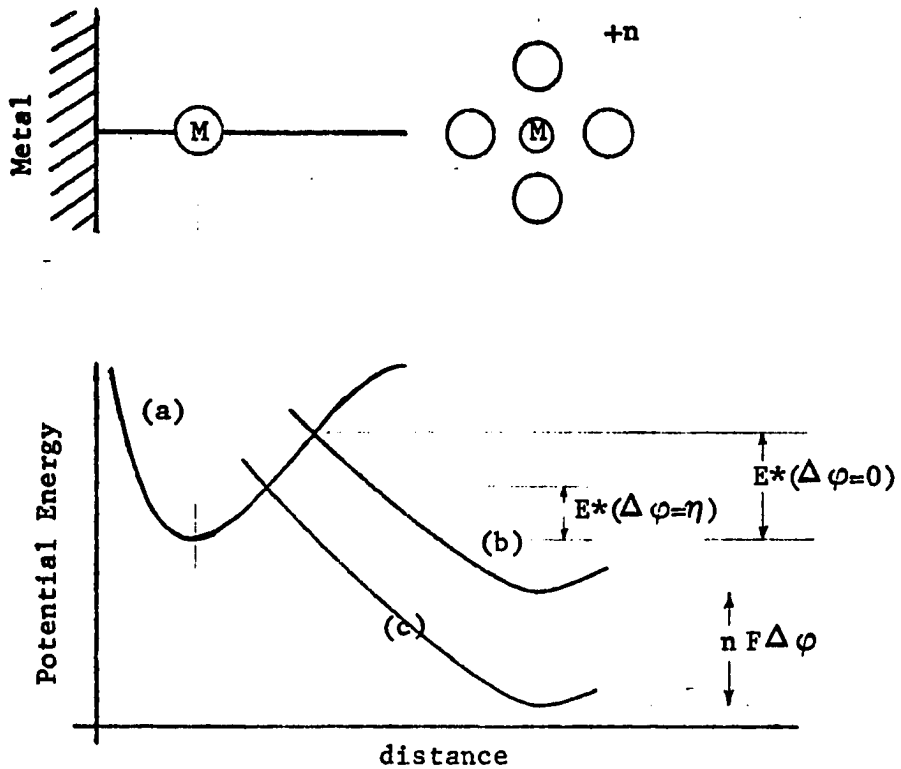

Fig. B.1.--Potential Energy-Distance Curves for the Dissolution of a Metal Atom.

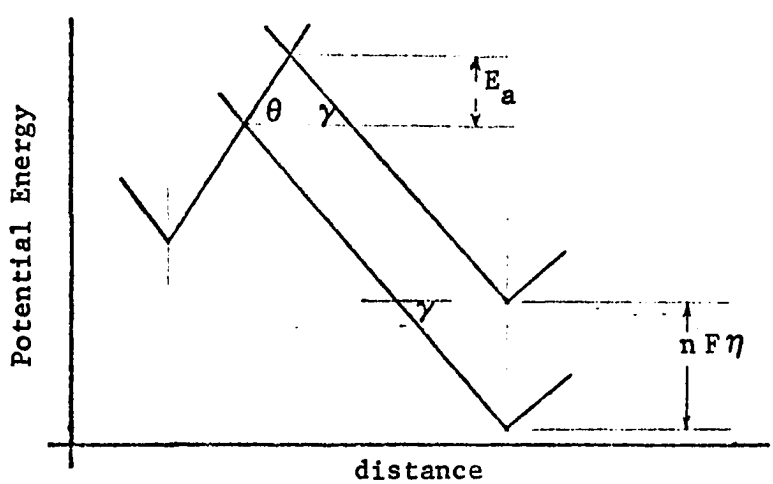

Fig. B.2.--Linearized Potential Energy-Distance Curves

potential on the activation energy.

Suppose that curves a and b of Figure B.1 represent the situation when no electrical potential is applied, i.e., it represents the situation described by chemical kinetics. Now if an electrical potential gradient is imposed at constant temperature no change in the M-M curve is expected since no charged species are involved, thus curve a will apply for all potentials. Also the applied potential will have little effect on the relatively weak M^{+n}—m H_2O bonds. Consequently, the major source of change is attributable to the $M(ne^-)$ term in Reaction B.1. Since

$$(\Delta \text{ electron energy}) = (\text{electronic charge}) \cdot (\Delta \varphi) \qquad \text{Equation B.2}$$

the change in potential energy associated with the application of the potential gradient, $\Delta\varphi$, becomes $(ne^-)\cdot(\Delta\varphi)$ for one event or $nF\Delta\varphi$ for Avagadro's number of events where F is the Faraday. This result can be plotted into Figure B.1 by recognizing that the imposition of $\Delta\varphi$ affected only the potential energy of the electrons, therefore, the distances are unaffected and the right hand curve is shifted vertically downward by the amount $nF\Delta\varphi$ and the activation energy changes from $E^*(\Delta\varphi=0)$ to $E^*(\Delta\varphi=\eta)$.

All that remains is to relate $nF\Delta\varphi$ to the change in activation energy, $E_a = (E^*_0 - E^*_\eta)$. This can be accomplished rudimentarily by linearizing Figure B.1 as shown in Figure B.2. From the latter figure it follows that:

$$\frac{E_a}{\tan\theta} + \frac{E_a}{\tan\gamma} = \frac{nF\eta}{\tan\gamma} \qquad \text{Equation B.3}$$

or

$$\frac{E_a}{nF\eta} = \frac{\tan\theta}{\tan\theta + \tan\gamma} = (1 - \alpha) \qquad \text{Equation B.4}$$

where $(1 - \alpha)$ is used to maintain harmony with published works in which α is typically discussed in terms of cathodic processes.